US Army Corps
of Engineers
Construction Engineering
Research Laboratories

USACERL Technical Report 97/116
July 1997

Comparative Evaluation of Ultrafiltration/Microfiltration Membranes for Removal of Nitrocellulose (NC) Fines From Wastewater

by
Byung J. Kim
Mark M. Clark
Yonghun Lee

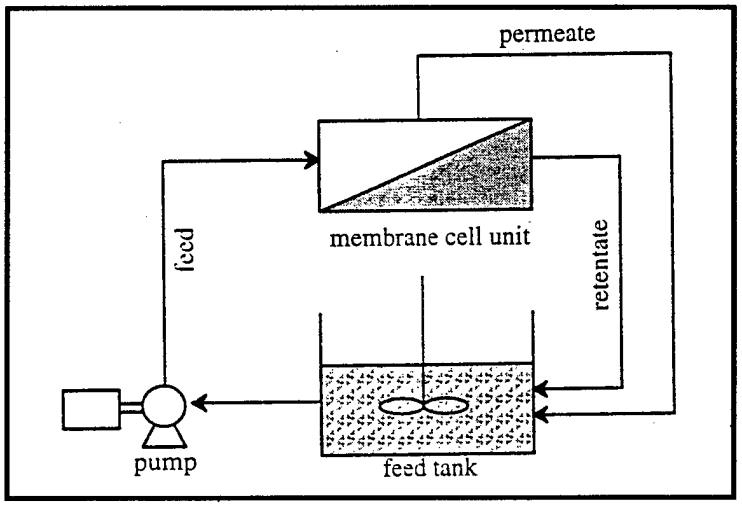

Nitrocellulose (NC) is a basic constituent for military gun propellants. NC wastewater is a byproduct of the NC manufacturing process. Crossflow microfiltration/ultrafiltration (MF/UF) may recover NC fines and allow the wastewater to be recycled. This bench-scale crossflow membrane filtration system was constructed to test the application of MF/UF technology to NC wastewater. This study was conducted in two phases. The results of Phase I were used to select a candidate membrane. In Phase II, a pilot-scale crossflow membrane filtration system was constructed to: (1) investigate the concentration polarization and fouling mechanism caused by NC fines during crossflow filtration of NC wastewater, (2) explore flux decline behavior of NC wastewater streams with various membranes, and (3) study the effects of operating parameters on flux decline behavior.

This study found that:

1. UF membranes have a lower flux decline rate and a higher flux recovery than MF membranes, but UF membranes have a relatively low permeate production rate compared to MF membranes.
2. A critical membrane pore size of about 0.1 μm exists, at which point the worst flux performance occurs.
3. The cellulose-based hydrophilic membranes have the best flux performance.

DESTROY THIS REPORT WHEN IT IS NO LONGER NEEDED

DO NOT RETURN IT TO THE ORIGINATOR

REPORT DOCUMENTATION PAGE

Form Approved
OMB No. 0704-0188

1. AGENCY USE ONLY *(Leave Blank)*	2. REPORT DATE	3. REPORT TYPE AND DATES COVERED
	July 1997	Final

4. TITLE AND SUBTITLE
Comparative Evaluation of Ultrafiltration/Microfiltration Membranes for Removal of Nitrocellulose (NC) Fines From Wastewater

5. FUNDING NUMBERS
4A162720
D048
TE6

6. AUTHOR(S)
Byung J. Kim, Mark M. Clark, and Yonghun Lee

7. PERFORMING ORGANIZATION NAME(S) AND ADDRESS(ES)
U.S. Army Construction Engineering Research Laboratories (USACERL)
P.O. Box 9005
Champaign, IL 61826-9005

8. PERFORMING ORGANIZATION REPORT NUMBER
TR 97/116

9. SPONSORING / MONITORING AGENCY NAME(S) AND ADDRESS(ES)
Headquarters, U.S. Army Corps of Engineers (HQUSACE)
ATTN: SFIM-AEC-ET
20 Massachussetts Ave, NW.
Washington, DC 20134-1000

10. SPONSORING / MONITORING AGENCY REPORT NUMBER

11. SUPPLEMENTARY NOTES
Copies are available from the National Technical Information Service, 5285 Port Royal Road, Springfield, VA 22161.

12a. DISTRIBUTION / AVAILABILITY STATEMENT
Approved for public release; distribution is unlimited.

12b. DISTRIBUTION CODE

13. ABSTRACT (Maximum 200 words)
Nitrocellulose (NC) is a basic constituent for military gun propellants. NC wastewater is a byproduct of the NC manufacturing process. Crossflow microfiltration/ultrafiltration (MF/UF) may recover NC fines and allow the wastewater to be recycled. This bench-scale crossflow membrane filtration system was constructed to test the application of MF/UF technology to NC wastewater. This study was conducted in two phases. The results of Phase I were used to select a candidate membrane. In Phase II, a pilot-scale crossflow membrane filtration system was constructed to: (1) investigate the concentration polarization and fouling mechanism caused by NC fines during crossflow filtration of NC wastewater, (2) explore flux decline behavior of NC wastewater streams with various membranes, and (3) study the effects of operating parameters on flux decline behavior.

This study found that:

1. UF membranes have a lower flux decline rate and a higher flux recovery than MF membranes, but UF membranes have a relatively low permeate production rate compared to MF membranes.

2. A critical membrane pore size of about 0.1 μm exists, at which point the worst flux performance occurs.

3. The cellulose-based hydrophilic membranes have the best flux performance.

14. SUBJECT TERMS
wastewater treatment systems
nitrocellulose fines
crossflow microfiltration

15. NUMBER OF PAGES
94

16. PRICE CODE

17. SECURITY CLASSIFICATION OF REPORT	18. SECURITY CLASSIFICATION OF THIS PAGE	19. SECURITY CLASSIFICATION OF ABSTRACT	20. LIMITATION OF ABSTRACT
Unclassified	Unclassified	Unclassified	SAR

Foreword

This study was conducted for Headquarters, U.S. Army Corps of Engineers (HQUSACE) under Project 4A162720D048, "Industrial Operations Pollution Control Technology"; Work Unit TE6, "Nitrocellulose Fines Abatement." The technical monitors were Gene Fabian, SFIM-AEC-ET and James Small, DCS-AMSIO-EQC.

The work was performed by the Industrial Operations Division (UL-I) of the Utilities and Industrial Operations Laboratory (UL), U.S. Army Construction Engineering Research Laboratories (USACERL). The USACERL principal investigator was Dr. Byung J. Kim. Walter J. Mikucki is Chief, CECER-UL-I; John T. Bandy is Operations Chief, CECER-UL; and Gary Schanche is the associated Technical Director, CECER-UL. The USACERL technical editor was William J. Wolfe, Technical Resources.

COL James A. Walter is Commander and Dr. Michael J. O'Connor is Director of USACERL.

Contents

List of Figures and Tables

Figures

Tables

Tables (Cont'd)

1 Introduction

1.1 Background

Nitrocellulose (NC) is a basic constituent for military gun propellants, and NC wastewater is a byproduct of NC manufacturing process. The Radford Army Ammunition Plant (RAAP), Radford, VA, generates an approximate maximum of 3.5 million gal of NC wastewater per day, which contains about 2,000 lb of colloidal and supracolloidal NC fines.* NC wastewater is generated at several points in the NC manufacturing and purification processes, including acid wash from boiling tub, and washwater from beating, poaching, blending, and wringer operations (Figure 1).

Currently, NC fines are separated from washwater by gravity settling at an acid boiling tub house settling pit and poacher house settling pit and by DeLaval Centrifuges for poacher pit effluent. Most of NC that is recovered at the poacher pit is reused as a lower grade propellant known as "pit cotton." If this pit cotton is not used and becomes waste, it will be considered a hazardous waste because of its flammability. The sludge produced by this process is also a listed hazardous waste. The Army is seriously considering terminating the reuse of pit cotton and will consequently need to develop some other reuse or treatment technology.

At RAAP, centrate from the DeLaval centrifuges containing small amounts of NC fines is pumped to Hill Top tank. For long periods, substantial amounts of NC fines accumulate in the Hill Top tank. When the Hill Top tank water is discharged to the acid boiling tub settling pit, a part of the accumulated NC fines is released; when this occurs, the water agitates and elevates the pH of the acid boiling tub pit water, resulting in a resuspension of the NC fines. Then NC fines are resettled in the boiling tub pit by gravity settling and the acid water containing NC fines is neutralized with lime and discharged to settling lagoons. NC fines are captured at the settling lagoon in a calcium sulfate matrix. The settled sludge from the lagoon is a listed hazardous waste. RAAP sought delisting of this sludge, but delisting was not granted. The residual NC fines in discharged wastewater may have deleterious ecological effects—mainly a reduction of light penetration and blanketing of benthic habitats rather than toxicity (Sullivan 1978). The present National Pollutant Discharge Elimination System (NPDES) sets the 40 ppm limit as suspended solids for the discharging NC wastewater at RAAP.

---

* 1 gal = 3.78 L; 1 lb = 0.453 kg.

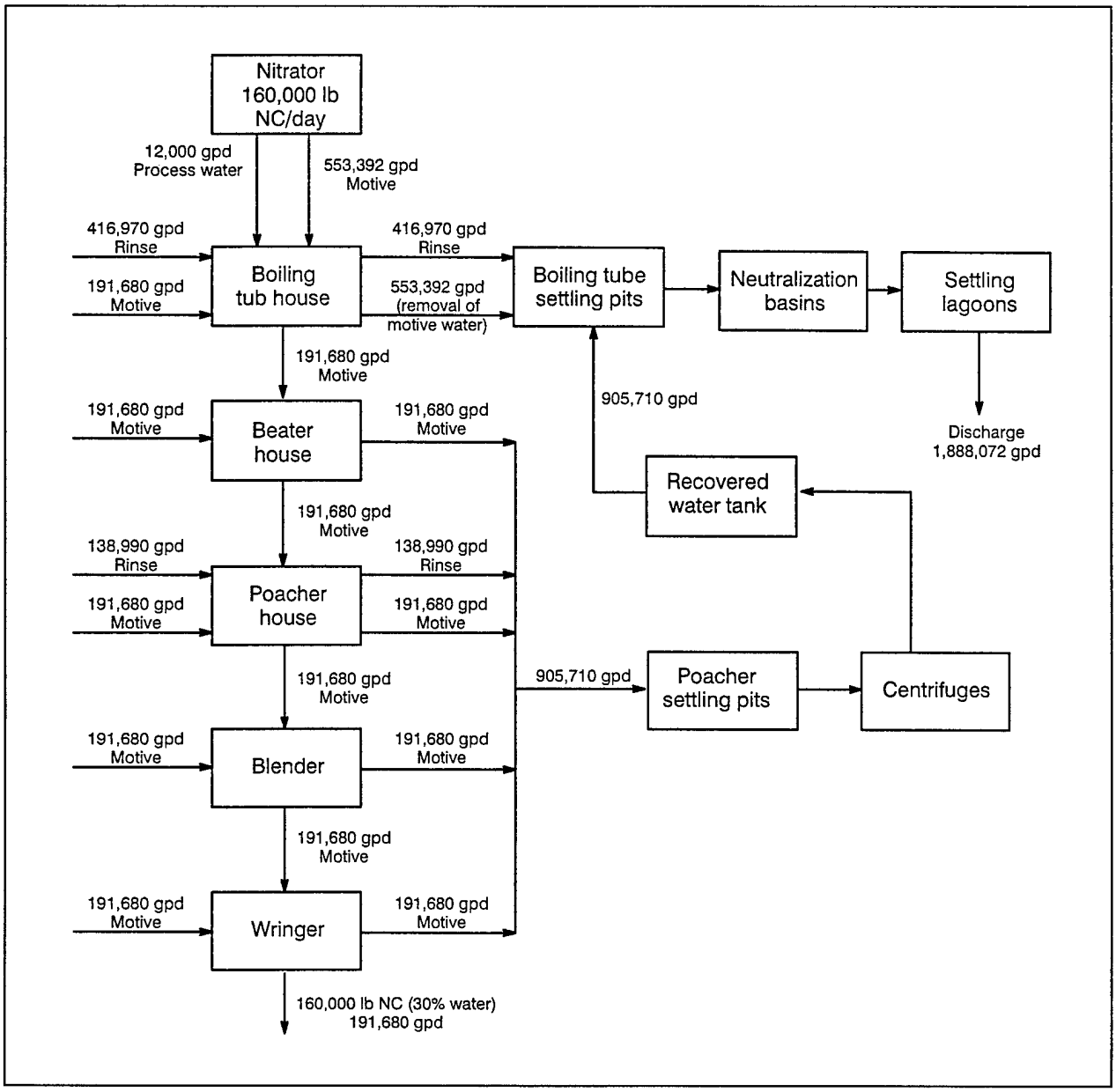

Figure 1. NC manufacturing process at RAAP (after Sullivan et al. 1978).

It is the Army's challenge to understand and develop technology to effectively separate NC fines from washwater. Among several alternatives (sliding bowl centrifugation, crossflow microfiltration, incineration, and alkaline digestion-biological treatment), the crossflow microfiltration membrane process is a technology that enables the NC fines to be recovered and the water to be recycled in the manufacturing process (Arthur D. Little, Inc. 1987). NC fines can be separated at each step and recycled to the next step of the process. NC fines can be also separated at poacher pit effluent, thereby replacing or supplementing the DeLaval centrifuges. Solid-liquid separation by a membrane process has many advantages: (1) it requires no phase change; (2) it has a low

energy requirement; and (3) it operates at ambient temperatures. However, the main problem in implementing the process is permeate flux decline due to concentration polarization and fouling phenomena. The crossflow membrane configuration tends to limit the negative effect of concentration polarization. However, research on crossflow membrane filtration of NC wastewater is quite limited. A bench-scale crossflow membrane filtration system was constructed to fill this information gap.

1.2 Objectives

This study consisted of two phases: Phase I, "dead-end filtration," and Phase II, "crossflow filtration." The objectives of the Phase I study were:

1. To investigate the physical/chemical characteristics of NC wastewater and NC fines
2. To explore the reactivity of various microfiltration/ultrafiltration (MF/UF) membranes in relation to flux decline behavior and reversible/irreversible fouling using an Amicon stirred dead-end filtration apparatus
3. To study the effects of transmembrane pressure and stirring on the flux decline behavior of NC wastewater.

Based on the results obtained in Phase I, a candidate membrane for NC wastewater treatment was selected. Because the Amicon stirred dead-end filtration apparatus is not appropriate to simulate the flux decline behavior during a practical crossflow filtration process, a pilot-scale crossflow membrane filtration system was constructed at University of Illinois at Urbana-Champaign for this project. The objectives of the Phase II study were:

1. To investigate the concentration polarization and fouling mechanism caused by NC fines during the crossflow UF/MF membrane filtration of NC wastewater.
2. To explore the flux decline behavior of each NC wastewater stream with various types of UF/MF membranes.
3. To study the effects of operating parameters like transmembrane pressure and crossflow velocity on the flux decline behavior.

1.3 Approach

A market survey was conducted to compile data on available membranes. The bench scale research was conducted in two phases: dead end filtration and cross flow filtration, using synthetic microfiltration/ultrafiltration membranes. Actual NC wastewater samples at various generation points were characterized. Flux decline behavior and its relationship to reversible/irreversible fouling for each membrane was analyzed using dead filtration. A candidate membrane was selected and membrane fouling behavior and factors affecting microfiltration/

ultrafiltration were analyzed using a bench scale crossflow microfiltration/ultrafiltration.

1.4 Scope

This study focused on the performance of synthetic microfiltration/ultrafiltration membrane using a bench-scale experimental system. Although 11 different membranes for dead filtration and three different membranes for crossflow filtration were evaluated, the study was not meant either to be inclusive for all membranes or to select any specific membranes. Rather, this study evaluated microfiltration/ultrafiltration membranes with different properties under various operational conditions. Transmembrane pressures were varied from 5 to 15 psi and flow velocity varied from 0.2 to 0.5 m/sec. Temperature effects were not considered; membranes in this study cannot be used for high temperature wastewater directly from the boiling tub or poacher house. Economic analysis and configuration of crossflow systems were beyond the scope of this work.

1.5 Mode of Technology Transfer

It is anticipated that the results of this study will contribute to further work involving the fouling behavior of synthetic microfiltration/ultrafiltration membranes with NC fines containing wastewater, especially to evaluate and develop NC fines separation and treatment technologies. If microfiltration/ ultrafiltration technology is selected for use at the RAAP NC lines, the data derived from this work will be useful for the selection of a membrane for application a that site.

2 General Background

2.1 Characteristics of NC

The discovery of NC is attributed to Branconnot, around the year 1832 (Albert and Weston 1917) for his creation of what he termed "xyloidines," or readily combustible products formed by treating various plant and wood fibers with nitric acid. Later, in 1845, Schönbein developed the process of nitrating cellulose fibers using a mixture of nitric and sulfuric acids (Quinchon et al. 1989). Nitration baths composed of nitric/sulfuric acid mixtures significantly improve nitration levels and form the basis for many commercial nitration processes used today. These first NC products were of little practical use owing to their extreme instability. Not until Abel and Brown determined that the instability of the compound was due to easily decomposable impurities in the final product, which could be removed by a purification process of boiling and pulping (Urbanski 1965), was the doorway opened to NC development for military and civil use.

The primary military uses for NC have been in the production of smokeless propellants (which significantly reduce the fouling of gun barrels over their predecessor, black powder), the production of multiple base propellants for missiles and rockets, and in high explosives. In addition to military use, the ability of NC to form extremely thin, high-strength films and its excellent chemical resistivity provide for a broad spectrum of civil uses for the compound. The first major civil uses were celluloid (Hyatt 1870) and in photographic films (Godwin 1898). Today, NC enjoys wide applicability in industry, most notably in lacquers and varnishes, printing inks, and membranes used to purify biological molecules (Quinchon et al. 1989).

Nitrocelluloses are broadly defined as nitrated derivatives of cellulose, a polymer of glucose linked by (1-4) glycosidic bonds. Since both the nitration level and the degree of polymerization may vary, Urbanski (1965) offers the following chemical formula for NC:

$$[C_{24}H_{40-x}O_{20-x}(ONO_2)_x]_p$$

where x, the degree of substitution, may take on values from 0 to 12, and p is a variable polymerization degree. Quinchon and Tranchant (1989) offer a less rigorous formula based on the monomer:

$$C_6H_7O_2(OH)_{3-x}(ONO_2)_x$$

molecule, varying to a maximum of 14.14 percent for the fully nitrated form (x=3). According to Quinchon and Tranchant (1989), the degree of polymerization may vary from approximately 100 to 2000 linkages per macromolecule. Figure 2 shows the chemical structures of cellulose and NC.

2.2 Physical/Chemical Properties of NC

Molecular Weight: variable to 297 amu/monomer

Density: 1.66 g/cm3 (dependent on % nitrogen)

Solubility: variable (dependent on % nitrogen)

acetone, ethyl acetate (% N > 10.0)

ether-alcohol mixtures (11.0 < % N < 12.0)

Appearance: white powder

Specific Heat: 0.48 kcal/kg/°K

Ignition Temperature: 180 °C (variable)

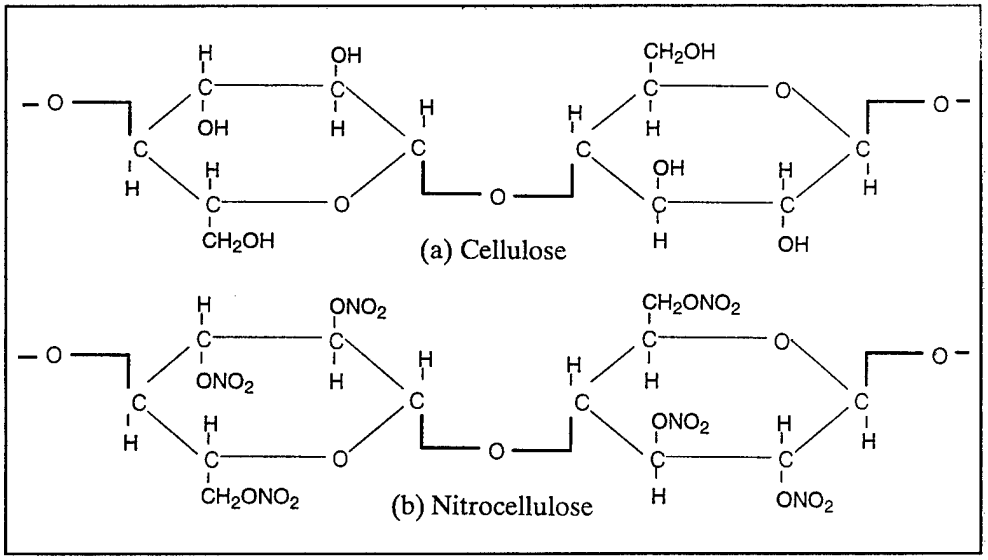

Figure 2. Chemical structures of cellulose and nitrocellulose.

2.3 NC Properties Related to Health and Safety Aspects

2.3.1 Effects of Temperature

Thermal degradation of purified NC proceeds very slowly at room temperature. However, an increase in temperature produces an exponential increase in the rate of decomposition. The self-ignition temperature varies not only with the

rate of heating, but also is dependent on the purity of the NC product; it becomes less predictable as the purity of the product decreases. As the percentage of water increases, the rate of thermal decomposition decreases, becoming virtually incombustible when the percentage of water exceeds 25 percent (Quinchon and Tranchant 1989). Precautions must be taken to ensure against the dehydration of significant quantities of the NC samples while in storage to avoid creation of a potentially hazardous situation.

2.3.2 Effects of Pressure

Ewing and Kristoff (1986) studied the combined effect of pressure and temperature on wet, unstabilized, and wet, partially stabilized NC in a confined cell. Tests were performed with both a wet slurry containing up to 10 percent NC, and packed plugs. The percent nitrogen of the samples used in the tests were typical of those most likely to detonate under test conditions. Filled cells equipped with pressure relief valves set at 45 psig and 100 psig were heated in three phases to internal temperatures of 140-160 °C.

No explosive decompositions occurred for any of the slurry samples, but two samples run with packed plugs reacted violently under the test conditions. However, on examination of the test fixture, it was determined that the damage resulted from overpressurizing the test fixture and not from a transition from decomposition to detonation (Ewing and Kristoff 1986). Although no information regarding the effect of pressure alone on NC decomposition was found, the results from these tests indicate no violent reactions resulting within the first 2-hour heating phase where pressures reached 45 psig. Since the effect of temperature greatly increases the rate of decomposition, pressures of 1-2 atm at room temperatures encountered in the Amicon stirred ultrafiltration cell should pose no excessive hazards in our experimentation.

2.3.3 Other Physical Effects

NC is sensitive in varying degrees, depending on nitration level, to shock, abrasion, and spark (Quinchon and Tranchant 1989). In the dry state, any of these effects may lead to ignition and/or detonation. However, as the percent water increases, the stability increases until at 40 percent water the NC is completely insensitive to shock or open flame (Quinchon and Tranchant 1989).

2.3.4 Chemical Reactivities

NC will react with concentrated acids or bases causing a denitration of the polymer (Quinchon and Tranchant 1989). This decomposition is capable of producing localized increases in temperature, which may in turn produce increases in the decomposition rate. Care should be exercised whenever treating NC with either acids or bases.

2.3.5 Other Chemical Effects

The combustion of NC produces NO and NO_2 gases, which are toxic and should be avoided.

2.4 Handling and Disposal of NC Wastewater

The following procedures are recommended to ensure the safe handling and storage of NC containing aqueous solutions for the duration of our experimentation. An effort has been made to address areas of anticipated problems, and as such, should not be considered to be a complete presentation of the hazards associated with all NC products or NC-containing materials.

2.4.1 Exposure to High Temperatures

NC's susceptibility to temperature-induced ignition is a function of both its nitrogen content and its purity. Although this temperature is predicted to be in excess of 160 °C, the probability of autoignition increases rapidly with temperature. The rate of decomposition of the NC also increases with temperature. Therefore, the temperature of both NC solutions and NC should be maintained at the lowest temperature conveniently possible during any portion of the experimentation and that bulk samples were stored under refrigerated conditions until needed. The temperature should not be elevated above 110 °C in any case.

2.4.2 Maintenance of Moisture Content

The most efficient method used to stabilize NC is to maintain a minimum moisture content of at least 25 percent water. Under normal temperatures and these moisture conditions, the NC is incapable of sustaining a flame front and is therefore insensitive to spark and flame. During experimentations, moisture content of the NC at a level less than 25 percent was avoided as much as possible. Whenever the experimental methods necessitate a lower moisture content, the sample size was maintained at smaller than 10 mg (0.010 g). In addition, extreme care was taken when handling and storing low moisture content samples to eliminate exposure of the sample to combustible or flammable materials. If any samples or wastes are inadvertently allowed to dry, the material should be thoroughly saturated with water before any attempt is made to handle or clean up.

2.4.3 Disposal of Wastes

High NC-containing wastes should be treated by alkaline digestion before disposal. Since permeate analysis showed little indication of NC content, all permeates were wasted directly to the sanitary sewer. Retentate containing high concentrations of NC fines was collected and allowed to settle. After a sufficient time for settling, the water layer was decanted and re-filtered for volume reduction. The final concentrated volume of NC fines was hydrolyzed using NaOH solution (Alleman et al. 1993) and wasted to the sanitary sewer.

2.5 Concentration Polarization and Fouling During Membrane Filtration

Membrane processes can be either dead-end filtration or crossflow filtration. In the case of dead-end filtration (Figure 3a), the membrane cell is initially filled

with feed water, and permeate is produced by pressurizing the cell. The cell can be stirred to improve permeate flux. This configuration is used to concentrate specific solutes in a small amount of feed water, mainly in laboratory studies of membrane fouling. Unlike dead-end filtration, in the case of crossflow configuration (Figure 3b), the pressurized feed stream continuously flows along the membrane surface, and permeate is produced due to the pressure difference between inside and outside of the membrane cell.

During the pressure-driven membrane filtration process, particles within the feed stream are convectively driven to the membrane surface and accumulate near the membrane surface since most particles are rejected by the membrane. Some particles may form a gel-layer (which is more resistant to shear stresses), some may be adsorbed to the membrane pore wall, and some may block the membrane pores. All these phenomena tend to increase the hydraulic resistance against permeate flux so the flux decreases with time and eventually reaches a certain steady-state value. The flux decline behavior is generally caused by *concentration polarization* and *fouling* phenomena. *Concentration polarization* occurs within a relatively short time, and is reversible. On the other hand, *fouling* refers to a long-term and irreversible phenomena due to deposition and adsorption of submicron-size particles and molecules to the membrane surface and membrane pores.

2.6 Factors Affecting Flux Decline During Membrane Filtration

In general, the permeate flux, J can be expressed as:

$$J = \frac{\Delta P}{\mu R_t} \qquad \text{Eq 1}$$

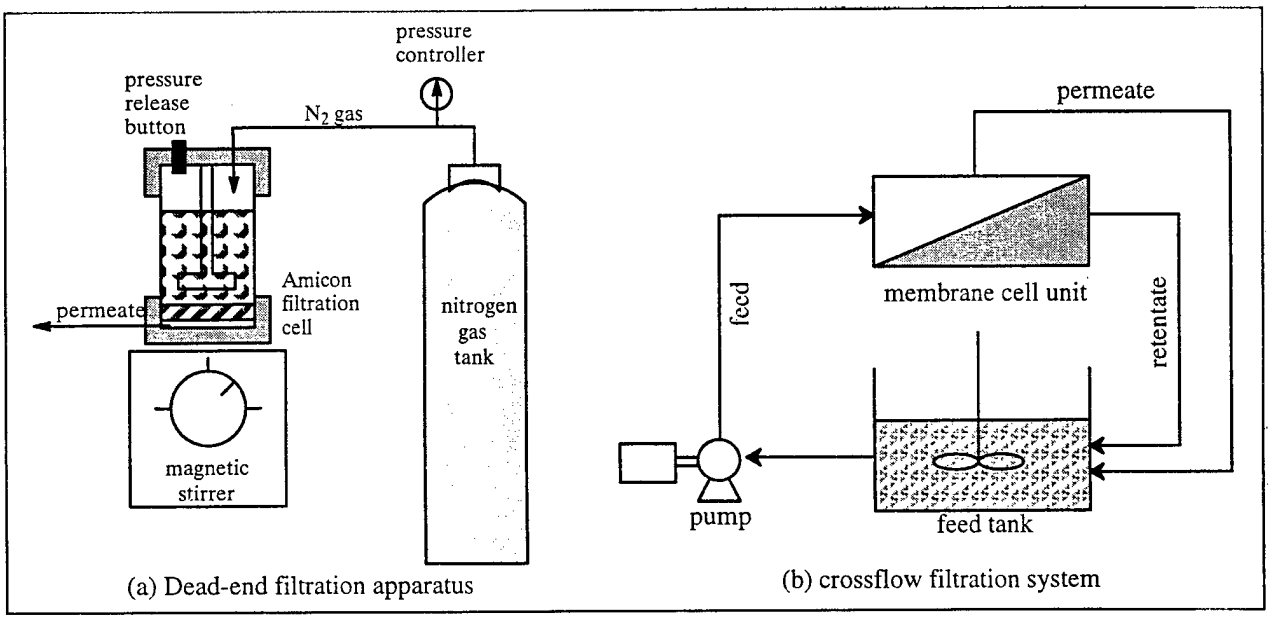

Figure 3. Dead-end filtration vs. crossflow filtration.

where ΔP=transmembrane pressure, μ=dynamic viscosity, and R_t=total resistance, which consists of many components such as the intrinsic membrane resistance (R_m), resistance due to reversible concentration polarization (R_c), and resistance due to irreversible fouling (R_i).

The permeate flux decreases with time since the degree of concentration polarization and fouling increases. Eventually, it reaches a certain steady-state value (Figure 4). The permeate flux during membrane filtration process is influenced not only by operating parameters such as transmembrane pressure, crossflow velocity (or stirring), and feed concentration, but also by physicochemical interactions between the feed solution and membrane itself.

2.6.1 Effect of Transmembrane Pressure

In the case of pure water, the permeate flux for an ideal noncompacting membrane is linearly proportional to the transmembrane pressure, since the total resistance is constant and just equal to the intrinsic membrane resistance (R_m). In case of dirty water, although the permeate flux increases initially with the transmembrane pressure (pressure controlled region), the rate of increase in permeate flux eventually declines. Finally, the flux will not increase any more even though the transmembrane pressure increases further (mass transfer controlled region) (Figure 5) because the total resistance is also increasing with ΔP (Porter 1972; Cheryan 1986). In other words, an additional increase in ΔP results in formation of more compacted concentration boundary layer or gel-layer, which makes the total resistance increase. The permeate flux at that point is referred to as the *limiting flux*, and the transmembrane pressure for the limiting flux is defined as the threshold transmembrane pressure.

2.6.2 Effect of Crossflow Velocity

A major advantage of crossflow configuration is the self-cleaning mechanism, i.e., surface washing and/or scouring. It is clear that a higher crossflow velocity results in a higher shear stress at the membrane surface, and thus reduces the concentration polarization and fouling. The back diffusion rate will be also augmented as the crossflow velocity increases.

2.6.3 Effect of Feed Concentration

As the feed concentration increases, its density and viscosity increase and its diffusivity decreases. These changes will affect the permeate flux, and higher feed concentrations usually aggravate fouling. Fane et al. (1984) conducted batch cell UF tests with silica-based particulate solutions of four different sizes, and observed that higher feed concentration caused lower permeate flux (Figure 6). There could be two possible explanations for this phenomenon. First, particle deposition rate increases with feed concentration, which results in greater cake growth rate. Secondly, back diffusion process is retarded as feed concentration increases because of lower concentration gradient.

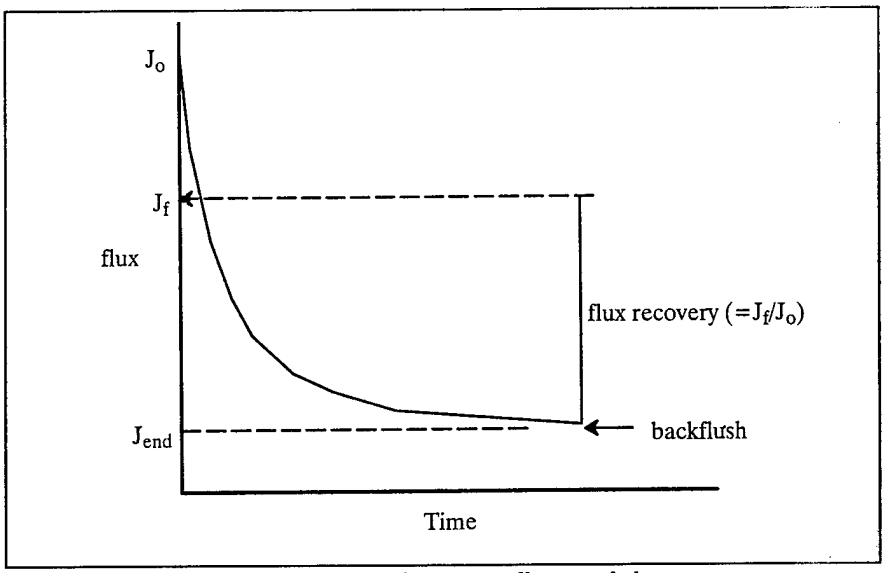

Figure 4. General relationship between flux and time.

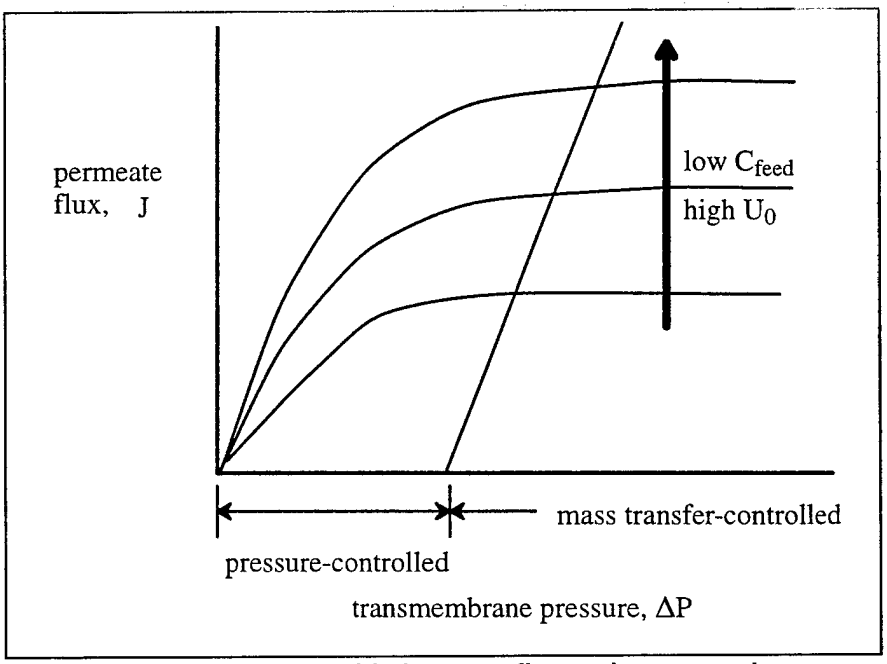

Figure 5. General relationship between flux and transmembrane pressure.

2.6.4 Physico-Chemical Factors

Since fouling results from specific interactions between the membrane and various solutes in the feed stream, it is difficult to establish general rules about the nature and extent of fouling. Each component of a feed stream will react differently with the membrane depending the type of membrane, charge characteristics of solutes, zeta potential, etc. Protein, lipids, and salts are usually known foulants during membrane filtration.

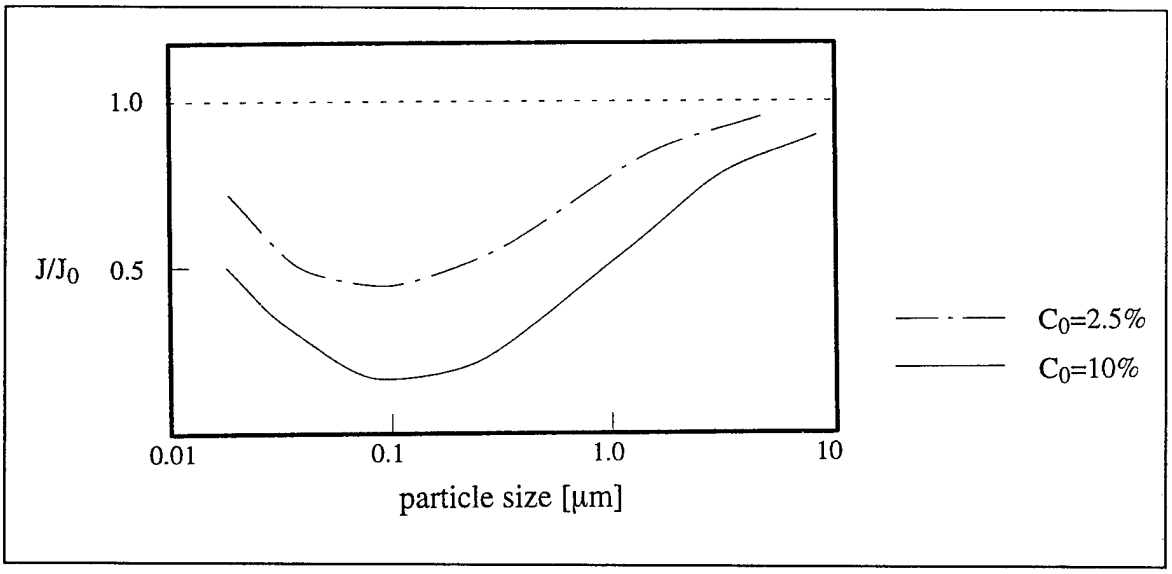

Figure 6. Effects of feed concentration and particle size (after Fane et al. 1984).

3 Materials and Experimental Methods

3.1 Phase I: Dead-End Filtration

3.1.1 Description of NC Wastewater Samples

Samples were received from the RAAP sealed in plastic-lined steel containers. On receipt, all samples were transferred to plastic containers and stored in the temperature controlled room at 5 °C. All samples were equilibrated to room temperature and remixed at a high mixing rate with a laboratory paddle stirrer before performing chemical analysis or other experimentation. Table 1 lists sampling dates and locations of the NC wastewater samples received from RAAP. Notable big differences were seen in their appearance such as color and suspended solids. The samples taken from boiling tub and centrifuge (sample #8 and #5, respectively) were crystal clear, and contained no visible NC fines. The other four samples contained lots of suspended and settleable NC fines. Especially, the NC wastewater sample taken from poacher house (sample #1) was quite different from the other three. In case of sample #1, there were large amounts of big aggregates of NC fines strongly bonded together, which could be settled within a minute. In addition, the supernatant of sample #1 appeared slightly yellow, which implied the existence of dissolved organic matter. NC fines in sample #3, #10, and #11 were difficult to settle (it took several hours), and the supernatant of these samples were crystal clear.

3.1.2 Properties of Membranes Used

Table 2 summarizes the properties of the membranes used in the experiments. A variety of membrane types, pore sizes, and base materials were tested. Figure 7 shows the characteristics of various pressure-driven membrane processes. Reverse osmosis (RO) membranes retain all components other than solvent (water) while ultrafiltration (UF) membranes retain only macromolecules or particles larger than about 0.01-0.2 μm (Cheryan 1986).

Table 1. Description of NC wastewater samples.

Sample ID	Dampling Time/Date	Sampling Location	Color
#1	9:45am, 9-23-93	Poacher decant after 1.5-hr settling	Yellow/white
#3	12:15pm, 9-23-93	Blend decant after 2.5-hr settling	Deep chalky white
#5	9:30am, 9-23-93	Centrifuge effluent	Crystal clear
#8	10:30am, 9-23-93	Boiling tub effluent	Crystal clear
#10	2:00pm, 9-23-93	Beater decant after 2-hr settling	Light chalky white
#11	10:40am, 9-28-93	Wringer effluent	Moderate chalky white

Table 2. Properties of membranes used.

ID	Membrane	Mfg.	Type	Pore size (MWCO)	Base material*	Pore structure**	Hydrophobicity/ hydrophilicity***	Clean water flux [ml/min/cm^2]	Temp/pH/ pressure limit
A1	Nova100	Filtron	UF	100K	PES	anisotropic	hydrophobic	5–14 @55psi, 25°C	50°C/1–12/55psi
A2	Omega100	Filtron	UF	100K	modified PES	anisotropic	hydrophilic	5–14 @55psi, 25°C	50°C/1–12/55psi
A3	Omega300	Filtron	UF	300K	modified PES	anisotropic	hydrophilic	5.5–20 @55psi, 25°C	50°C/1–12/55psi
A4	Omega 0.16	Filtron	MF	0.16 μm	modified PES	anisotropic	hydrophilic	16–60 @55psi, 25°C	50°C/1–12/55psi
A5	Omega 0.3	Filtron	MF	0.3 μm	modified PES	anisotropic	hydrophilic	20–60 @55psi, 25°C	50°C/1–12/55psi
B1	YM100	Amicon	UF	100K	cellulose acetate	anisotropic	hydrophilic	0.6–1.0 @10psi, 20°C	121°C/3–13/70psi
B2	XM300	Amicon	UF	300K	Acrylo nitrile vinyl chloride	anisotropic	moderately hydrophilic	0.5–1.0 @10psi, 20°C	70°C/2–10/70psi
C1	Filinert	Costar	MF	0.2 μm	PTFE	isotropic	extremely hydrophobic	15 @10psi, 20°C	130°C/NA
C2	Membra–Fil	Costar	MF	0.22 μm	mixed–esters of cellulos	isotropic	hydrophilic	15 @10psi, 20°C	120°C/NA
D1	RC02	Osmonics	MF	0.2 μm	Acrylo–co polymer	isotropic	moderately hydrophilic	20 @10psi, 20°C	100°C/1–13/100psi
D2	YC01	Osmonics	MF	0.2 μm	polypropylene	isotropic	extremely hydrophobic	20 @10psi, 20°C	100°C/1–13/100psi

* PES=polyethersulfone; PTFE=polytetrafluoroethylene

** A and B series membranes have thin top skin layer and more porous back support structure. C and D series have no skin and highly tortuous flow path.

*** C1 and D1 membranes are extemely hard to wet with water. These membranes should be wetted in alcohol in order to apply water, then they behave like moderately hydrophobic or hydrophilic membranes.

**** The surface of A and B series membranes are fairly smooth, but C and D membranes are rough. Especialy, C1 membrane has very rough surface.

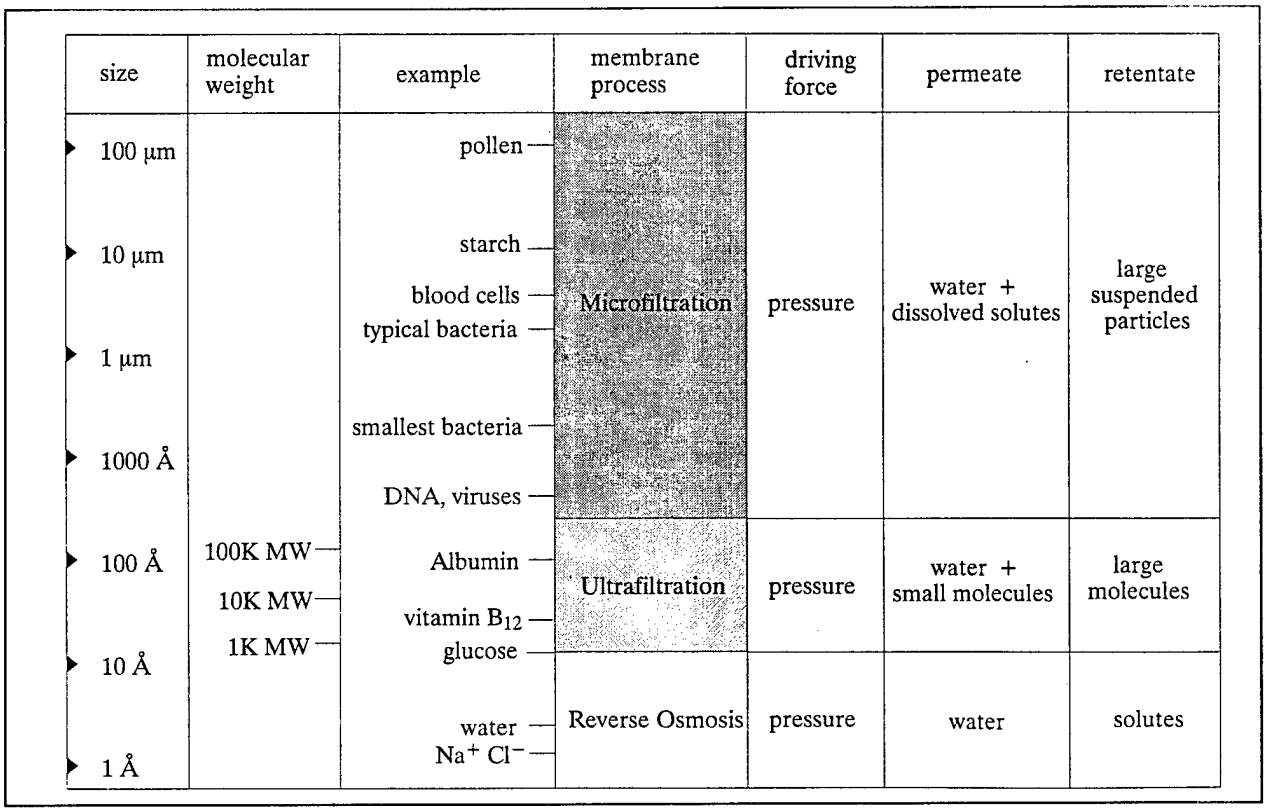

Figure 7. Characteristics of RO, UF, ad MF membrane processes (Cheryan 1986).

Microfiltration (MF) membranes are supposed to retain suspended particles in the range of 0.1 to 10 μm (Cheryan 1986). In classifying UF membranes, it is customary to use molecular weight cut-off (MWCO) instead of pore size. The range of membrane pore sizes examined in this study was from 100K MWCO (corresponding to about 0.01 mm) to 0.3 mm.

Membranes can also be classified as either isotropic (microporous) or anisotropic (asymmetric) based on their ultrastructures. In general, UF membranes have a thin skin on the face of the membrane with an extremely porous supporting body (asymmetric structure) whereas MF membranes have isotropic microporous structure. Note that Omega series MF membranes manufactured by Filtron have also asymmetric structure. The asymmetric membranes rarely get plugged the way that microporous membranes do although they are also susceptible to flux decline phenomena like concentration polarization and fouling (Cheryan 1986).

Hydrophilicity is another important factor affecting the flux performance. (Hydrophilicity depends on the membrane base materials.) Besides those factors mentioned above, pore density/porosity, pore tortuousness, and surface roughness also affects flux decline behavior. In general, the membranes having a thin skin structure have a relatively smooth surface in comparison to microporous or isotropic membranes—Filinert and RC02 MF membranes have

an especially rough surface. The MF membranes manufactured by Costar have about 10^8 pores per cm^2, and their porosity is 70 to 75 percent.

3.1.3 Flux and Static Adsorption Tests

All membranes were conditioned before use by presoaking for 4 hours in Milli-Q water. The Milli-Q water was changed and membranes rinsed with Milli-Q water every 30 minutes, up to 2 hours, after which no additional water exchanges were made. Additionally, each membrane was flushed in the Amicon stirred dead-end filtration cell with approximately 450 ml of Milli-Q water at 25 psi before initial clean water flux tests. The YC01 (Osmonics) and the Filinert (Costar) MF membranes were wetted with 100 percent ethanol before applying water as prescribed by the manufacturers. After the membranes were conditioned, three flux tests of 120 ml each were performed with Milli-Q water to establish the clean water flux of the membrane.

All flux tests were performed using an Amicon model 8200 stirred dead-end filtration cell. During the flux tests, compressed nitrogen gas was used to pressurize the filtration cell (Figure 8). Samples were stirred throughout the flux tests (except during the unstirred flux testing) using the Amicon model MT2 magnetic stir table. Flux tests for membranes were conducted in 1-stage (short-term), 3-stage and 6-stage (long-term), with total permeation of 120, 300, and 600 ml, respectively (Figure 9). Flux readings were taken until the desired amount of permeate was collected, at which time the pressure on the cell was released and permeate flow was stopped. The cell was then carefully refilled so as not to disturb the formation of any compacting layer above the membrane surface.

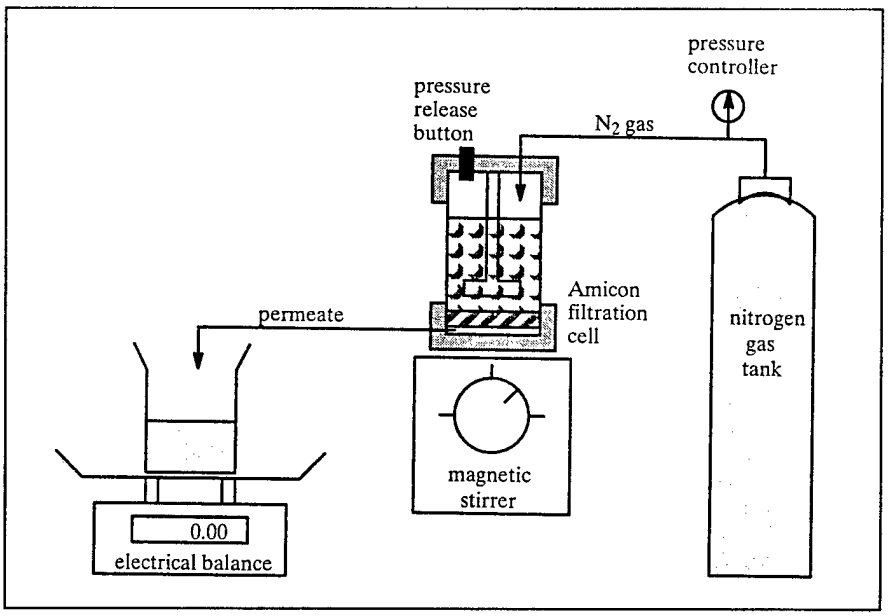

Figure 8. Amicon filtrtion apparatus.

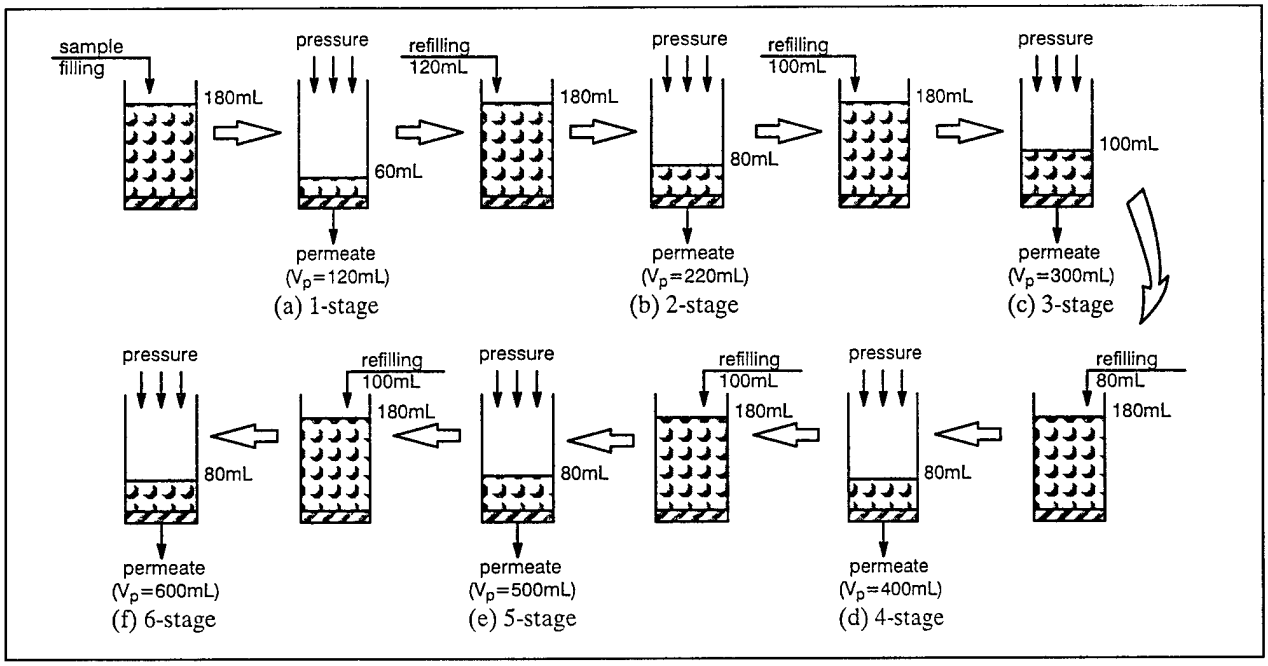

Figure 9. Multi-stage flux tests.

After refilling, the cell was repressurized, and the next stage of the flux test was conducted. Permeate mass was measured with a Johnson Prescisa electronic balance. The temperature effects were neglected in calculating flux. Since all flux tests were performed in the range of 21 to 23 °C, there is less than 0.4 percent error due to the density/viscosity difference.

At the end of the flux tests, the cell was carefully disassembled and any cake layer formation noted. Compactness, uniformity of coverage and color of the cake layer were all qualitatively assessed, as well as the cake layer's attachment to the membrane surface. After observation, the surface layer was removed by flushing with a water spray. This method was used after determining that even the most tightly attached layer encountered was removed by backflushing the membrane at 10 psi with Milli-Q water, except in areas where the membrane was supported so the permeation was restricted. After removing the surface layer, the membrane was again visually inspected, and any remaining color change was noted. Membranes were then backflushed with 120 ml of Milli-Q water at 10 psi. Following the backflush procedure, a clean water flux trial was performed to determine flux loss. This loss was considered irreversible fouling.

For the static adsorption tests, virgin membranes were conditioned according to the above procedure, and a volume (180 ml) of well-mixed NC wastewater sample was placed in the Amicon stirred cell assembled with the membrane. During the exposure, the outlet of the cell was maintained at a level above the liquid level in the cell to prevent any flow from transporting NC particles by convection while permeating the membrane. All samples were stirred continually during the exposure to the membrane. After the exposure period,

the wastewater sample was poured from the cell, and the cell was rinsed twice with Milli-Q water to remove any traces of NC particles remaining on the cell walls and on the membrane surface. A flux test was then performed using 120 ml of Milli-Q water to determine flux loss due to adsorption. After the flux test, the well-mixed sample of the wastewater was again added to the cell and the cell returned to the stir table for additional exposure.

3.1.4 PAC Adsorption Isotherm and Batch Kinetic Tests (Adham 1993)

The bottle point technique was used to measure the adsorption isotherm, using powdered activated carbon (PAC) as the adsorbent, and NC wastewater as the adsorbate. Constant volumes of NC wastewater were placed in acid-washed glass bottles, which contained different masses of PAC. One bottle was kept without any PAC to serve as a blank. The bottles were covered with Teflon-lined silicon septa, and sealed with aluminum crimp caps (Wheaton, Milleville, NJ). Then, the bottles were vigorously agitated on a laboratory shaker for 4 days. After equilibrium, the samples were withdrawn using a gas-tight glass syringe (Hamilton Co., Reno, NV), and filtered through 0.22 μm nylon membrane filters (Magna, Wesborough, MA). The filtrates was analyzed for UV absorbance and total organic carbon (TOC).

The batch kinetic test was conducted to investigate the rate of adsorption. One liter of NC wastewater was placed in a 2-L beaker, and vigorously mixed with a magnetic stirrer. Before the PAC was added, a 5 mL sample was withdrawn with a gas-tight glass syringe (Hamilton Co., Reno, NV) to obtain the initial TOC concentration. Then, a specific amount of PAC was added to the reactor. The vigorous mixing was maintained throughout the test. After PAC addition, 5 mL samples were taken from the reactor with the glass syringe at regular time intervals, and filtered immediately with 0.22 μm nylon membrane filters (Magna, Wesborough, MA) for TOC analyses.

3.1.5 Analysis Techniques and Instruments

Turbidity tests were performed using a turbidimeter (Model 43900, Hach Co., Ames, IA), calibrated with Gelex secondary turbidity standards (0-2, 0-20, 0-200, 0-2000 NTU). Total suspended solid (TSS) was determined by vacuum filtration of samples using tared crucibles with 0.45 μm Whatman filter paper (Standard Methods, 2540 D).

The optical quality of NC samples are determined by three successive measurements of the light absorption in a spectrometer (Quinchon and Tranchant 1989):

- at 254 nm where the optical density is related to the dissolved organic contents
- at 460 nm where the optical density is the sum of the coloration and turbidity
- at 630 nm where the optical density is only related to the turbidity.

The UV/VIS analysis was performed at 254 nm, using a Perkin Elmer Lambda 3B UV/VIS spectrophotometer (Oak Brook Instrument Division, Oak Brook, IL).

TOC was determined by the persulfate-ultraviolet oxidation method (Standard Methods, 5310 C) using a TOC analyzer (Dohrmann model DC-80, Xertex Corp., Santa Clara, CA) calibrated with the 10 ppm KHP standard solution. Before TOC measurements, all samples were acidified by adding 3 drops of concentrated phosphoric acid per 10-20 ml sample. Following acidification, the samples were purged for 3 minutes to remove inorganic and purgeable organic carbon.

Alkalinity tests were done using the volumetric titration method (Standard Methods, 2320 B). Hardness tests were performed by the EDTA titration method (Standard Methods, 2340 C). All pH measurements were taken using an Orion model 520A temperature compensated pH meter.

Particle size analysis was performed, using a microscope and image analysis system (Figure 10). A drop of NC wastewater sample was placed on a microscope slide using a transferring pipette. The image of NC particles was transferred from the optical microscope to the high resolution color video monitor (Model PVM-1943MD, Sony Inc., Japan) through the video camera (Model JE3462HR, Javelin Elec., Japan). After acquiring and freezing the image by an image analysis software called OPTIMAS (Bioscan Inc., Edmonds, WA), the threshold was adjusted such that particles concerned should be accounted for particle size measurements.

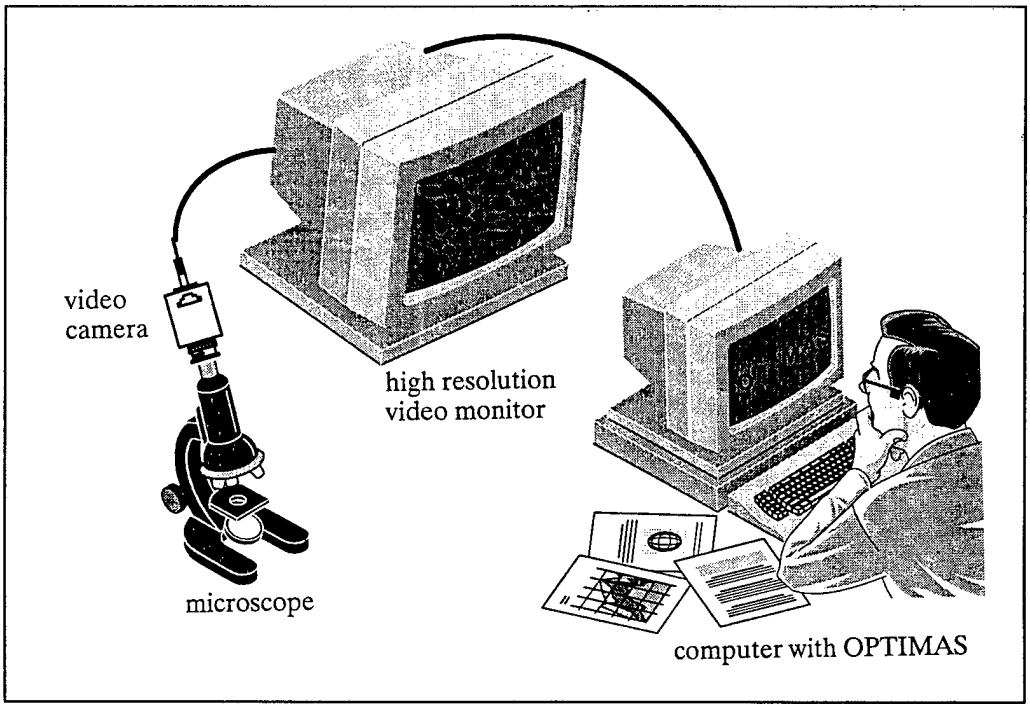

Figure 10. Image analysis system.

Then, the projected area of each particle was measured and exported into a spreadsheet (Excel) by the OPTIMAS calibrated with the S8-stage microscope slide with 1 mm/0.01 division (Graticules Ltd., England). The effective particle sizes were calculated from the measure areas.

3.2 Phase II: Crossflow Filtration

3.2.1 Description of NC Wastewater Samples

NC wastewater was sampled at each manufacturing process including beater, poacher, blender, and wringer houses. Samples were delivered from the Radford plant sealed in 5-gal, plastic-lined steel containers. At each sampling location except the wringer house, an RAAP employee sampled the NC wastewater at the initial, mid, and ending stages of decanting process. Since there was little variance in turbidity, UV absorbance and total suspended solid contents among these three samples, it was decided to mix these three samples to make a representative sample for each NC wastewater stream. In the case of wringer decants, NC wastewater was sampled when the wringer basket was empty and full with NC fines. (There was a big discrepancy in visual turbidities between the empty and full basket samples.) The storage and remixing requirements were the same as those described in Section 3.1.1.

Table 3 lists sampling dates and locations of the NC wastewater samples. The color of NC wastewater samples was milky white, but the degree of transparency was quite different. The samples taken from the beater and wringer (empty basket) were relatively clear, and NC fines of these samples were very hard to settle—it took more than 6 hours to settle down NC fines after mixing. The poacher house samples contained lots of suspended and easily settleable NC fines.

3.2.2 Properties of Membranes Used

Based on the flux test results of the Phase I study, two kinds of membranes (Filtron's Omega 300K UF and Costar's Membra-Fil 0.22 μm MF membranes) were selected as candidates for NC wastewater treatment. Both membranes are hydrophilic, and showed good flux performance and low irreversible fouling.

Table 3. Description of NC wastewater samples.

Sample ID	Sampling Time/Date	Sampling Location	Visual Description
#1-1	9:45am, 10-22-94	Beater decant mixture	Low turbidity
#2-1	10:30am, 10-23-94	Poacher decant mixture after 1hr boiling	High turbidity
#2-2	11:45am, 10-23-94	Poacher decant mixture after 2hr boiling	High turbidity
#2-3	4:30pm, 10-23-94	Poacher decant mixture after 4hr boiling	Very highly turbidity
#3-1	10:30am, 10-24-94	Blender decant mixture	Low turbidity
#4-1	10:00am, 11-28-94	Wringer decant (empty basket)	High turbidity
#4-1	11:40am, 11-28-94	Wringer decant (full basket)	Low turbidity

Although the manufacturer (Filtron Inc.) insists that the Omega 300K is hydrophilic, its base material (polyethersulfone) itself is hydrophobic so it was replaced it with the Millipore 100K UF membrane, the base material of which is cellulose acetate. (Unfortunately, the Millipore did not sell hydrophilic 300K UF membrane sheets at the time of this study.) For comparison, one hydrophobic 300K UF membrane was added. The properties of these membranes are summarized in Table 4.

3.2.3 Channel-Type Crossflow UF/MF Membrane System

Figure 11 shows a schematic diagram of the pilot scale membrane filtration system. A 12-L glass jar served as a feed tank, and a big magnetic stirrer was used for mixing the feed tank. A Masterflex peristaltic pump (Model H-07017-00, Cole-Palmer Instruments Co., Chicago, IL) was used to drive the feed water to the membrane cell. The pump was driven by an adjustable speed gearmotor (Model Type 42DSBEPM-E1, Bodine Electric Company, Chicago, IL) and a permanent magnet control with analog interface board (Model Type FPM 856, Bodine Electric Company, Chicago, IL). A computer was used to acquire analog signals from all gauges and to control the pumping speed.

Two pulsation dampeners (Model H-07596-20, Cole-Palmer Instruments Co., Chicago, IL) were installed serially close to the pump to reduce the large pulsations created by the peristaltic pump. Then, almost pulsation-free feed was provided to the channel-type crossflow UF/MF membrane filtration unit (Model SEPA CF System B, Osmonics Inc., Minnetonka, MN) (Figure 12). A feed spacer is placed on the bottom half of the membrane cell body, and a rectangular membrane sheet is placed on the top of the feed spacer. The top half of the membrane cell fits over the guideposts of the bottom half. Then the cell body is inserted into the cell holder. The pressure provided by a nitrogen gas tank is applied through a fitting on the top of the cell holder. This pressure causes the piston to move downward and compress the cell body. Double O-rings in the cell body prevent any leakage.

Table 4. Properties of membranes used.

Membrane ID	MF 0.22	UF100K	UF300K
Manufacturer	Costar	Millipore	Millipore
Membrane name	Membra-Fil	NA	NA
Membrane type	MF	UF	UF
Pore size	0.22 mm	100K MWCO	300K MWCO
Base material	mixed-esters of cellulose	cellulose acetate	polysulfone
Pore structure	isotropic	anisotropic	anisotropic
Hydropilicity	hydrophilic	hydrophilic	hydrophobic
Clean water flux [L/m^2/hr]	9000@10psi,20°C	360-600@10psi,20°C	1500-2400@10psi,20°C
Temp/pH/pressure limit	130°C/NA	100°C/4-11/55psi	100°C/4-11/55psi

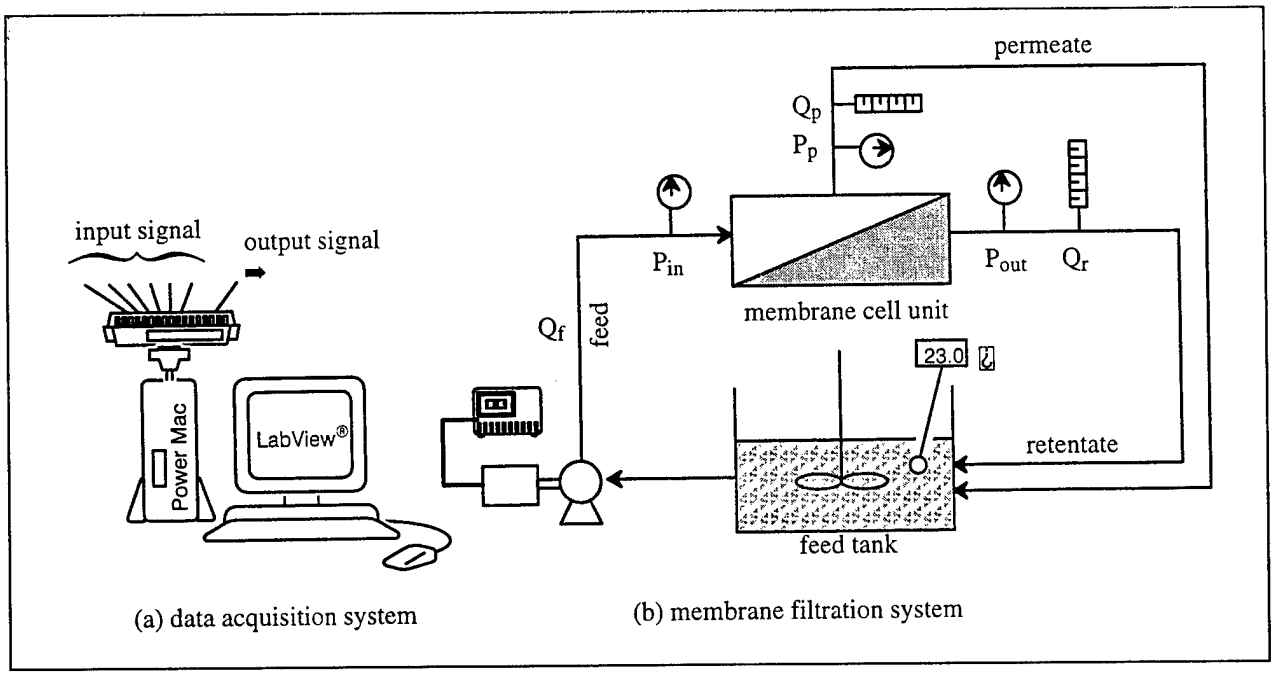

Figure 11. Channel-type crossflow UF/MF membrane pilot system.

A special feed spacer made with silicon rubber, which has a long rectangular channel (3.9 cm wide, 13.8 cm long, and 0.16 cm high), was used to induce the laminar flow conditions in the feed stream. The feed stream supplied by the pump only flows through this channel, so the effective membrane surface area is 53.8 cm^2 and the cross-sectional area is 0.62 cm^2. The permeate passing through the membrane sheet flows through the permeate carrier on the top half of the membrane cell, is collected in a manifold, and flows out through the permeate outlet.

All measurement instruments in the system shown in Figure 13 generate analog signals, which could be logged onto a computer. Inlet, outlet, and permeate pressures were measured by digital pressure transmitters (Model PG-4/20, PSI-Tronix, Tulare, CA) which supply a 4-20 mA current output signal proportional to the actual pressure. A 499-ohm resistor with 1 percent accuracy was connected across the current output, resulting in a 2 to 10 volt output that could logged onto a computer. Permeate and retentate flowrate were measured by 150 μm variable area flowmeters (Model H-03229-31 and H-03229-35, respectively, Cole-Palmer Instruments Co., Chicago, IL) equipped with flowmeter electronic conversion modules (Model H-03298 00, Cole-Palmer Instruments Co., Chicago, IL) which also provided a 4-20 mA current output signal proportional to the float position. A 499 ohm resistor was also used to convert the current to a voltage signal. Temperature was measured by a customarized RTD probe with a 3/8-in. NPT hex fitting (Model DD93560-02, Cole-Palmer Instruments Co., Chicago, IL), which was inserted to the permeate tube line.

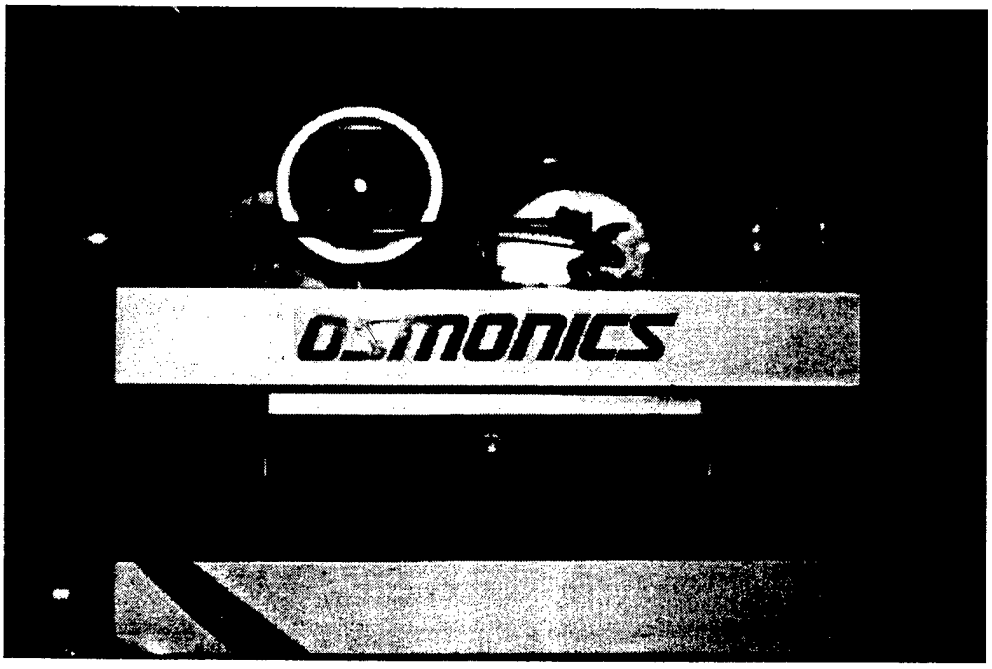

(a) Cell holder

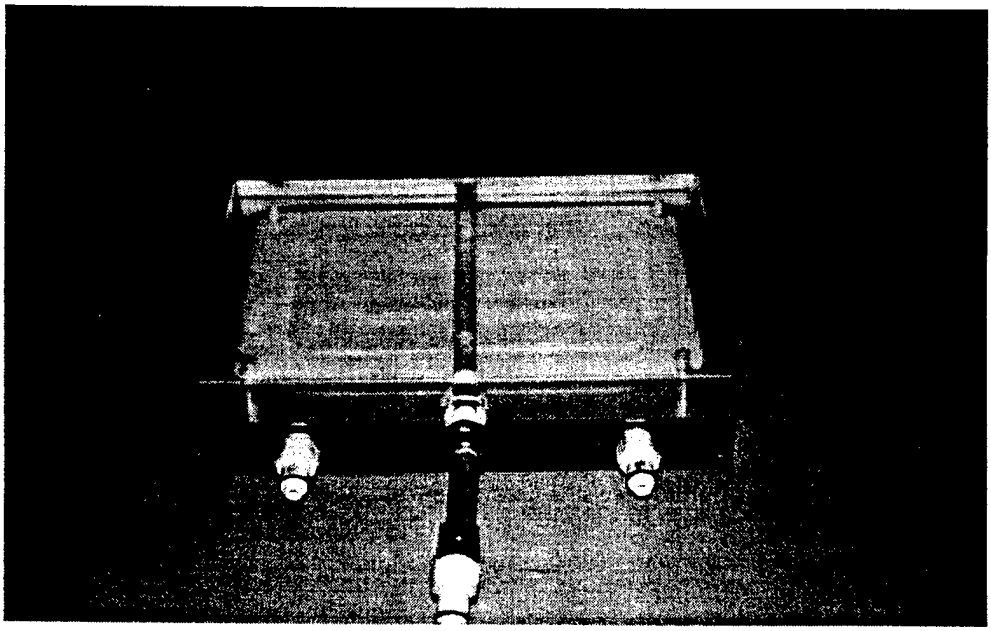

(b) Membrane Cell

Figure 12. Osmonics SEPA CF membrane cell unit.

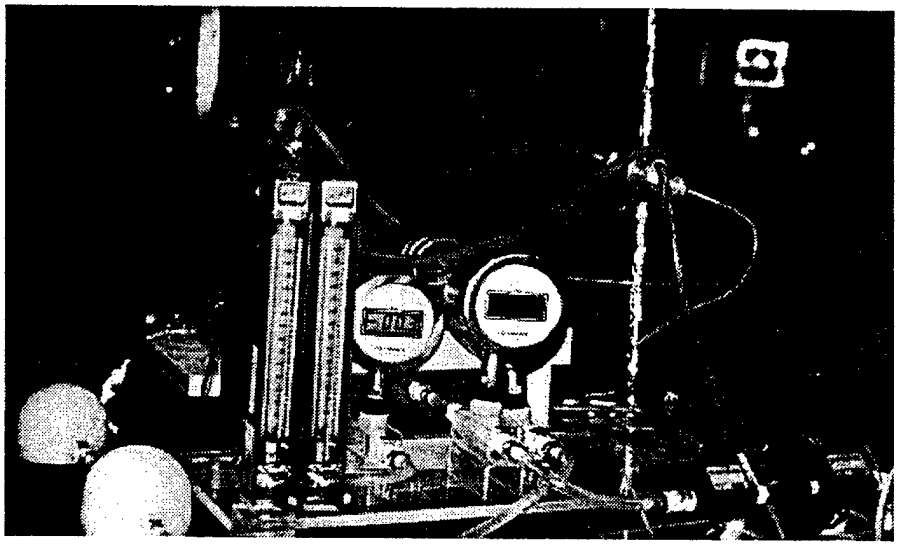

(a) Front view

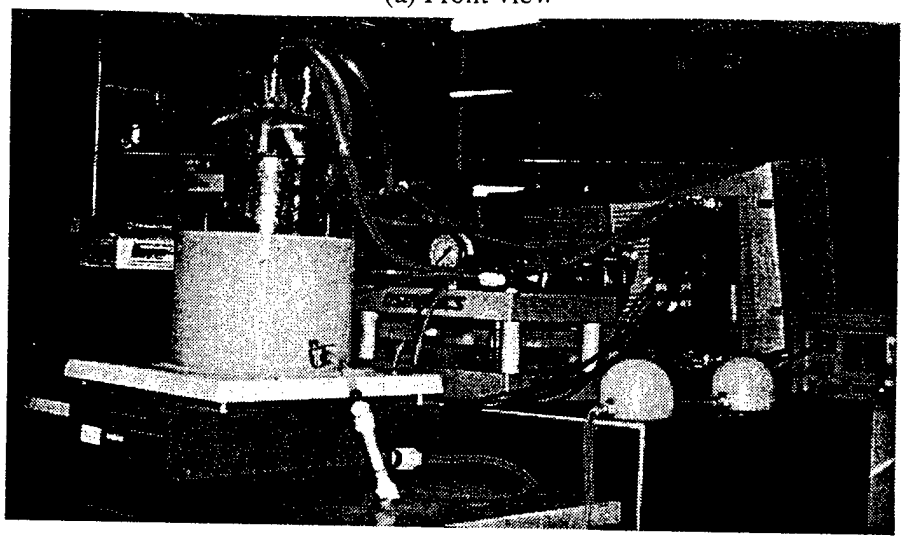

(b) Rear view

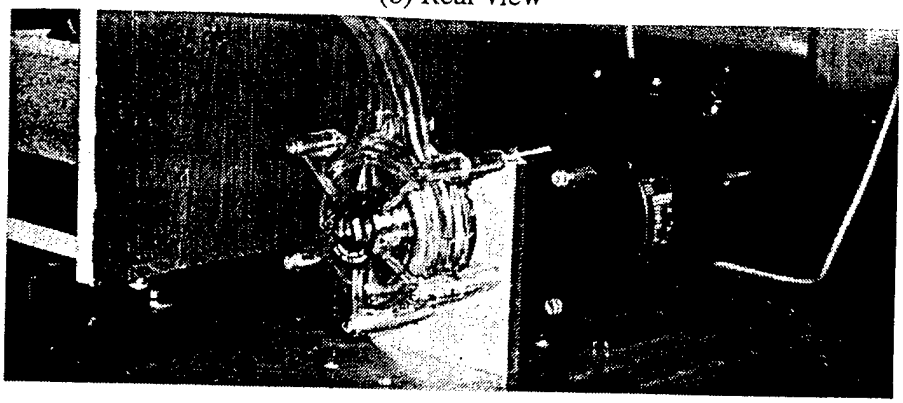

(c) Pump and mortor

Figure 13. Crossflow UF/MF membrane pilot system.

The temperature probe was connected to a RTD indicator-transmitter (Model H-08099-00, Cole-Palmer Instruments Co., Chicago, IL), which supplies a 4 to 20 mA current signal proportional to the actual temperature. Figure 14 shows the specifications and calibration results of each sensors.

The analog signals (voltage) from all measurement devices were continuously logged onto a computer (Macintosh Quadra650) through a multifunction I/O board (Model NB-MIO-16L-9, National Instruments Corp., Austin, TX), which converts the analog signals to digital signals that could be read by the computer. A general-purpose programming system called LabVIEW (National Instruments Corp., Austin, TX) was used for system control and data acquisition. LabVIEW is a program development application much like C or BASIC, but it is much different from those application in one important respect. Other program systems use text-based languages to create lines of code, while LabVIEW uses a graphical programming language, G, to create programs in block diagram form. LabVIEW programs are called virtual instruments (VIs) because their appearance and operation imitate actual instruments. A LabVIEW program consists of a front panel and a block diagram. The front panel is the interactive user interface that simulates actual instruments, and the block diagram is the source code for the VIs.

Figures 15 and 16 show the front panel and block diagram of the LabVIEW program developed for this research. As can be seen from the front panel, the system could be run in four different control modes: constant permeate flux, constant feed flowrate, constant inlet pressure, and constant transmembrane pressure mode (the distinctive characteristics of each mode are well explained in Section 3.2.4). The system can shut off in three different stop modes: inlet pressure limit, filtration time, and permeate flux limit.

For instance, if the constant inlet pressure mode is activated and if the permeate flux limit is set at a desired value, the computer would read all measurements continuously in a specified interval until a permeate flux reaches the set value. Any deviation between the set inlet pressure and the actual inlet pressure reading greater than a tolerance (e.g., 0.1 psi) would cause the computer to either increase or decrease the voltage supply to the drive pump to keep the inlet pressure constant. An additional safety trigger was put in so that the system would shut off if the inlet pressure ever exceeded its maximum allowable value (30 psi).

3.2.4 Control Modes for Crossflow UF/MF Membrane Process

The crossflow UF/MF membrane process can be operated in either constant pressure or constant flux mode. In the former case, the system keeps the inlet pressure constant during operation and the permeate flux declines due to fouling/concentration polarization. In the latter case, the system keeps the permeate production rate constant by increasing transmembrane pressure to compensate for fouling/concentration polarization. Figure 11 shows a schematic diagram of the channel-type crossflow UF/MF membrane pilot system.

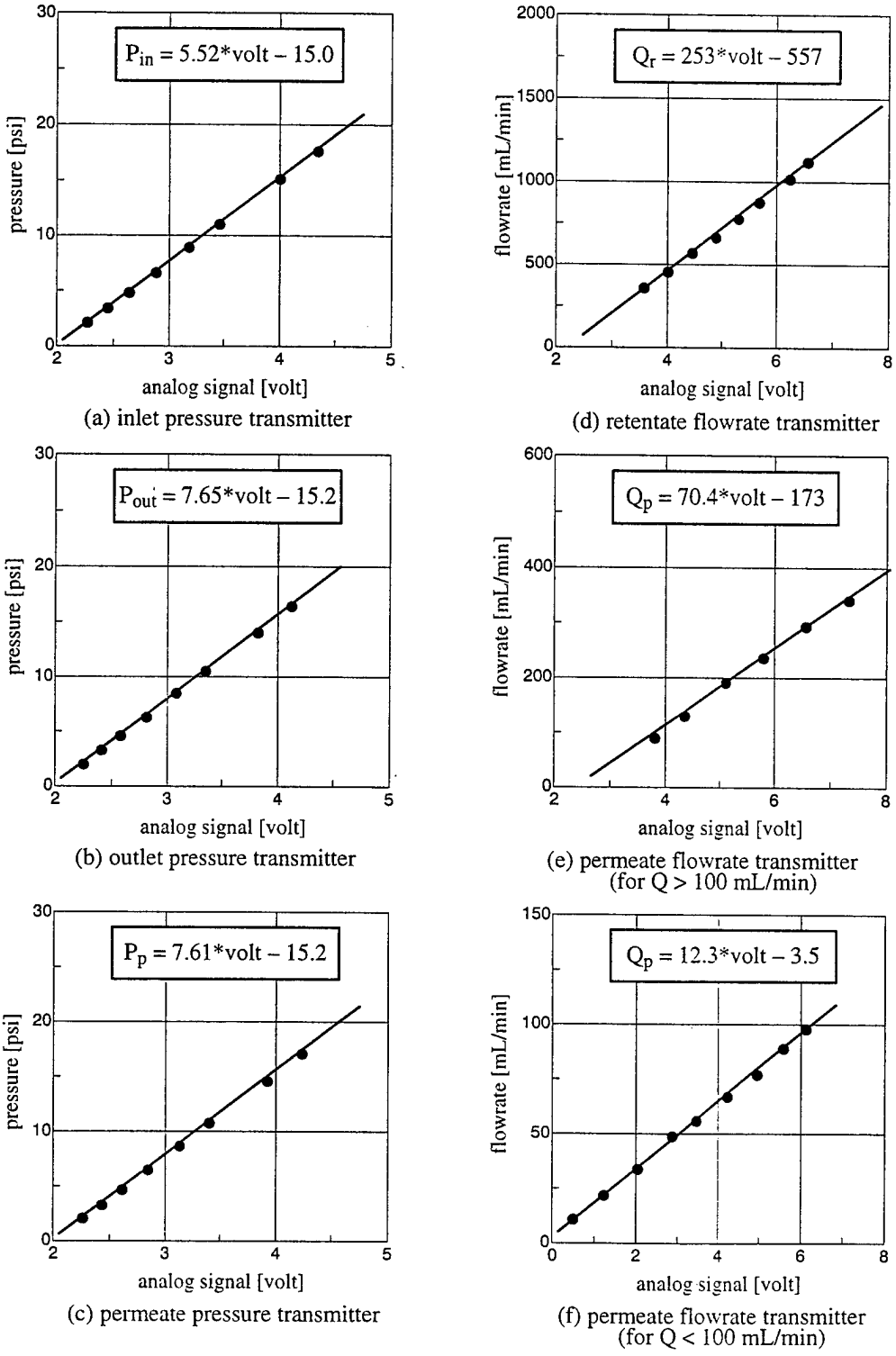

Figure 14. Calibration results for each measurement device.

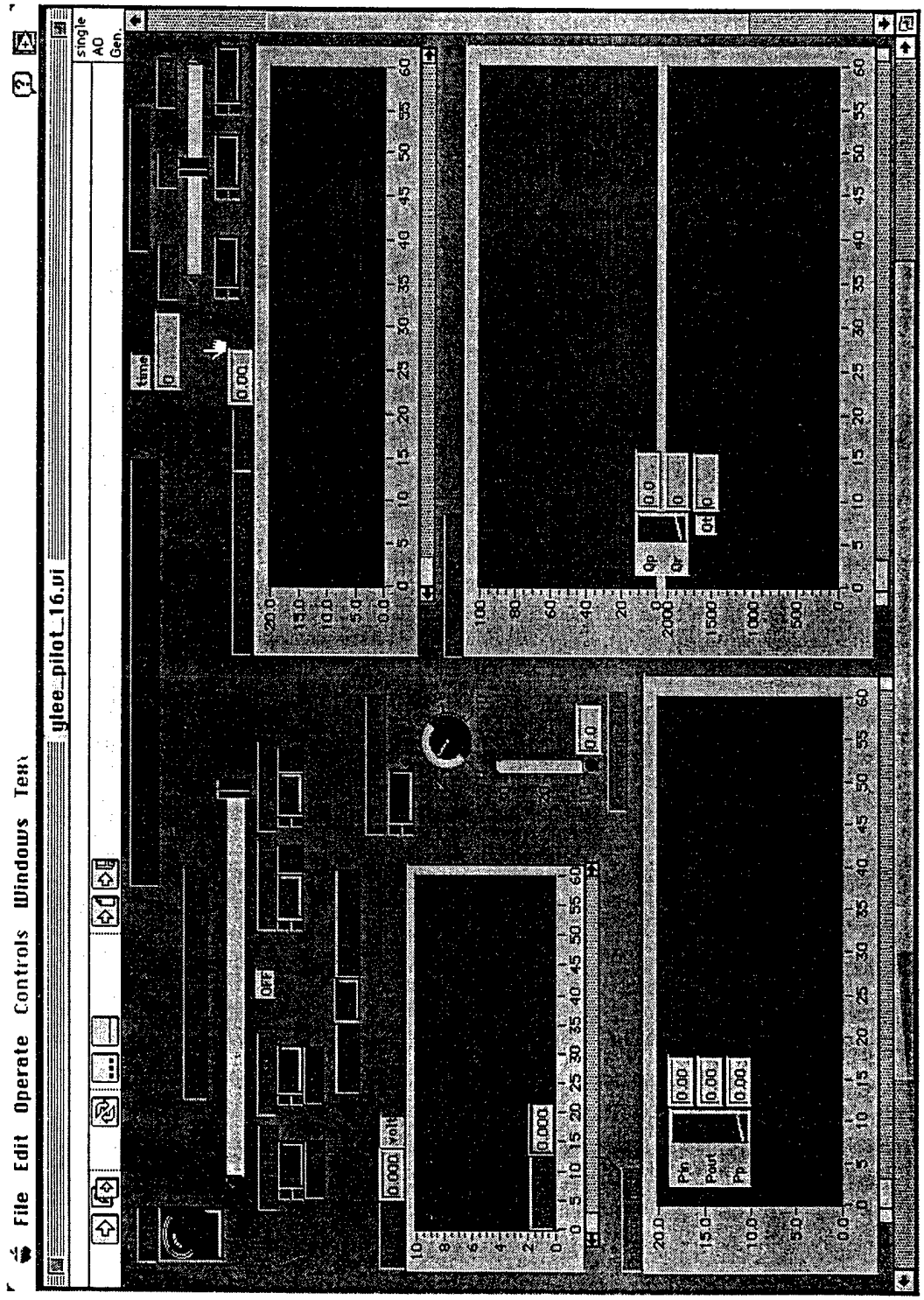

Figure 15. Front panel of LabView program for data acquisition and system control.

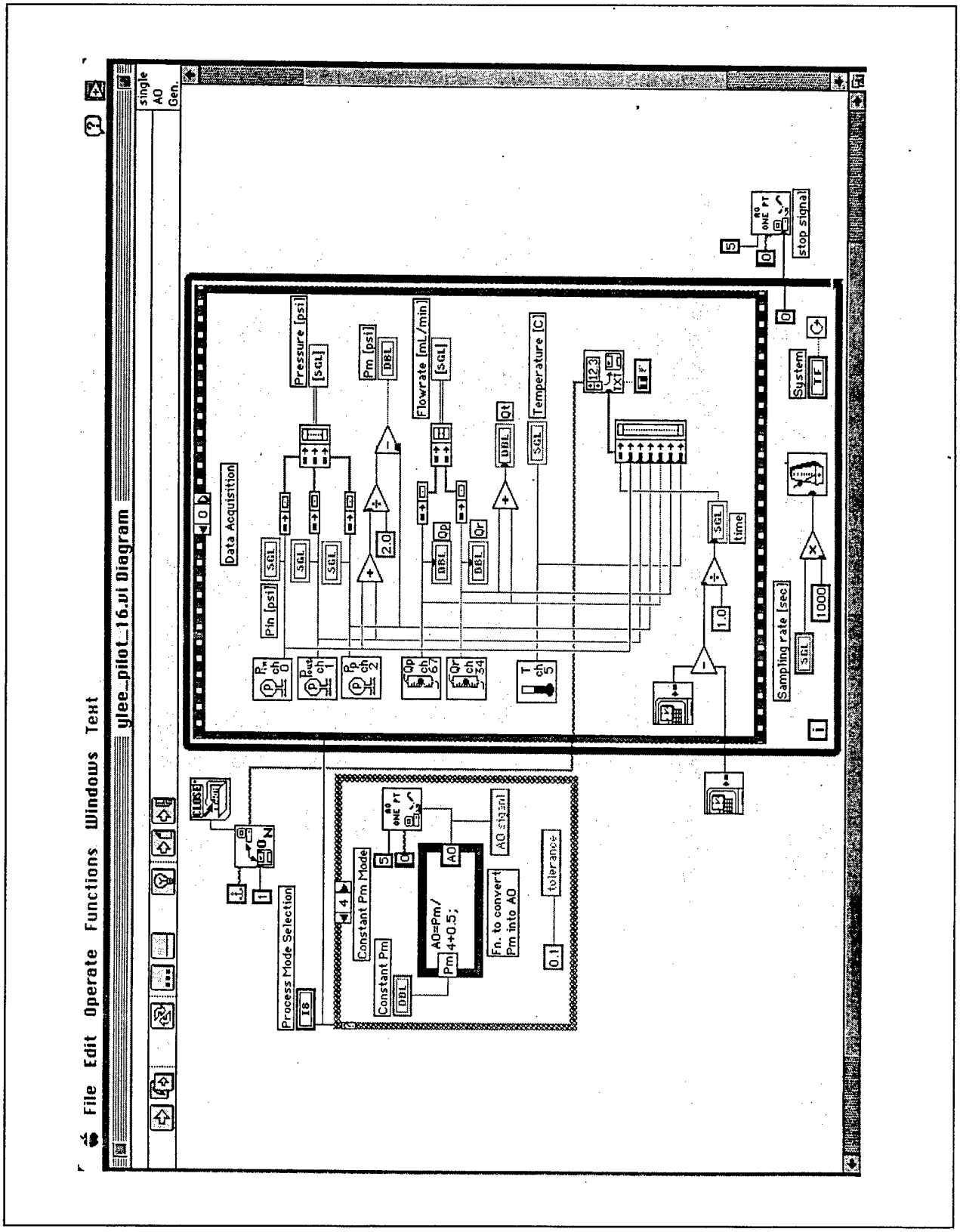

Figure 16. Block diagram of LabView program for data acquisition and system control.

All measurements are electrically monitored by the data acquisition system, and the pilot system is controlled by analog signals from the computer to an adjustable speed motor where a positive displacement pump head is attached. In addition to constant inlet pressure and constant flux modes, there can be two more possible controlling modes—constant transmembrane pressure and constant feed flowrate modes. Each of these four modes has distinctive characteristics of flow and pressure conditions, which are described in the following sections. The model simulation of each mode will be also discussed.

3.2.5 Constant Pressure Modes.

Constant Inlet Pressure Mode (Constant Pin Mode). This mode is usually referred to as "constant pressure mode"; in practice this mode is simulated by fixing a pumping speed. In fact, the inlet pressure can not be maintained as a constant by fixing a pumping speed, but would increase under these conditions. The permeate flux declines with time due to fouling/concentration polarization while the total feed flowrate generated by the pump is constant unless the pumping speed changes. So, more flow should go to the retentate side, which results in increasing the membrane cell pressures, P_{in} and P_{out}. In a true sense, the constant inlet pressure mode can be maintained by reducing the pumping speed with time in response to the flux decline. Wetterau (1992) pointed out the incorrectness of this terminology, which, unfortunately, is used extensively.

Figure 17 shows expected pressure and flowrate variations during the crossflow UF/MF membrane process in constant P_{in} mode. During this process, the permeate flowrate, Qp, decreases with time, and this makes both P_{in} and P_{out} tend to increase since more flow should pass to the retentate side. These variations in P_{in} and P_{out} are controlled by reducing the pumping speed (i.e., reducing Q_f) to compensate for the reduction in Q_p. So, in the constant P_{in} mode, Q_r as well as both P_{in} and P_{out} remain constant during the process.

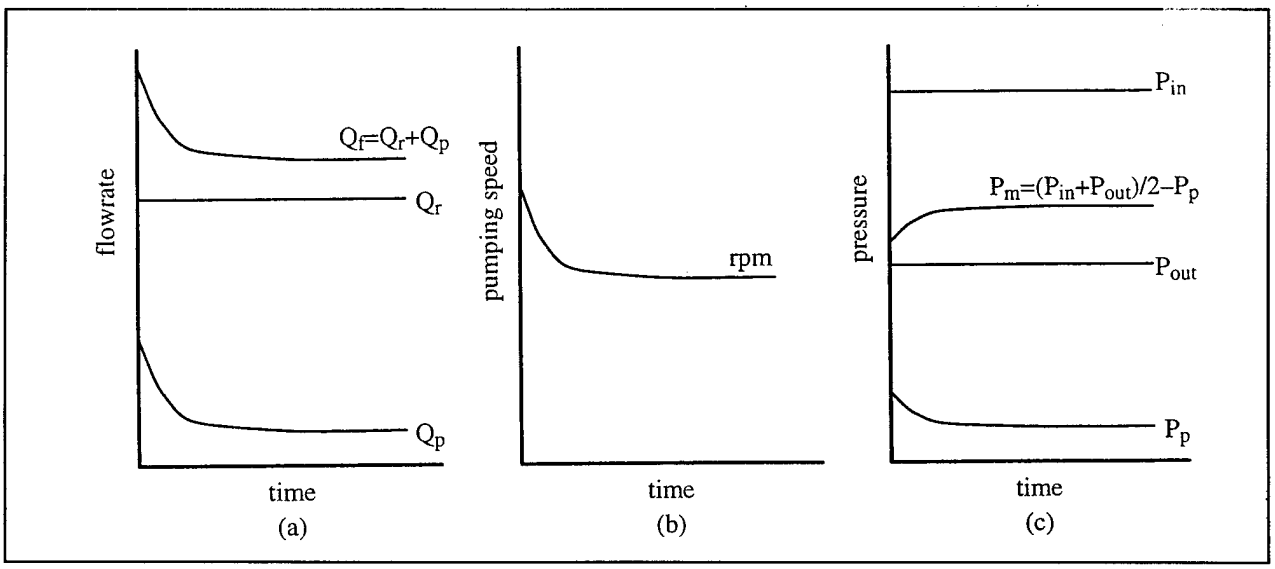

Figure 17. Variations in flow rates and pressures in constant P_{in} mode.

The next question is how to simulate this mode with a numerical model. The numerical model can predict a flux decline curve (i.e., the Q_p curve in Figure 17a) if the feed concentration and velocity field are given. Therefore, the problem is narrowed down to how to get the correct velocity field since the feed concentration is always assumed to be known. The velocity field is deterministic if the feed flowrate (Q_f) and the permeate flux profile (V_m) along the x direction are known. The feed flowrate is easily determined as follows since Q_r is always constant with time and the permeate flux at the previous time step, $Q_p(t)$, is known:

$$Q_f(t + \Delta t) = Q_r + Q_p(t) \qquad \text{Eq 2}$$

If a linear pressure profile along the x direction is assumed, the transmembrane pressure can be written as:

$$P_m(x,t + \Delta t) = (P_{in} - \frac{P_{in} - P_{out}}{L} x) - P_p(t) \qquad \text{Eq 3}$$

where L is the length of the membrane module.

The main problem is how to predict $P_p(t)$. We need a kind of pumping curve that describes the relationship between P_p and Q_p. Then, the permeate flux profile is determined as:

$$V_m(x,t + \Delta t) = \frac{P_m(x,t + \Delta t)}{\mu(R_m + R_t(x,t))} \qquad \text{Eq 4}$$

where:

m = viscosity

R_m = intrinsic membrane resistance

R_t = resistance due to fouling/concentration polarization.

If P_p is negligible (i.e., close to zero), the transmembrane pressure profile remains constant at all the time during the process.

Constant Transmembrane Pressure Mode (Constant P_m Mode). In the constant P_m mode, the average transmembrane pressure remains constant during the process by controlling the pumping speed. Figure 18 shows the expected pressure and flowrate variations during the process in the constant P_m mode. As the permeate flux declines with time, the pressure at the permeate side decreases. So, both P_{in} and P_{out} tend to arise since more flow should flow into retentate side. As a result, the transmembrane pressure tends to rise due to an increase in P_{in} and P_{out} as well as reduction in P_p. In this mode, lowering the pumping speed keeps Pm constant and makes Q_r, P_{in}, and P_{out} decrease. The feed flowrate is given by:

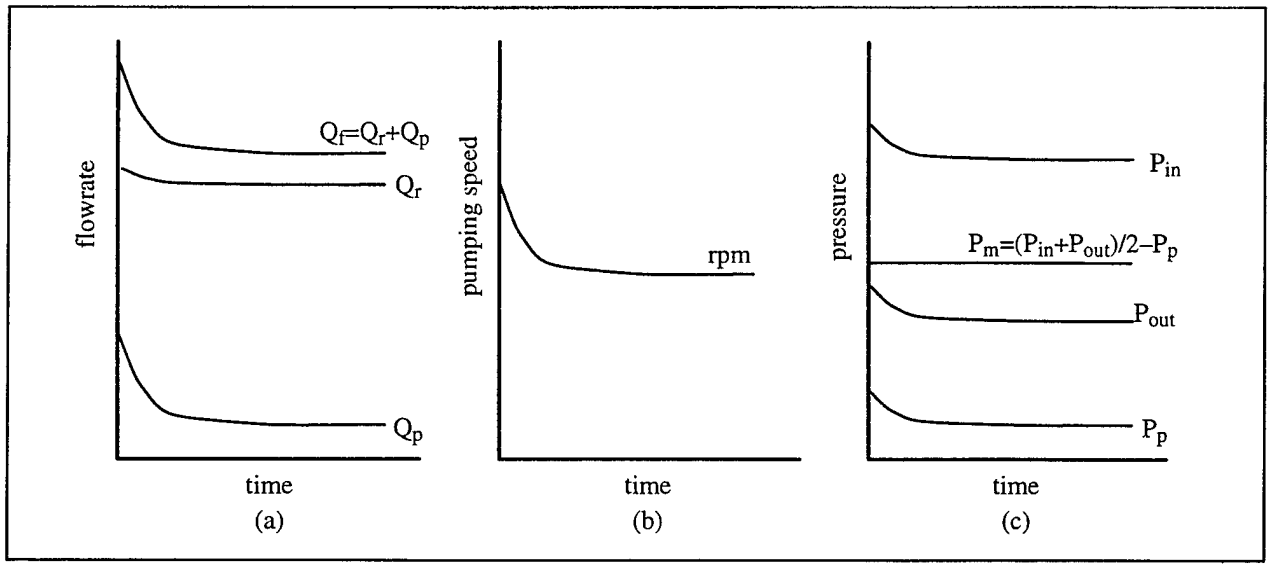

Figure 18. Variations in flowrate and pressures in consant P_m mode.

$$Q_f(t+\Delta t) = Q_r(t) + Q_p(t) \qquad \text{Eq 5}$$

where $Q_p(t)$ is known at the previous step but $Q_r(t)$ should be given as an input parameter for the proposed flux decline model. Q_r must be defined as a function of Q_p for a given P_m. Because the transmembrane pressure remains constant all the time in this mode, the permeate flux profile in axial direction is given by

$$V_m(x,t+\Delta t) = \frac{P_m}{\mu(R_m + R_t(x,t))} \qquad \text{Eq 6}$$

where: $$P_m = (P_{in} - \frac{P_{in} - P_{out}}{L} x) - P_p \qquad \text{at t=0.}$$

Constant Flowrate Modes.

Constant Permeate Flowrate Mode (Constant Q_p Mode). In constant Q_p mode, the permeate production rate remains constant during the process by increasing the transmembrane pressure to compensate for fouling/concentration polarization. Figure 19 shows the expected pressure and flowrate variations during the process in the constant Q_p mode. During the process, the membrane is subjected to fouling/concentration polarization, so the permeate flux tends to decrease.

As mentioned before, the transmembrane pressure tends to increase slightly due to both an increase in Q_r and a decrease in P_p. However, this increment in P_m is usually too small to overcome an additional hydraulic resistance due to fouling/concentration polarization. To keep Q_p constant, the pumping speed should increase to provide a necessary transmembrane pressure.

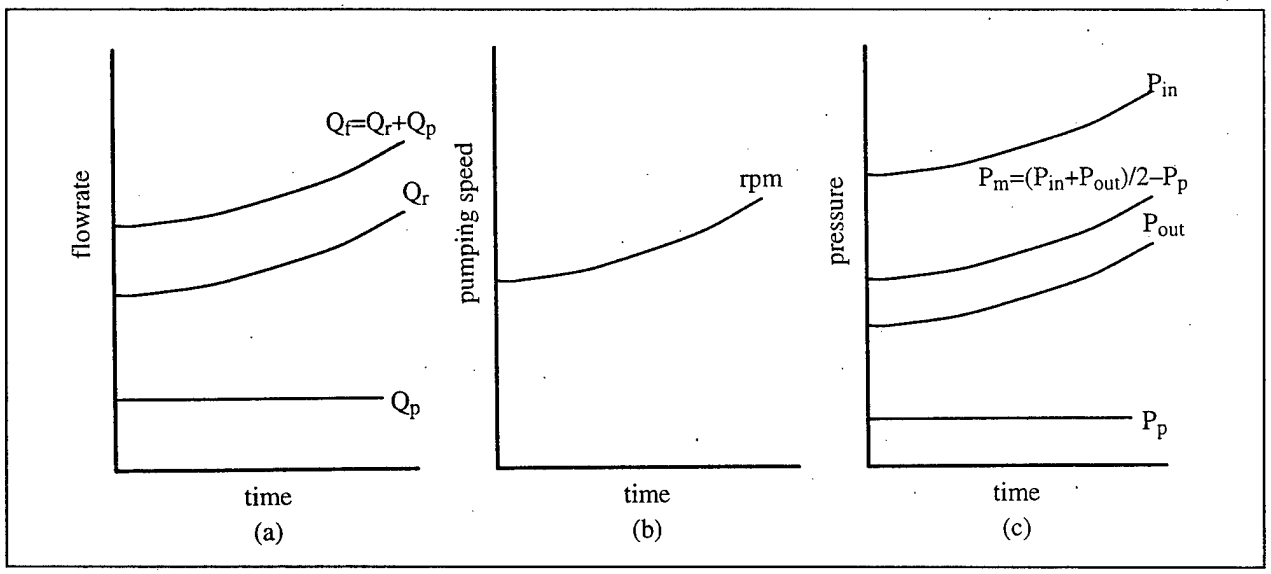

Figure 19. Variations in flow rates and pressures in constant Qp mode.

Constant Feed Flowrate Mode (Constant Q_f Mode). This is the right terminology for so-called "constant pressure mode" in practice. In constant Q_f mode, the pumping speed remains constant during the process, so the total feed flowrate flowing into the system remains constant. Figure 20 shows the expected pressure and flowrate variations during the process in the constant Q_f mode. As the permeate flux declines with time, the pressure at the permeate side decreases. So, both P_{in} and P_{out} tend to arise since more flow should flow into retentate side. As a result, the transmembrane pressure tends to rise due to an increase in P_{in} and P_{out} as well as reduction in P_p. Unlike the constant pressure modes, there is no means to control these variations. Since Q_f remains constant in this mode, Q_r should increase to compensate for an reduction in Q_p. As a result P_{in} and P_{out} increase, so P_m increases more rapidly than in the constant P_{in} mode.

Since the feed flowrate remains constant, the axial inlet velocity remains constant. Similar to the previous cases, the transmembrane pressure at any axial location is given by:

$$P_m(x,t+\Delta t) = (P_{in}(t) - \frac{P_{in}(t) - P_{out}(t)}{L} x) - P_p(t) \qquad \text{Eq 7}$$

Then, the permeate flux profile can be written as

$$V_m(x,t+\Delta t) = \frac{P_m}{\mu(R_m + R_t(x,t))} \qquad \text{Eq 8}$$

So, to explicitly define a velocity field for the proposed flux decline model, one should define P_{in}, P_{out} and P_p as a function of Q_p. Note that the transmembrane pressure does not remain constant even though P_p is negligible.

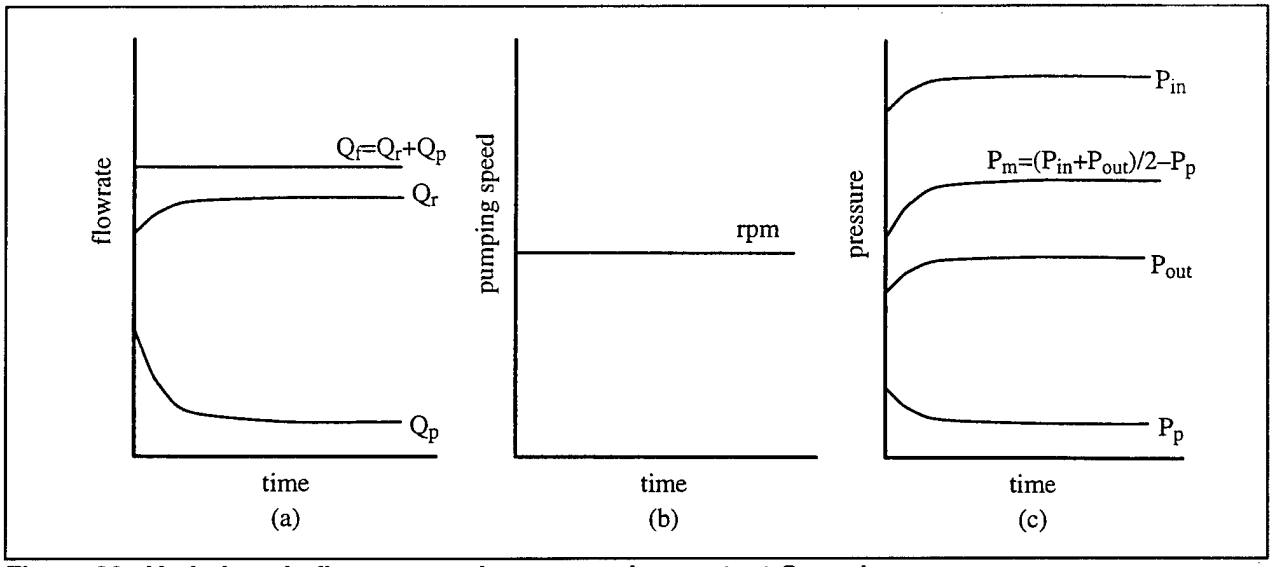

Figure 20. Variations in flowrates and pressures in constant Q_f mode.

4 Experimental Results and Discussion

4.1 Phase I: Dead-End Filtration

4.1.1 Characterization of NC Wastewater Samples

The analytical experiments were performed to characterize the NC wastewater samples described in Section 3.1.1. Raw NC wastewater samples were analyzed for hardness, alkalinity, pH, TSS, turbidity, UV absorption, and TOC, for which the analytical procedures are described in Section 3.1.5. Figure 21 shows the experimental results. Main parameters to differentiate the NC samples were TSS, turbidity, UV, and TOC.

Although there were no specific relationships between turbidity and TSS, or UV absorption and TOC, TSS and TOC tend to increase with turbidity and UV, respectively. The turbidity/TSS and UV absorption/TOC relationships may not be valid from one sample to another. In other words, one may find a specific relationship between turbidity and TSS for one specific sample (Park 1992), but the relationship cannot be valid to other samples. In any event, turbidity and UV should be a good indicator for TSS and TOC, respectively.

The NC wastewater samples are divided into the following categories based on their characteristics as determined by the results of analytical experiments and their appearance:

- *Category 1*: Samples #5 and #8, which have no visible suspended solids, and relatively low turbidity and UV absorption so the NC samples in this category were excluded from further experimentations.
- *Category 2*: Sample #1, which has relatively high values of TSS, turbidity, UV, and TOC, and of which the filtrate through 0.45 μm with yellow color is suspected to have a significant amount of dissolved organic matter. Both NC fines and dissolved organic matter were suspected to be main foulants to cause reversible and/or irreversible flux decline.
- *Category 3*: Samples #3, #11, and #10, which have medium ranges of TSS, turbidity, UV, and TOC. Since the appearance of their filtrate through 0.45 μm filter paper is crystal clear, no significant amount of dissolved organic matter were expected; NC fines will be main foulants to cause flux decline. A main difference among these samples is the magnitude of TSS.

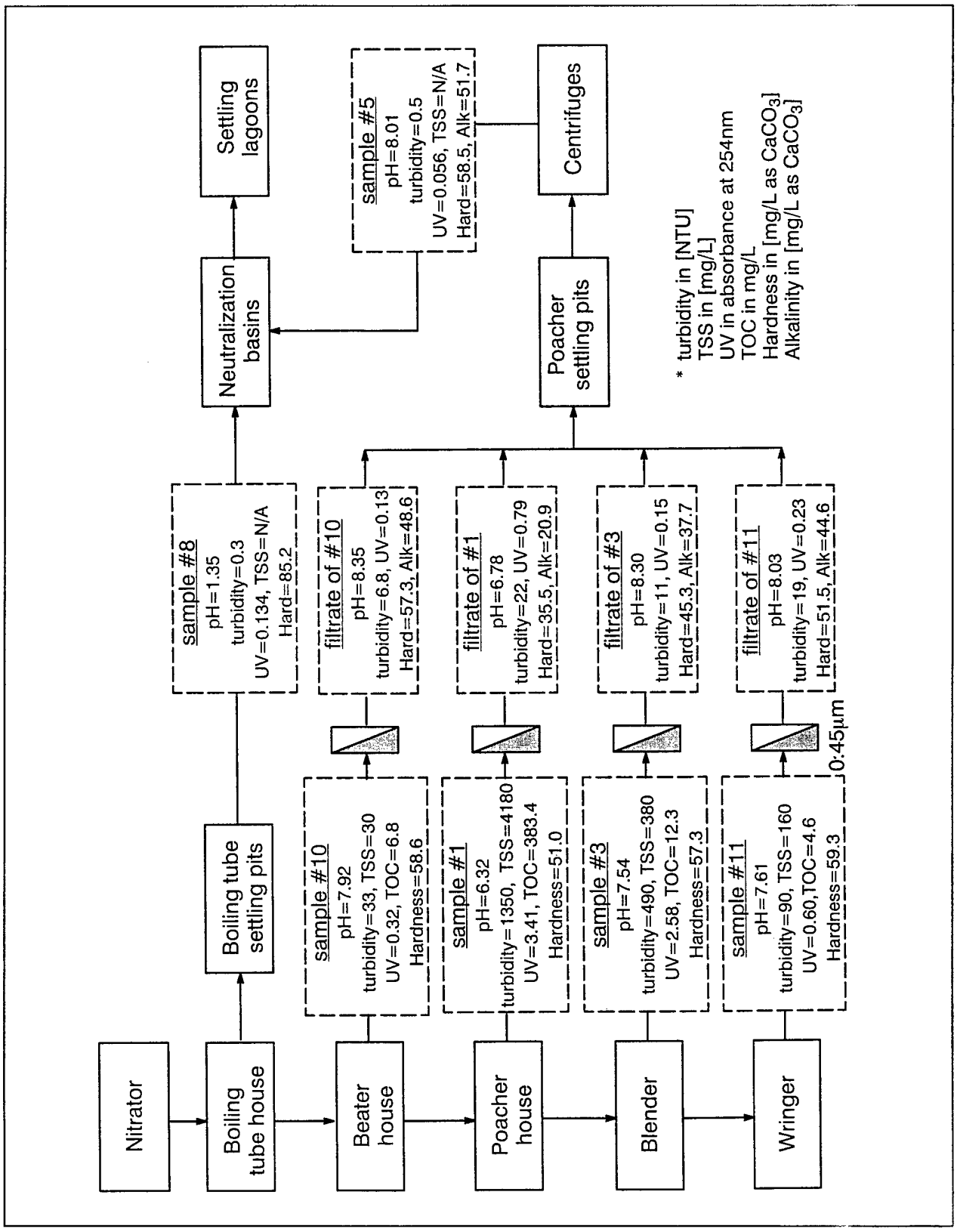

Figure 21. Characteristics of NC wastewater samples.

4.1.2 Characterization of NC Fines

The particle size distribution of NC fines is one of most critical factors in selecting membranes for filtration of NC wastewater. The pore size of membrane to be used depends on the minimum particle size of NC fines to be retained. Although NC cakes are built up during the filtration process and the cake layer acts as a secondary membrane to retain NC particles even less than the membrane pore size used, there are many adverse effects associated with selecting larger pore size membranes. The short-term advantage of higher initial flux with the larger pores will be outweighed by the long-term problems caused by higher fouling rate (Cheryan 1986).

Figure 22 schematically shows the relationship between membrane pore size and particle size. If the size of pores is similar to that of particles, some particles may lodge themselves in the pores, causing a physical blockage. In contrast, if the pores are much smaller than the particles, there is no chance for the particles to sit on the pores, but the particles are more likely to be swept by the shearing process generated by the crossflow or stirring. Many experienced workers believe the larger pores have an deleterious effect on the long-term flux decline (Merin et al. 1983; Patel 1985; Rogers et al. 1980).

The image analysis described in Section 3.1.5 was performed to obtain the particle size distribution of NC fines. Images of NC fines were taken through optical microscope and NC particle sizes were analyzed with the image analysis software, *OPTIMAS*. The level of magnification used for analyzing particle sizes was 100X, which could project about a 500 μm X 400 μm area. Under this magnification, particle sizes could be measured up to 2 μm. Increasing the magnification level makes the total number of particles per image so small that it cannot represent the particle size distribution of the sample. Similarly, lowering the magnification causes the loss of small size particles.

Because the representative sample of Category 2, sample #1, has NC fines/ aggregates that are too large—frequently greater than several hundreds micrometers in length, it was not possible to obtain images suitable for the particle size analysis (Figure 23). Based on observations with 100X to 1600X magnifications, the size range of NC fines in sample #1 is from submicrometer to several hundreds micrometer. The particle size analysis with sample #3 (Figure 24), which is the representative sample of Category 3, was successful (Table 5). Three images were taken from each sampling (trial), and the particle size data of each image were gathered and analyzed to give the particle size distribution.

The choice of class interval to present the particle size distribution is critical, and the basic requirement is that the resolution defined as the class interval divided by the mean class size should be fairly constant. If there is constant error in defining the class intervals, the effect of this error will be dependent on the particle size with an arithmetic progression being greater for small particles, whereas with a geometric progression, the effect is independent of particle size (Allen 1990).

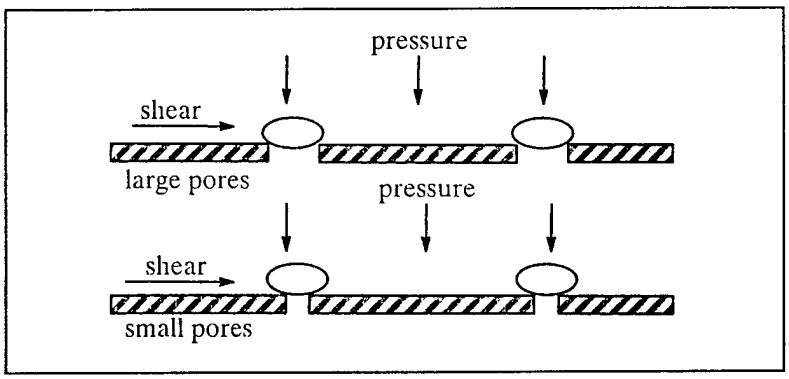

Figure 22. Effect of pore size and particle size on membrane fouling (after Cheryan 1986).

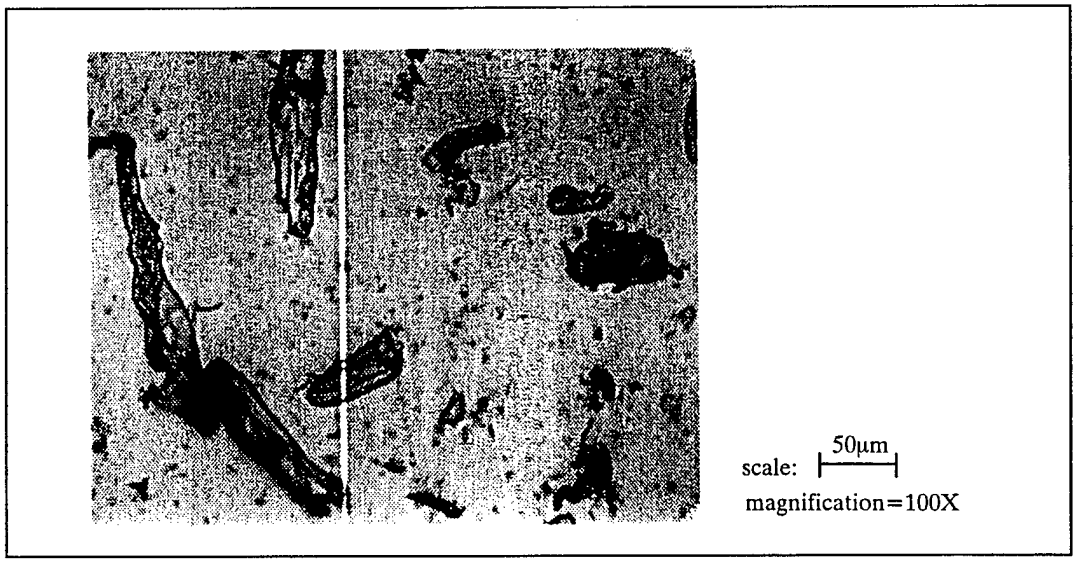

Figure 23. Microscopic observations of NC fines in sample #1.

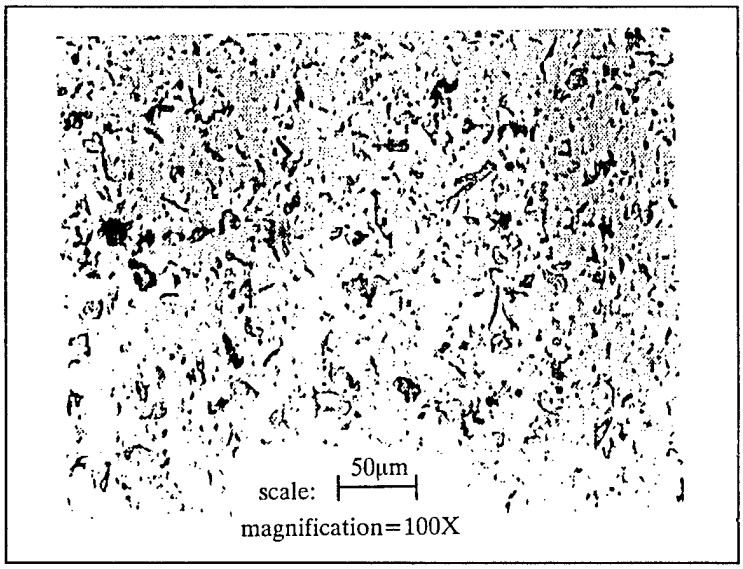

Figure 24. Microscopic observations of NC fines in sample #3.

Table 5. Particle size distribution of NC fines from 2 to 32 mm in sample #3.

	Trial 1	Trial 2	Average		
class in [mm]	% frequency	% frequency	% frequency	% area	% volume
2.0 - 2.4	0.5	0.3	0.4	0.0	0.0
2.4 - 2.8	0.8	0.2	0.5	0.1	0.0
2.8 - 3.4	11.4	9.4	10.3	2.5	0.9
3.4 - 4.0	19.8	17.2	18.3	6.4	2.7
4.0 - 4.8	16.0	18.3	17.3	8.5	4.3
4.8 - 5.7	16.4	16.5	16.5	11.5	6.9
5.7 - 6.7	13.6	11.8	12.6	12.5	8.9
6.7 - 8.0	8.3	9.4	8.9	12.4	10.5
8.0 - 9.5	5.9	8.8	7.5	14.8	14.8
9.5 - 11.3	5.4	4.3	4.8	13.5	16.1
11.3 - 13.5	1.3	1.9	1.6	6.3	8.9
13.5 - 16.0	0.4	1.0	0.7	4.1	7.0
16.0 - 19.0	0.3	0.2	0.2	1.8	3.6
19.0 - 22.6	0.1	0.3	0.2	2.5	6.1
22.6 - 26.9	0.0	0.2	0.1	1.8	5.1
26.9 - 32.0	0.0	0.1	0.1	1.3	4.3
mean diameter	5.47	5.79	5.65	5.98	6.78

The particle size distribution data of sample #3 listed in Table 5 are in a geometric progression with 16 class intervals, of which the resolution is constant at 0.17. If the class interval is arithmetic progressing with 2 μm from 2 to 32 μm, then the resolution varies from 0.67 to 0.07 for 2 to 4, and 30 to 32 size classes, respectively. Figure 25 shows histograms for relative frequencies, area fractions, and volume fractions versus particle size ranges. Figure 25d also shows the cumulative volume fractions. The shape of particle size distribution depends entirely on selection of class intervals (Table 4.1). Figure 25 is included to show the best resolution of size distribution of NC fines in sample #3 ranging from 2 to 32 μm. One should not predict that there be no or a very few particles less than 2 μm based on Figure 25. Although the area or volume fraction of NC fines less than 2 μm are negligible, the number of particles less than 2 μm may be quite big. In fact, many NC fines less than 1 μm were found under the higher magnification, as well as a large amount of NC fines larger than 32 μm. Remember that the membrane pores are more easily blocked or fouled by small size particles.

In addition to the particle size distribution of NC fines, the shape of NC fines is also important to explain and interpret the membrane fouling mechanisms. Figure 26 shows that the shapes of NC fines are too diverse to be defined as a single shape. There are many rod-like NC fines with sharp edges, which are subjected to be plugged into membrane pores and may cause membrane fouling. Due to the diversity in shapes and sizes of NC fines, the cake layer during filtration will be expected to be more compact and dense.

4.1.3 Flux Test Results

1, 3, and 6-stage flux tests were performed, as described in Section 3.1.3, to investigate the performance of each membrane. With a resistance model (Clark 1991; Lâiné et al. 1989), the permeate flux can be expressed as:

$$J_o = \frac{\Delta P}{\mu R_m} \qquad \text{Eq 9}$$

$$J_{end} = \frac{\Delta P}{\mu R_t} = \frac{\Delta P}{\mu (R_m + R_c + R_i)} \qquad \text{Eq 10}$$

$$J_f = \frac{\Delta P}{\mu (R_m + R_i)} \qquad \text{Eq 11}$$

where J_0=clean water flux, J_{end}=flux at the end of each stage, J_f=flux after backflush, ΔP=transmembrane pressure, m=dynamic viscosity of permeate, and R_t=total resistance, which consists of many components such as intrinsic membrane resistance (R_m), resistance due to reversible cake and/or gel layer (R_c), resistance due to irreversible fouling (R_i).

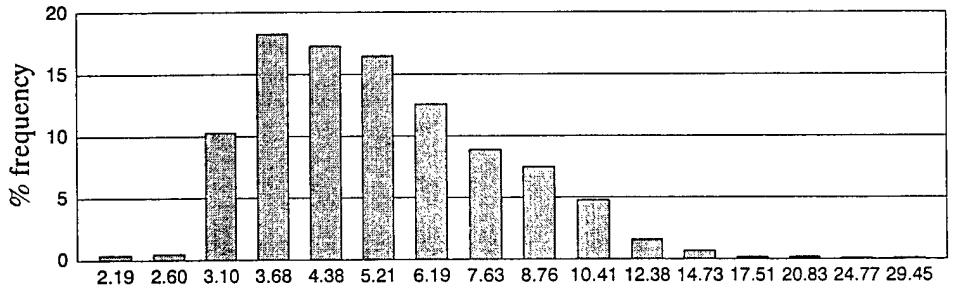

(a) relative frequency versus mean particle size

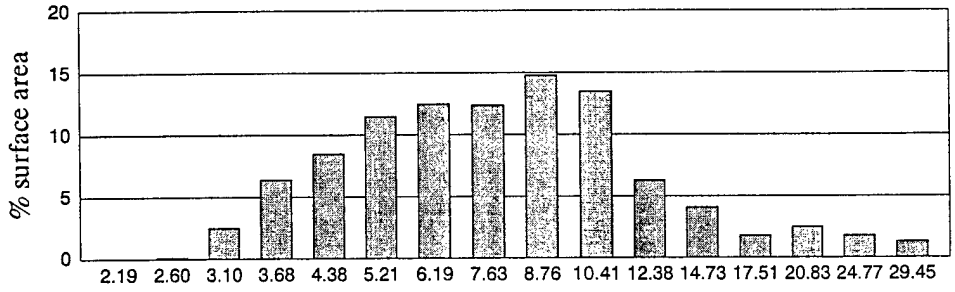

(b) surface area fraction versus mean particle size

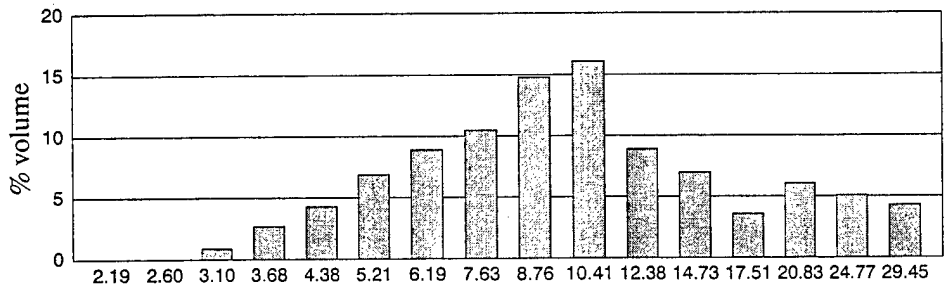

(c) volume fraction versus mean particle size

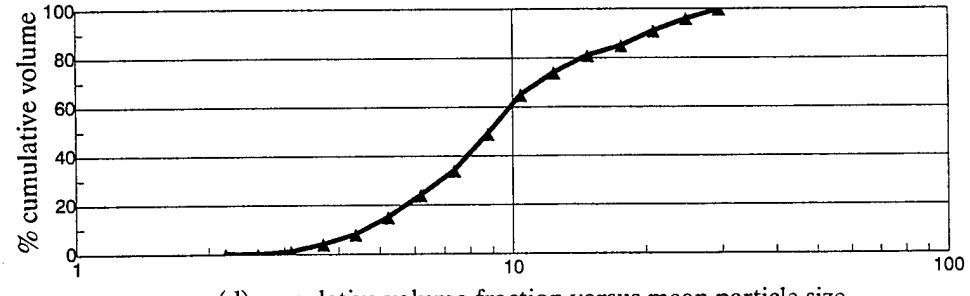

(d) cumulative volume fraction versus mean particle size

Figure 25. Particle size distribution of NC fines from 2 to 32 μm in sample #3.

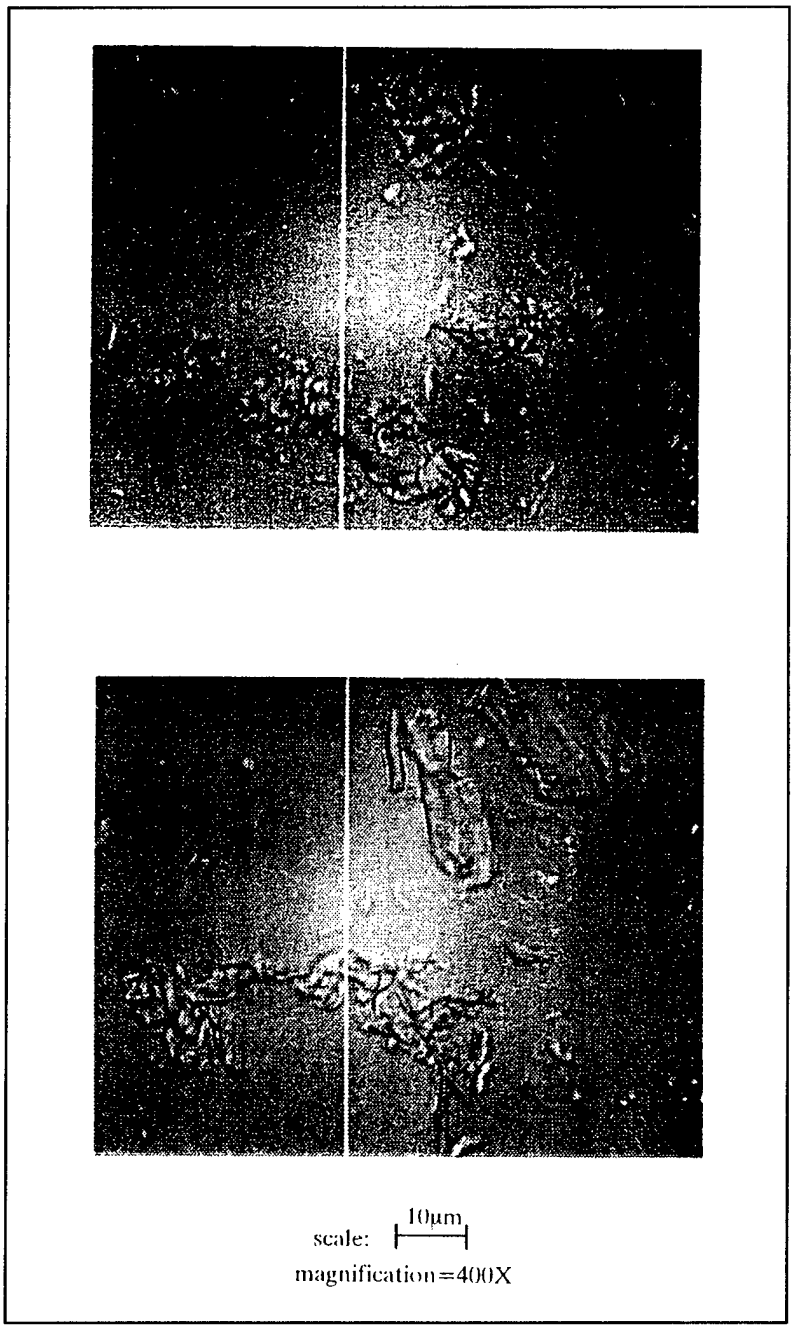

Figure 26. Shapes of NC fines in sample #3.

Using equations 9 through 11, each resistance component can be calculated from the flux test results. All flux test results are tabulated in Appendix.

There are many ways to present the flux decline behavior during filtration. In this report, five different kinds of formats will be used to explain and compare the flux test results:

1. Relative flux (J/J_0) versus time in sec (t)
2. Flux in LMH ($L/m^2 \cdot hr$) (J) versus t
3. J/J_0 versus permeate volume (V_p)
4. J versus V_p
5. t/V_p versus V_p.

Each plot has its own advantages and disadvantages. For example, the (J/J_0 vs. t) plot shows clearly how fast the permeate flux for each membrane declines with time, while it is difficult to compare the real flux data of several membranes at the same time. In case of the (J/J_0 vs. V_p) or (J vs. V_p) plots, it is helpful to compare the flux data after a certain amount of permeate production, but they do not provide any information on how long it takes to produce that amount of permeate. Although the (t/V_p vs. V_p) plot cannot show the flux decline data explicitly, we can reduce the complexity of presenting many curves in one figure since our flux test results show a linear relationship between t/V_p and V_p. In addition to reducing the complexity, we can induce the magnitude of resistances due to reversible and irreversible, i.e., (R_c+R_i) from its slope. According to the cake filtration model (Van Den Berg and Smolders 1990):

$$\frac{t}{V_p} = \frac{1}{J_o} + KV_p \qquad \text{Eq 12}$$

where K is a function of many parameters such as feed concentration, density of cake layer, and specific cake resistance, and which is proportional to the cake resistance.

In the case that the clean water flux is much greater than the dirty water permeate flux, i.e., $R_m << (R_c+R_i)$, equation 12 becomes the well-known relationship for unstirred dead-end filtration, $V_p \alpha t^{0.5}$. From equation 12, the y-intercept of the (t/Vp vs. Vp) plot can be said to be inversely proportional to the clean water flux, and the slope is proportional to the cake resistance.

1-Stage Flux Test Results of Sample #1. 1-stage flux tests of sample #1 were performed described in Section 3.1.3. The experimental results are provided in Table A.1. Although there is a small variance, the turbidity, UV absorption, and TOC values of permeates of all tested membranes are similar. Turbidity data of all permeates are very satisfactory comparing to that of Milli-Q or tap water, i.e., it is enough to meet the current and future discharge limits for NC manufacturing effluent of 40 and 25 mg/L, respectively. Therefore, in selecting candidates among the tested membranes, the permeate quality does not seem to be an issue regardless of membrane types, pore sizes, and materials (see Table A1). However, TOC data give evidence that there must be a considerable amount of dissolved organic matter in sample #1 that can pass through 100K MWCO membrane and that may cause flux decline during membrane filtration. In addition to TOC data, another indication of organic foulants was found in sample #1. After 1-stage flux tests of sample #1 (i.e., after 120 mL permeate

production), cake formation was seen on the membrane surface. There was no noticeable NC cake layer formation. Instead, a very thin layer, more like an organic gel layer rather than a NC cake layer, was found. Considering the high TSS of sample #1, it is somewhat strange that there is no significant cake formation. One possible explanation is that large NC fines, which have higher inertia arising from shearing force by stirring, tend to take small particles and/or themselves away from membrane surface, and prevent from NC cake formation. In the case of sample #1, the organic matter is suspected to be another foulant in addition to NC fines; this will be confirmed in next section. In this section, the effects of membrane types, pore sizes, and materials on flux decline behavior of sample #1 will be discussed with 1-stage flux test results.

Effects of Membrane Types (UF vs. MF) on Flux. Figure 27 (a) and (b) show how fast and how much the permeate flux of sample #1 declines with time. Figure 27a shows that the flux decline rates of MF membranes (A4, A5, C1, C2, D1, and D2) were higher than that of UF membranes (A1, A2, A3, B1, and B2). This is consistent with the effect of membrane pore size on fouling (Figure 22). However, keep in mind that the initial fluxes of MF membranes were much greater than UF under the same operating conditions, and that J_{end} of most MF membranes except Filinert 0.2 μm (C1) were still greater than those of UF membranes (Figure 27b). The flux recovery of UF membranes after backflush was better than that of MF membranes (Table A1). Of course, there were a few exceptions—XM300 (B2) and YC01 (D1). The flux decline rate of XM300 was similar to MF membranes (Figure 27) and the flux recovery was also bad (81 percent), while the flux decline rate of YC01 was similar to that of UF membranes and the flux recovery was also good (95 percent).

As mentioned before, two different kinds of foulants exist in sample #1—NC fines and organic matter. Each foulant will cause membrane fouling differently. Considering the relatively small pore size of UF membranes, one expects UF membranes to be more easily fouled by organics rather than NC fines. In contrast, NC fines will be a major foulant with MF membranes.

Effects of Membrane Pore Size and Pore Density/Porosity on Flux. According to the manufacturers of UF membranes used in this projects, the pore sizes of 100K and 300K UF membranes are 0.01 to 0.03 μm, respectively. (Table 2 lists the pore sizes of MF membranes.) Although it was not possible to find the pore density/porosity data of all membranes, the relative pore density/porosity can be estimated by comparing the clean water flux provided in Table A1. It can be aid that the Filtron's UF membranes (A1, A2, and A3) have much higher pore density than the Amicon's because J_0 of Filtron's UF membranes is more than 2 times greater than the Amicon's even though they have the same MWCO. If comparing the flux decline behaviors of Omega100K and YM100 membranes (Figure 27), Omega100K shows faster and higher flux decline rate whereas it has higher pore density and/or porosity. However, note that the flux decline rate depends on many other factors like base materials as well as pore density/porosity.

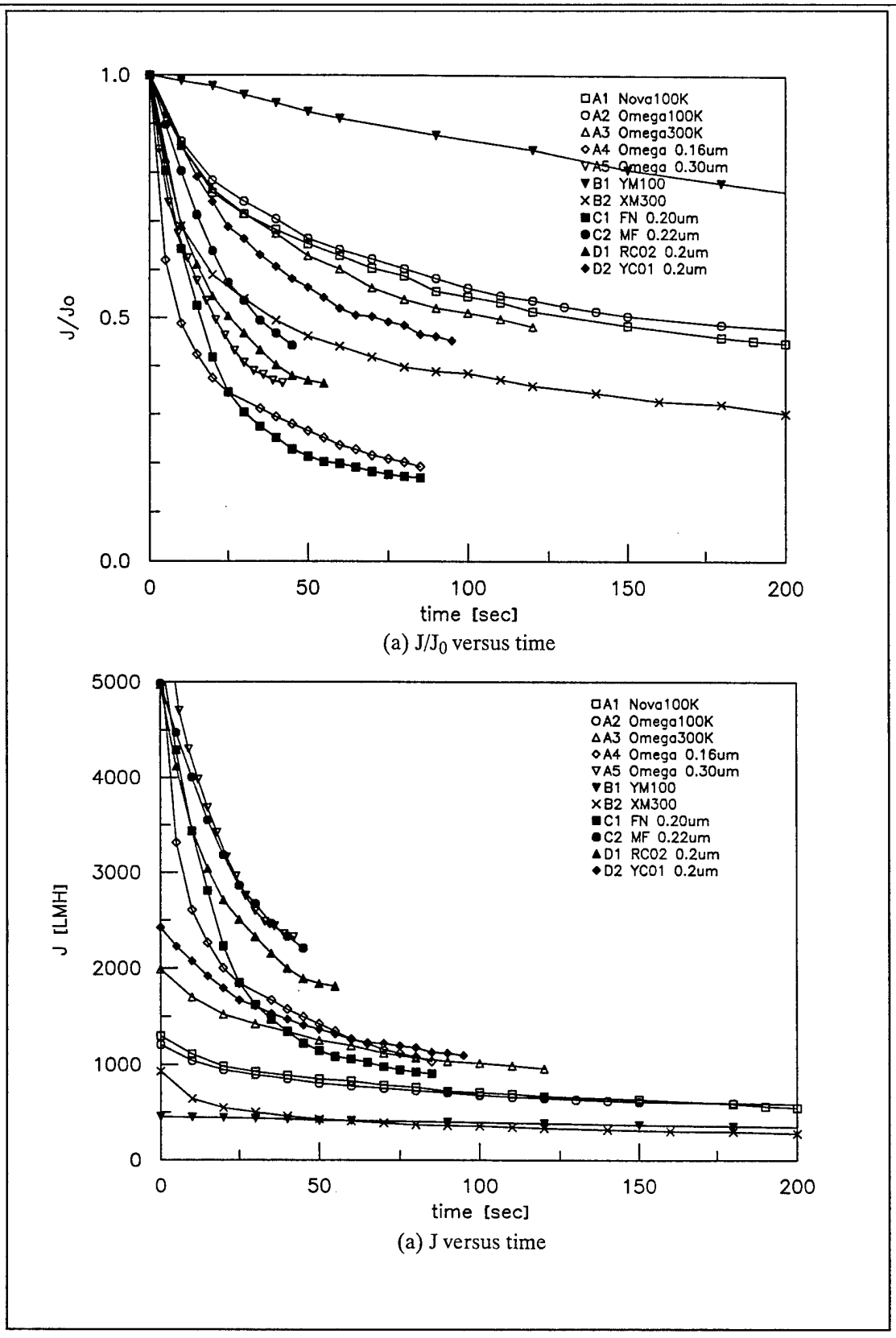

Figure 27. 1-stage flux test results of sample #1.

Based on the clean water flux data, the tested MF membranes except Omega0.16 μm (A5) and YC01 (D2) have about same order of pore density. A comparison of J_0 of Omega0.3μm to that of Omega0.16μm and other MF membranes (Tables 2 and A1) shows that Omega0.3μm has relatively lower pore density/porosity. YC01 also shows relatively lower J_0 as compared to other 0.2 μm MF membranes, which also means it has a relatively low pore density/porosity. Note that YC01 is naturally hydrophobic, and it behaves like moderate hydrophilic after wetted in alcohol.

It is hard to tell the pore size effects on the flux decline behavior unless the membrane base materials and other operating conditions are kept constant. Note the flux data of Omega series membranes only. As mentioned in Section 4.1.2, the flux decline rate and flux recovery tend to become deteriorated with the membrane pore size (Figure 28). This study, however, found somewhat different and very interesting experimental results. The flux decline rate and flux recovery of the smaller pore size membranes (Omega100K and Omega300K) were better than the larger pore size membranes (Omega0.16 μm and Omega0.3 μm) as expected, but Omega0.16μm shows much worse flux decline rate and flux recovery than Omega0.3μm (see Figures 27 and 28). In summary, there exists a critical pore size at which the flux decline and recovery is worst (Figure 28). The same trend was observed in case of sample #3 (Figure 29).

Effects of Membrane Base Materials on Flux. The membrane base materials were found to be a very critical factor affecting the filtration flux performance of NC wastewater samples. Among UF membranes tested, the acrylo nitrile vinyl chloride UF membrane, XM300, shows the worst performance in regard to flux decline rate and flux recovery (Figures 27 and 30a, respectively). The cellulose acetate UF membrane, YM100, is the best. The polyethersulfone (PES) based UF membranes (Nova100K, Omega100K and Omega300K) show fairly good performance during 1-stage flux tests, but the long-term flux test results will show how badly the PES-based membranes are fouled by organic matter in sample #1 (Section 4.1.3.2). Comparing experimental results of Nova100K (hydrophobic) and Omega100K (hydrophilic), the hydrophilicity appears to have no significant effects on the flux performance of NC wastewater samples.

Among MF membranes tested, the PES-based MF membranes (Omega0.16μm and Omega0.3μm) and the polytetrafluoroethylene (PTFE) MF membrane (Filinert FN 0.2μm) show the worst flux performance, and the next worst is the acrylo-co polymeric MF membrane (RC02 0.2μm) (Figure 30b). The mixed-ester cellulose MF membrane, Membra-Fil MF 0.22μm, and the polypropylene MF membrane, YC01 0.2μm, show the best performance.

In summary, the PES, acrylo-co polymer, and PTFE-based membranes are not good choices for membrane processing of sample #1 whereas the cellulose and polypropylene based membranes tend to give the better flux performance.

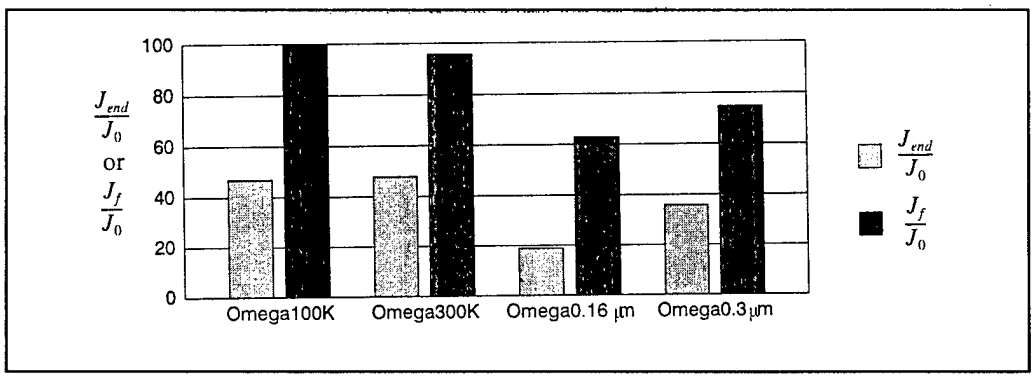

Figure 28. Effects of membrane pore sizes on 1-stage flux of sample #1.

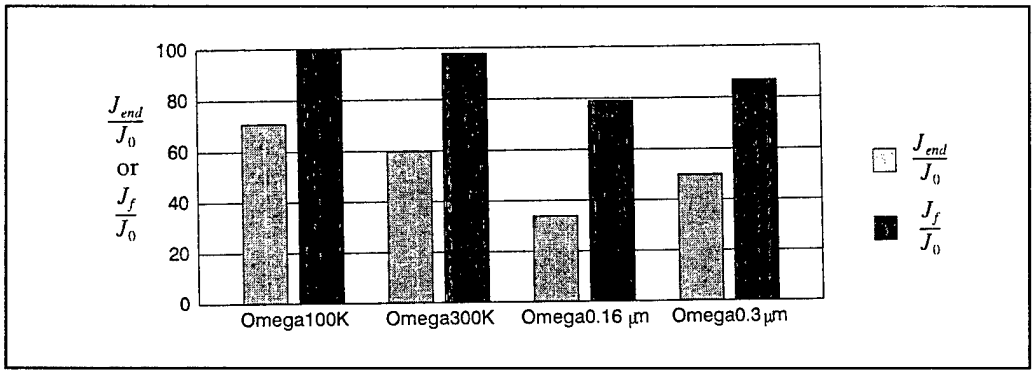

Figure 29. Effects of pore size on 1-stage flux of sample #3.

Effects of Organic Matter on Flux Decline Behavior of Sample #1. To confirm that organic matter in sample #1 is another major foulant in addition to NC fines, permeates of sample #1 passing through Omega0.3μm were collected and 3-stage flux tests were performed with various MF and UF membranes. Table A2 lists the flux test results. Figure 31 shows how the flux declines with the permeate volume. Two discontinuities of the flux decline curves correspond to the sample refilling points when the total permeate volume reaches 120 and 220mL, respectively.

Figure 31a shows that the MF membranes tested (Omega0.16μm and Membra-Fil MF 0.22μm) appear not to be significantly fouled by organic matter, and the local flux has never been below 80 percent of the initial flux. This fact is much clearer if the slopes of MF membranes in Figure 31c are examined, which are almost flat as compared to those of UF membranes. This means that there is no severe reversible and/or irreversible fouling during filtration. The flux recovery data of MF membranes in Figure 32 also show that there is no noticeable irreversible fouling by organic matter in sample #1. A possible explanation is that the molecular sizes of organic matter in sample #1 are much smaller than the pore sizes of MF membranes, so most organic matter can pass the MF membrane pores without causing severe fouling.

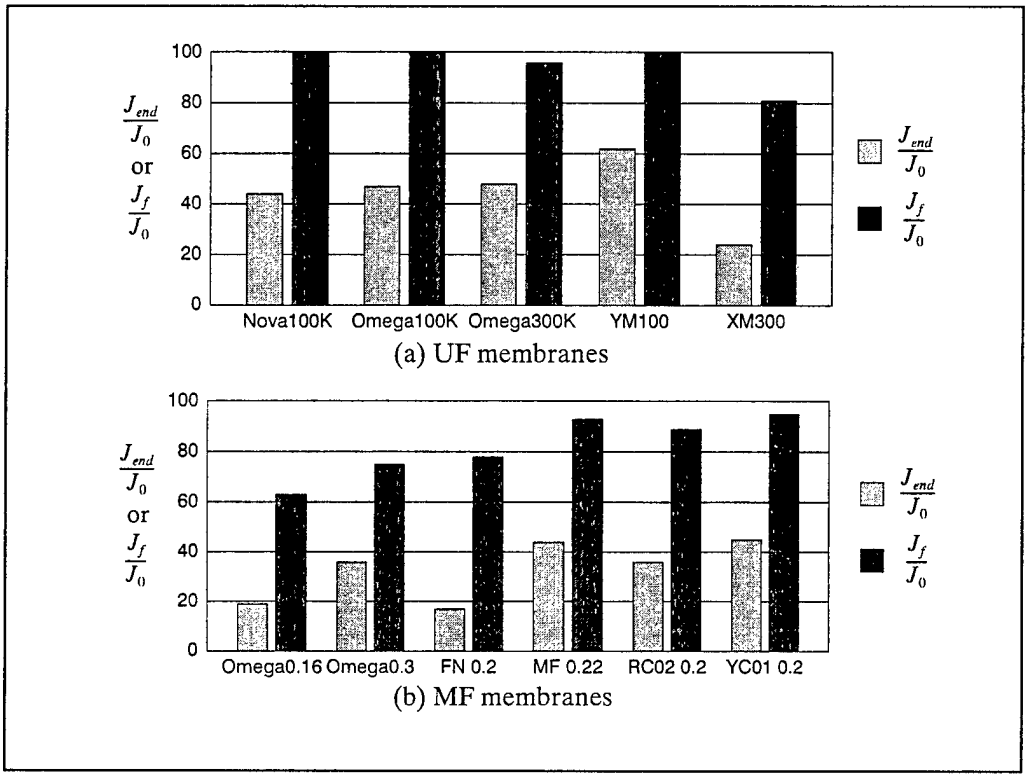

Figure 30. Effects of membrane base materials on 1-stage flux of sample #1.

However, UF membranes are badly fouled by organic matter in sample #1 (Figures 31 and 32). The degree of reversible and irreversible foulings is greater in case of the PES-based UF membranes, Omega100K and Omega300K, than the cellulose-based UF membrane, YM100. Big jumps of the permeate flux at the time of sample refilling, which were not observed in case of sample #3, can be explained as destruction of the concentration boundary layer. During filtration of the organic solution, the concentration boundary layer is created near the membrane surface, providing another major resistance component in addition to other resistance components like a gel layer. This concentration boundary layer is disturbed and re-established at the time of sample refilling due to dilution effects.

A comparison of the flux performances of Omega100K and Omega300K shows that Omega100K has a similar flux recovery to Omega300K (Figure 32), but a higher flux decline rate than Omega300K (Figure 31a) even though the initial clean water flux of Omega100 is less than that of Omega300K (Figure 31c). A possible explanation is that the chance for organic matter to pass membrane pores of Omega100K is less than Omega300K, so more organic matter tends to be accumulated on membrane surface in the case of Omega100K, which increases the gel layer and/or concentration boundary layer resistances.

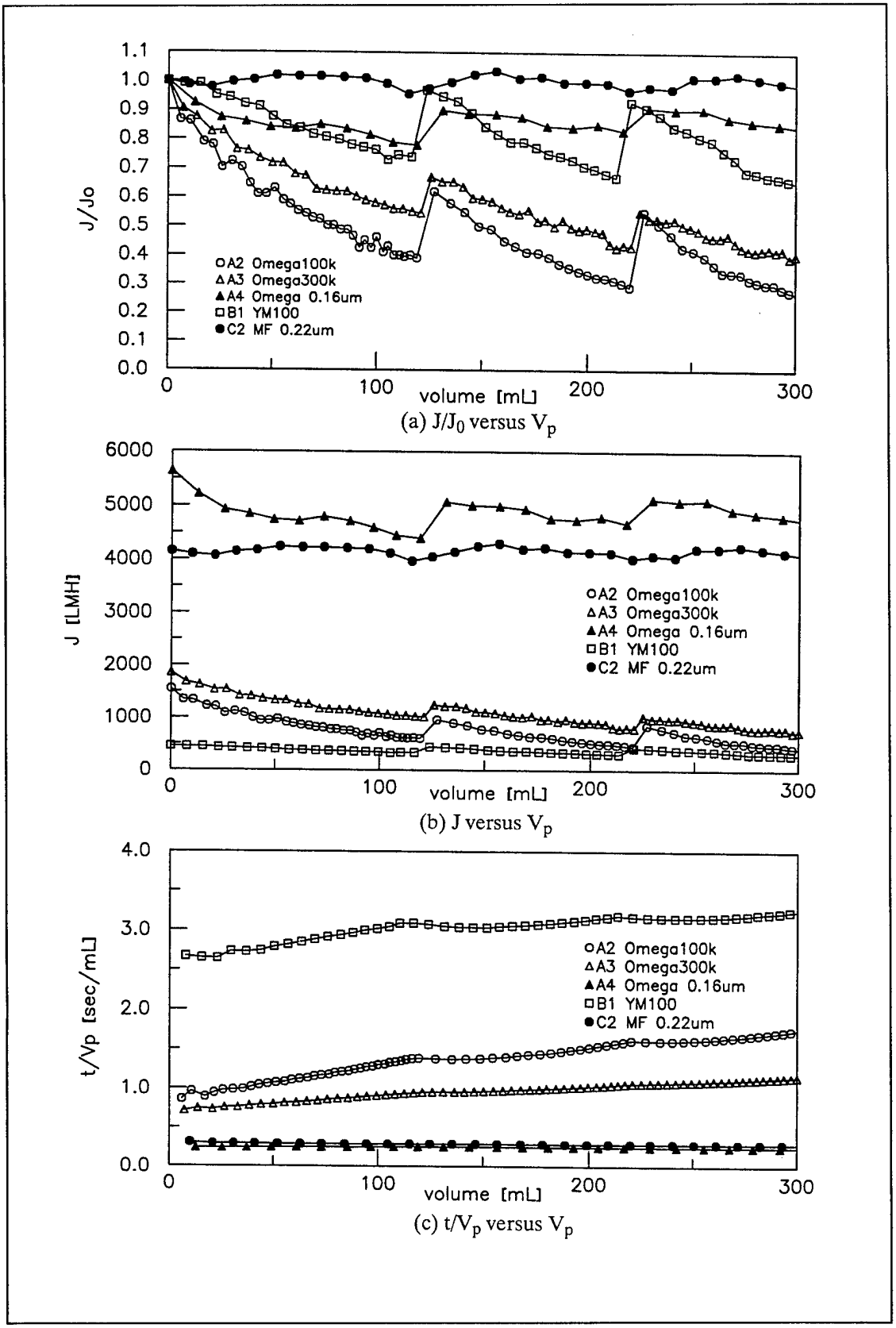

Figure 31. 3-stage flux test results of permeate #1.

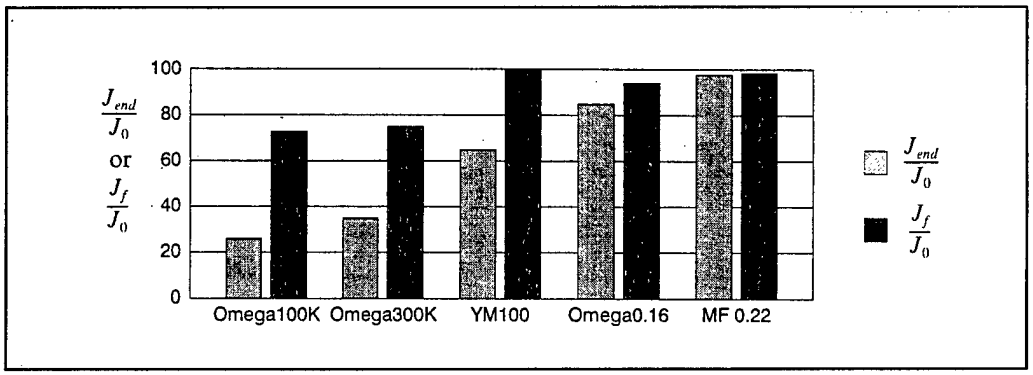

Figure 32. Effects of organic matter on 3-stage flux of sample #1.

To minimize organic fouling, sample #1 should be pretreated; the effectiveness of PAC pretreatment for sample #1 will be discussed in Section 4.1.6. If the permeate quality (like TOC values) is not an issue, MF membranes like Membra-Fil MF 0.22μm will be better for filtration process of sample #1.

1, 3, and 6-Stage Flux Test Results of Sample #3. The general trends of flux decline behaviors of sample #3 were very similar to those of sample #1, and the overall membrane performance of sample #3 can be summarized as follows:

1. *Effects of membrane types*: The flux performance of UF membranes is better than that of MF membranes in regarding to flux decline rate and flux recovery while UF membranes have lower actual flux (J_0 and J_{end}) than MF membranes.

2. *Effects of membrane pore sizes*: As Figure 29 and sample #1 (Figure 28) show, there exists a critical membrane pore size at which the flux performance is the worst.

3. *Effects of membrane base materials*: Again, the acrylo-co polymer based UF membrane (XM300) is not a good choice for sample #3, and the PES- and PTFE-based MF membranes (Omega0.16μm, Omega0.3μm, and FN 0.2μm) also show very bad flux performance (see Table A3).

The previous two sections have discussed the flux performance of each membrane for sample #1 with regard to the effects of membrane types, pore sizes, and base materials. This section will establish the membrane screening criteria to determine candidates membranes for the filtration process of sample #3, and will focus on selecting candidates.

In selecting candidates, we should consider the flux performance (flux decline rate and flux recovery) as well as the permeate production rate (J_0 and J_{end}). It is not possible to narrow down candidates based only on short-term (1-stage) flux test results. Also, it was not necessary to perform long-term (3 and 6-stage) flux tests for all membranes. Therefore, the following 3-step membrane screening criteria was set up to determine candidate membranes for further research:

1. 1-stage flux tests will be performed with all membranes, and the membranes that have a bad flux performance and a low permeate production rate will be excluded from candidates whereas the others will pass this criteria. For example, although a membrane shows relatively rapid flux decline, it will not be excluded if it has relatively high J_0 and J_{end}.

2. 3-stage flux tests will be performed with membranes that pass the first criterion, and the membranes that pass the first criterion regardless of their bad flux performance because of their superiority in J_0 and J_{end}, but which prove no more advantage of the permeate production rate, will be excluded from the list of candidates.

3. 6-stage flux tests will be performed with membranes passing the second criterion, and the candidate membranes will be determined based on the flux performance and permeate production rate.

1-Stage Flux Test Results of Sample #3 (First Criterion). Table A3 and Figure 33 give 1-stage flux test results of sample #3. According to the first membrane screening criterion, XM300 UF membrane and Filinert FN 0.2μm MF membrane will be excluded from candidate membranes. XM300 shows not only bad flux performance, but also relatively low J_0 and J_{end} (Table A3), and as mentioned before, its base material (acrylo nitrile vinyl; chloride) is responsible for its bad flux performance rather than membrane type (UF vs. MF) or pore size. As shown in Figure 33b, although FN 0.2μm has relatively high J_0, the permeate flux declines very rapidly and J_{end} is relatively very low compared to other MF membranes. FN 0.2μm is extremely hydrophobic, but according to the manufacturer, it behaves like a hydrophilic membrane after alcohol wetting. Its originally hydrophobic characteristics may be responsible for the strong interaction with NC fines. Also, its highly tortuous pore structure and rough membrane surface tend to make small NC fines easily trapped inside membrane pores or on membrane surface, and to make it hard to remove the trapped NC fines. The backflushed water of FN 0.2μm was seen to contain many small NC fines while the backflushed water of other membranes was clear.

Figure 33c shows relative reversible/irreversible resistances of each membrane—the slope is proportional to the reversible/irreversible resistance. The slopes of XM300 and FN 0.2μm are noticeably different from the others, which means the reversible/irreversible resistance of these two membranes are much greater than the others. This agrees well with the Rc and Ri values calculated using equations 9 to 11, and listed in Table A3.

Other UF membranes except XM300 passed the first criterion because of their superior flux performances during 1-stage flux tests although their actual fluxes are much less than MF membranes. Figure 33a and Table A3 show that the J_{end}/J_0 values of UF membranes except XM300 are greater than 60 percent, and their flux recoveries are almost 100 percent. MF membranes other than FN 0.2μm also passed owing to their higher permeate production rates although their flux performances were not as good as UF membranes.

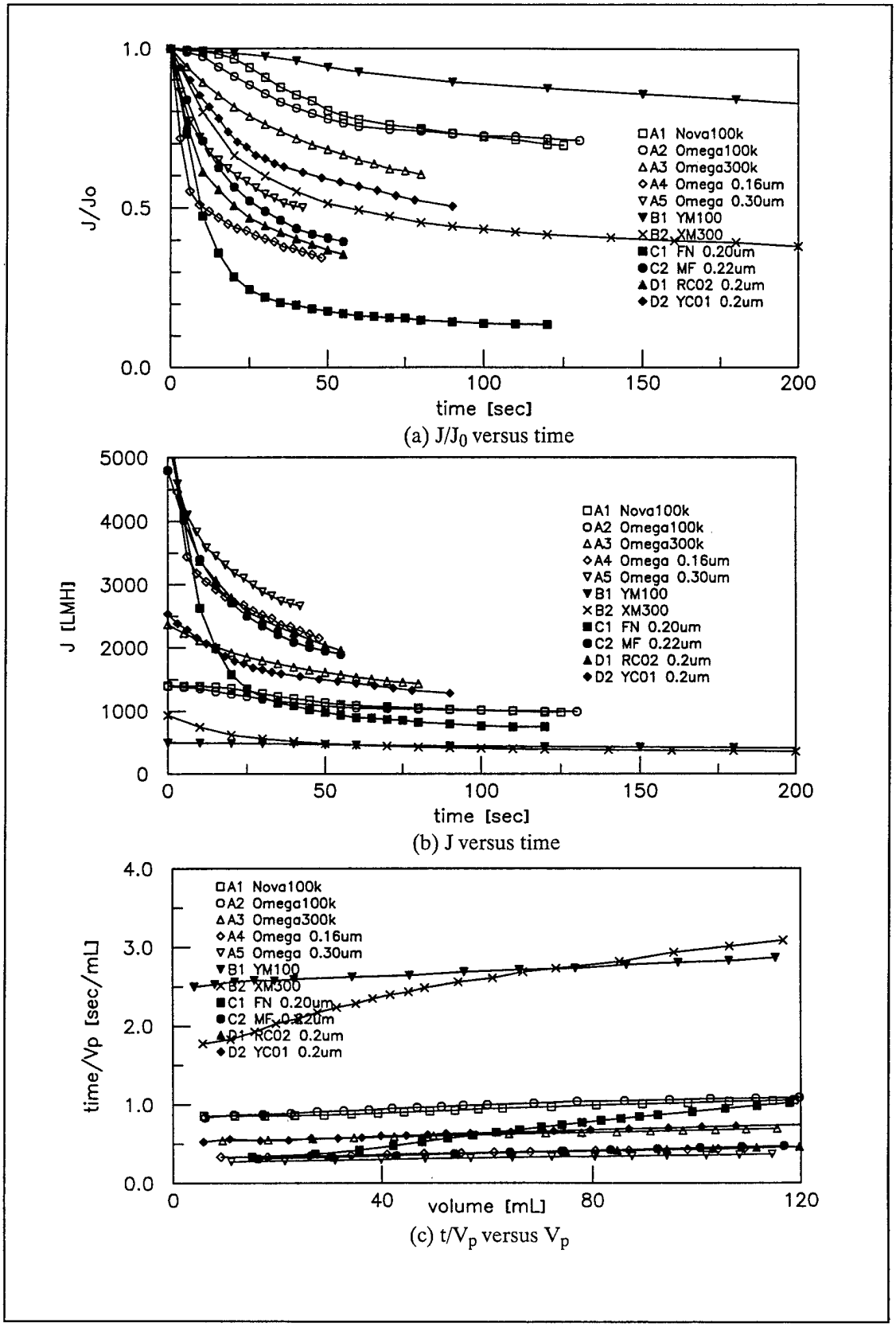

Figure 33. 1-stage flux test results of sample #3.

For example, although Omega0.16μm, Omega0.3μm and RC02 0.2μm have relatively bad J_{end}/J_0 and J_f/J_0 values (Table A3), their actual J_{end} and J_f values are greater than the other membranes (Figure 33b).

3-Stage Flux Test Results of Sample #3 (Second Criterion). Three-stage flux tests were performed with the membranes passing the first criterion, Table A4 and Figure 34 give the experimental result. According to the second criterion, Nova100K, Omega0.16μm, YM100 and RC02 0.2μm will be excluded from candidates.

Both Nova100K and Omega100K have about same initial clean water flux; the only difference is hydrophilicity. Both membranes are made with PES, and the PES-based membranes are well-known hydrophobic membranes with strong protein binding characteristics (Cheryan 1986). The membrane surface of Omega100K is modified to become hydrophilic. However, we observed there was no significant difference in the flux performance of sample #3, and Omega100K is slightly better than Nova100K (Figure 35a and 35b). It can be said that there is no difference between Nova100K and Omega100K for the filtration process of sample #3, so Nova100K was excluded from the list of candidates.

Although YM100 shows the best flux performance in regard to flux decline rate and flux recovery (Table A4), its permeate production rate (J_{end}) is relatively too low (Figure 35b). For 300mL permeate production, YM100 required a much longer time (2 or 3 times) than other membranes.

Omega0.16μm and RC02 0.2μm passed the first criterion only because of their superiority in permeate production rate (J_{end}) regardless of their low flux recovery (i.e., high irreversible fouling). However, their superiority in J_{end} begins to diminish as the filtration time (permeate volume) increases; if considering adverse long-term effects due to their high irreversible fouling (Figure 35a), these two membranes will not show any superiority in the permeate production rate.

6-Stage Flux Test Results of Sample #3 (Third Criterion). Only five membranes remain—two UF membranes (Omega100K and Omega300K) and three MF membranes (Omega0.3μm, MF 0.22μm, and YC01 0.2μm). The 6-stage flux tests were performed to determine final candidate membranes. Table A5 and Figure 36 give the experimental results.

Figures 36a and 37a, Omega100K has a similar flux recovery to Omega300K, and a slightly better flux decline rate than Omega300K. However, in regard to the permeate production rate—J_0, J_{end}, and the time required for 600mL permeate production, Omega300K is better than Omega100K. Omega100K requires about 30 percent longer time period than Omega300K (Figure 36a). The flux decline rate increases with the initial clean water flux (Figure 36a) because the mass flux of NC fines is also increasing with the permeate flux, so NC cakes are formed more quickly.

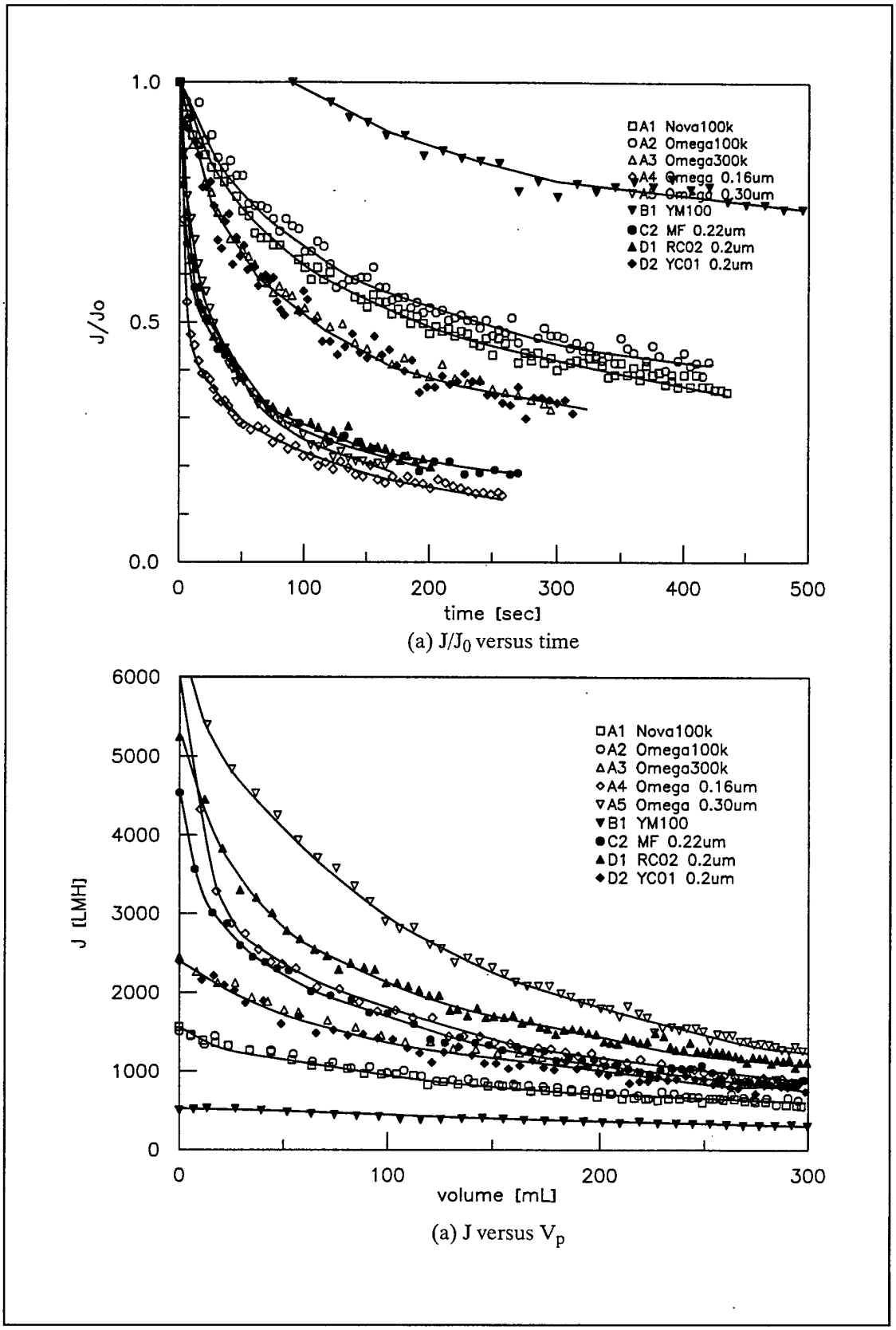

(a) J/J_0 versus time

(a) J versus V_p

Figure 34. 3-stage flux test results of sample #3.

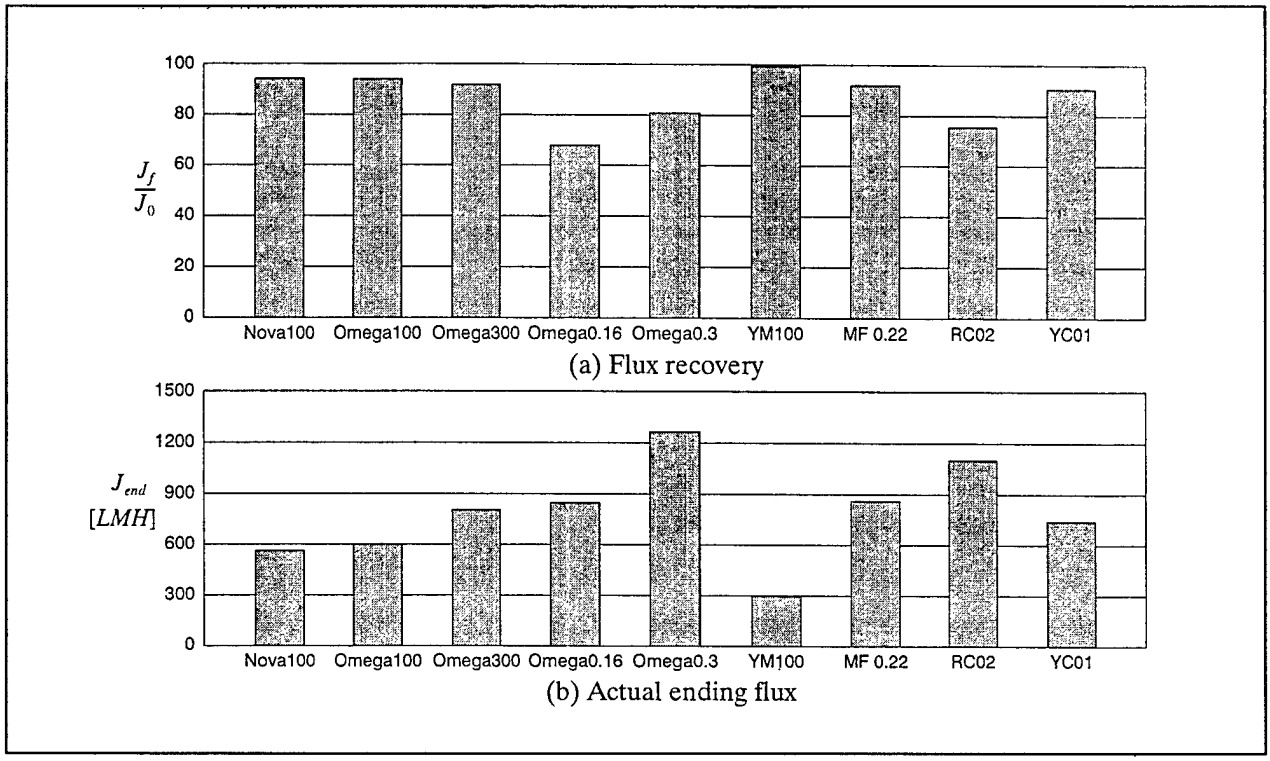

Figure 35. Flux performance during 3-stage flux test of sample #3.

In this context, it is clear that the time period required to produce the same amount of permeate volume (600mL) should decrease with the initial clean water flux. However, Figure 36a shows that YC01 requires a longer period of time than Omega100K and Omega300K although its initial clean water flux is greater. This seems to be owing to the base material of YC01, polypropylene, and its naturally hydrophobic characteristics. These two factors tend to make the physicochemical interactions between membrane surface and NC fines stronger. It becomes even clearer by comparing the slopes of the t/Vp versus Vp plot (Figure 36c). The slope of YC01 is much greater than the others, which means its reversible/irreversible cake resistance is much greater than the others (Table A5).

As filtration proceeds, an NC cake layer begins to form and increase the hydraulic resistance against permeate flux in addition to the intrinsic membrane resistance. If the NC cake resistance is much greater than the intrinsic membrane resistance, the permeate flux will be controlled by the NC cake resistance as filtration proceeds. Figures 36b and 37b show how, regardless of values of the initial clean water flux, the permeate flux of Omega300K, Omega0.3μm and MF 0.22μm approaches the same steady value. As provided in Table A5, the total resistances (R_t) of these membranes are about same regardless of their intrinsic membrane resistance (R_m).

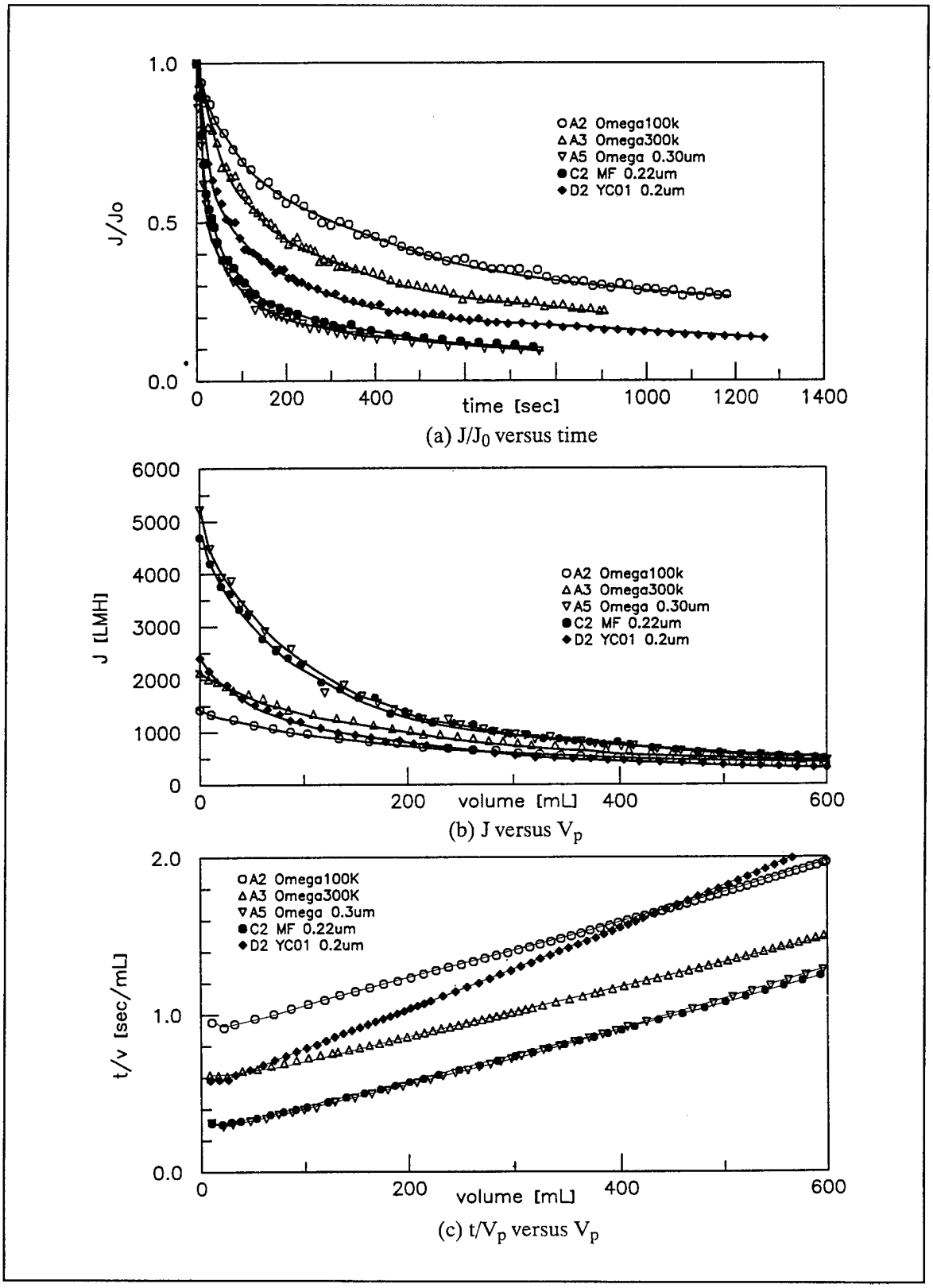

Figure 36. 6-stage flux test results of sample #3.

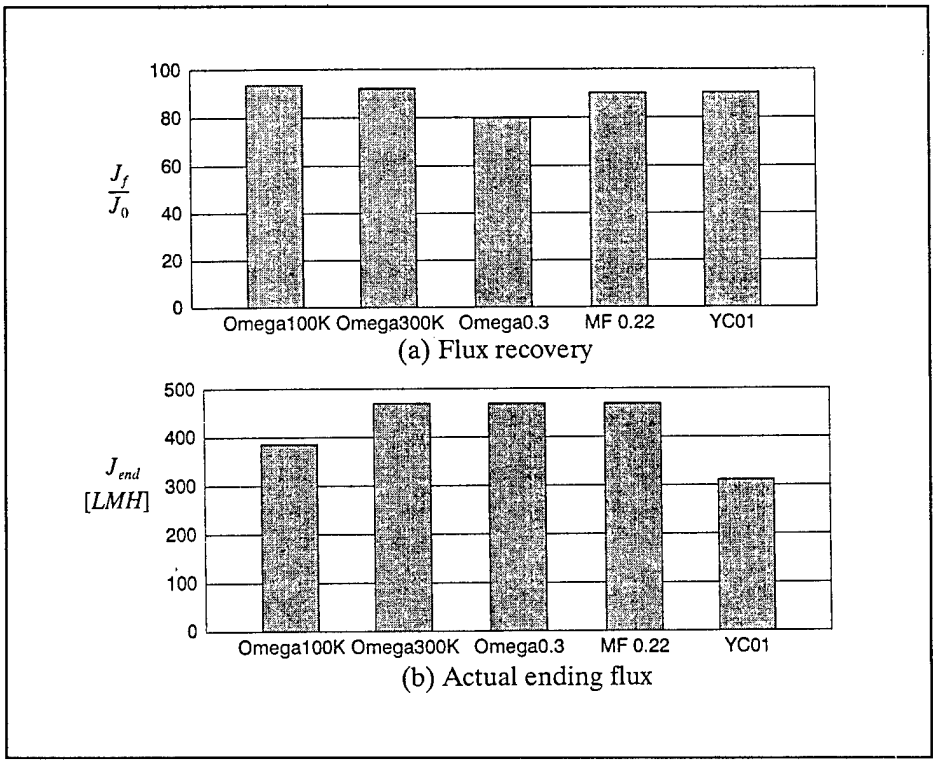

Figure 37. Flux performance during 6-stage flux test of sample #3.

Figure 37a shows that the flux recovery of Omega0.3μm is too low whereas its permeate production rate is similar to Omega300K and MF 0.22μm. Considering the adverse long-term effects of irreversible fouling, Omega0.3μm were excluded from candidates. Therefore, Omega300K and MF 0.22μm were selected as the candidate membranes for filtration of sample #3.

4.1.4 Static Adsorption Test Results

The static adsorption tests were performed as described in Section 3.1.3 to investigate the long-term adsorption of organics and/or NC fine particles in NC wastewater to membrane surface. Since any flow through membrane pores is prevented during static adsorption tests, one may assume that there was no membrane fouling by physical pore blockage and/or dynamic adsorption which are used to occur during filtration. However, in addition to surface adsorption, there might be membrane pore adsorption due to the diffusion process of organic matter and/or small size of NC fines. The water flux was measured after exposing membrane surface to NC wastewater samples for 24 hr (Figure 38).

For sample #1, YM100 shows the least flux loss while Omega300K shows the greatest flux loss. Considering that organic matter in sample #1 is a major foulant during static adsorption tests, it is not surprising that UF membranes tend to show more flux loss than MF membranes (Figure 32).

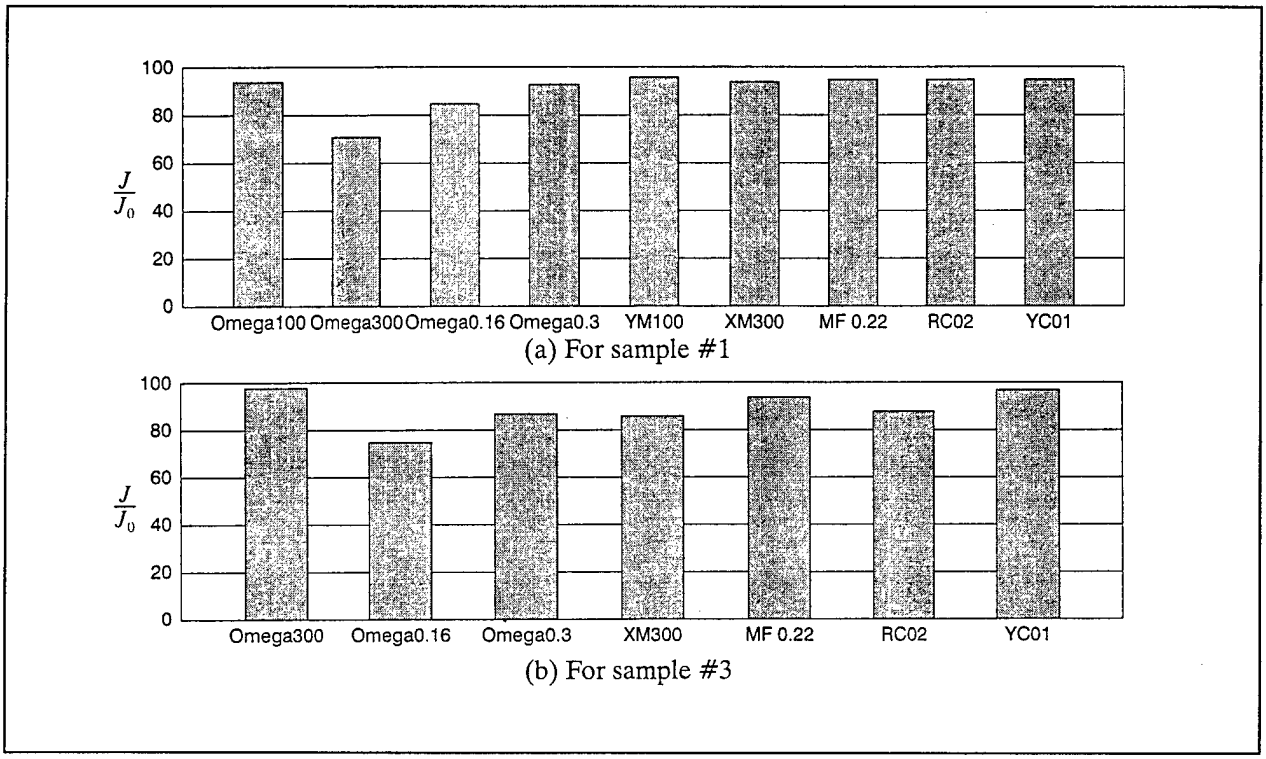

Figure 38. Static absorption test results.

The least flux loss of YM100 can be explained in relation to its base material—the cellulose-based membranes like YM100 and MF 0.22μm have showed the best flux performance throughout this project. Also, the bad flux loss of Omega0.16μm seems to result from its base material (PES). However, the flux loss of Omega100K and XM300 due to static adsorption was not as bad as the flux loss caused by filtration (see Figure 30a).

The flux losses of MF membranes for sample #3 tend to be greater than those for sample #1. Considering the particle size of sample #3 is smaller than that of sample #1, it appears that there is more active diffusion of small NC fine particles in sample #3. The greatest flux loss of Omega0.16μm agrees with the results of critical pore size at which flux loss caused by filtration is the greatest.

4.1.5 Effects of Pressure and Stirring on Flux Decline Behavior

The effects of transmembrane pressure and stirring on flux decline behavior of sample #3 were investigated by performing three-stage flux tests with the selected candidate membranes (Omega300K and MF 0.22μm). Table A6 lists the experimental results. Both Omega300K and MF 0.22μm show the same trend of effects of pressure and stirring.

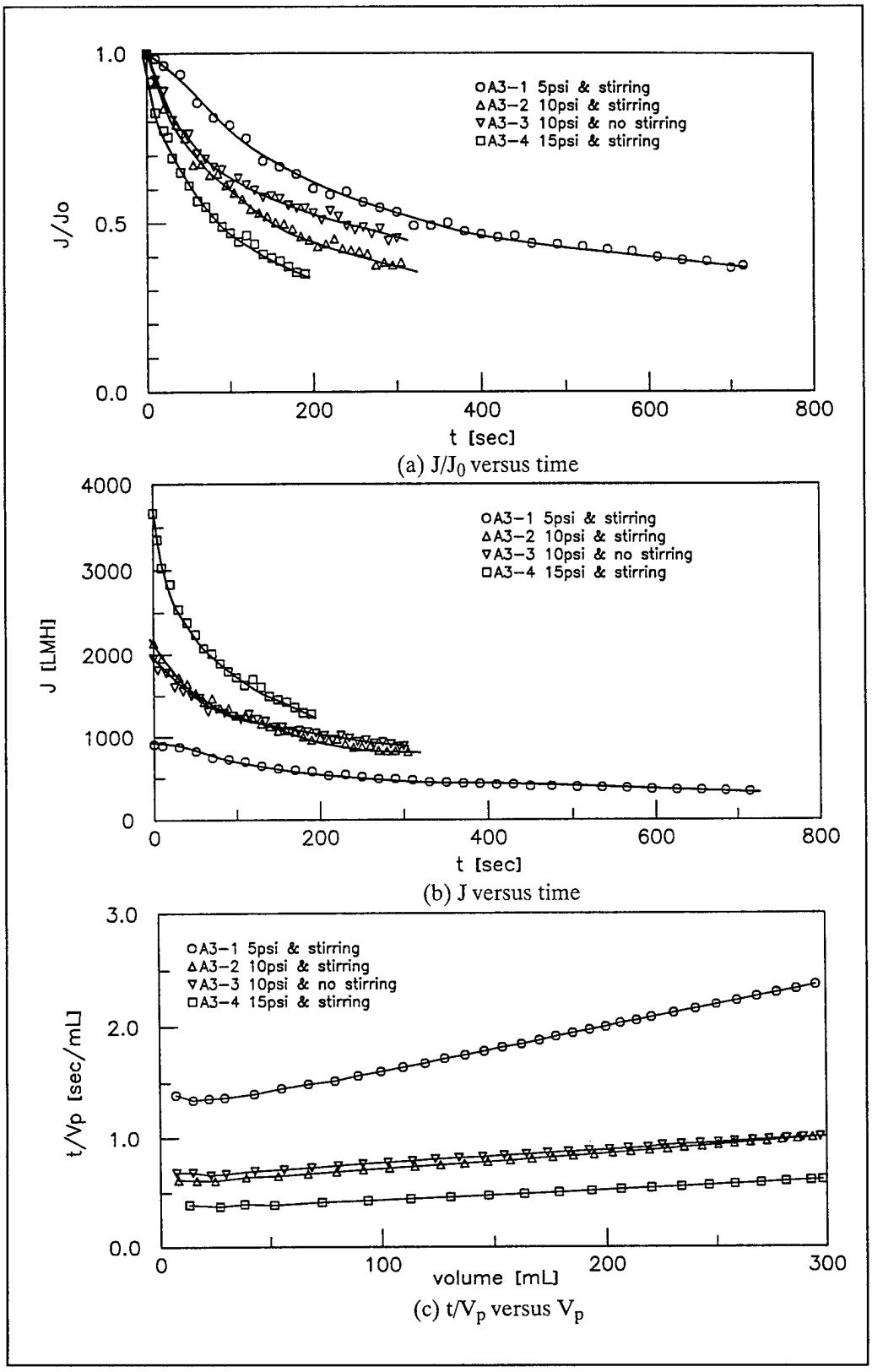

Figure 39. Effects of presure on flux of sample #3 (Omega300K).

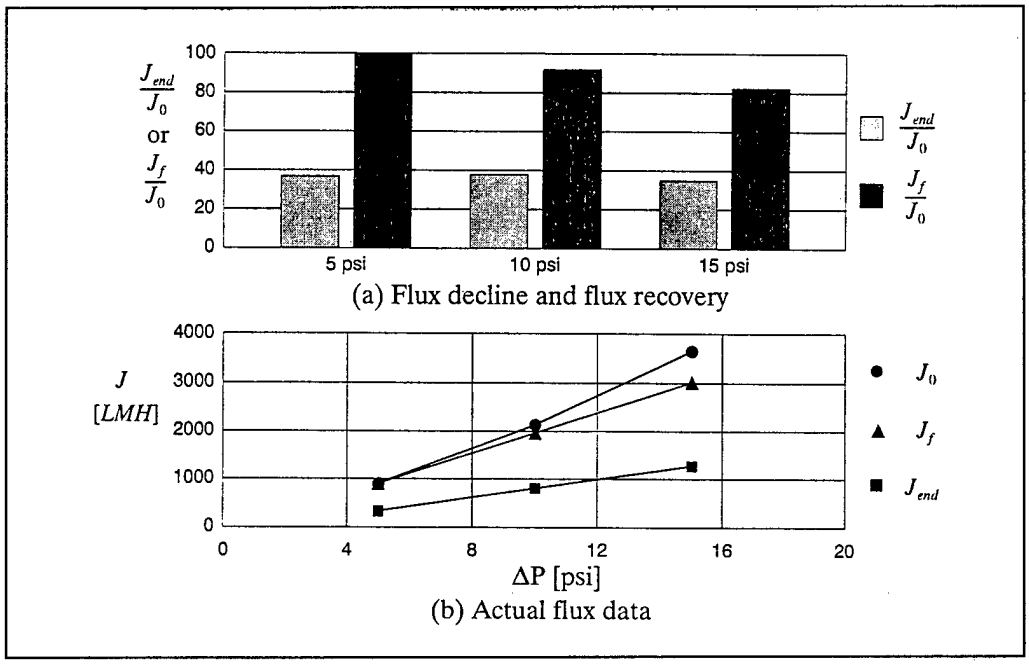

Figure 40. Effects of pressure on flux decline and recovery of sample 33 (Omega300K).

With Omega300K UF Membrane. As shown in Figure 39 (a), the permeate flux declines more quickly as the pressure increases. The flux recovery (J_f/J_0) decreases with the transmembrane pressure as shown in Figure 40a. Therefore, one may conclude that increasing the transmembrane pressure results in deteriorating the flux performance, so the transmembrane pressure should be low as possible (Shen et al. 1993). However, this does not appear to be true for NC wastewater, especially for sample #3. It is well-known that the permeate flux increases with the transmembrane pressure up to a certain point (pressure-controlled region), but after a certain point, increasing the transmembrane pressure merely results in a thicker and/or denser cake layer, so the permeate flux does not further increase by increasing the transmembrane pressure (mass-transfer controlled region).

Figure 40b shows that the actual flux values of J_0, J_f, and J_{end} increase linearly with the transmembrane pressure, i.e., the permeate flux is still in the pressure-controlled region rather than mass-transfer controlled region. It becomes much clearer when the slopes in Figure 39c are compared. The slope tends to decrease with the transmembrane pressure, which means that the NC cake resistance is less in case of the lower transmembrane pressure. So, one can expect a higher permeate flux by increasing transmembrane pressure, but one must keep in mind that the flux recovery tends to decrease with the transmembrane pressure (Figure 40a), which results in increasing operating costs. Therefore, one may possibly optimize the transmembrane pressure for the required permeate production rate and the operating cost.

Generally speaking, the flux performance is expected to be enhanced by stirring since stirring generates shearing force to take NC fines away from membrane surface and/or cake layer. However, the experimental results show that the flux performance without stirring is slightly better than that with stirring (Figure 39). This result could be explained in relation to the different nature of NC cake formation on the membrane surface under stirred and unstirred conditions. First, the NC cake layer under stirred condition is continuously exposed to shearing force, and a harsh shearing environment would make the NC cake layer become denser and tighter. Secondly, the larger NC fines convectively driven onto the cake layer tend to move back into feed stream due to their higher inertia arising from shear force, and the NC cake layer would consist of smaller NC fines (Baker et al. 1985). These two phenomena would give a higher resistance of the NC cake layer. Kim et. al (1993) found a very similar results with colloidal silver particles—stirred filtration shows a more finely dispersed cake than unstirred filtration.

With MF 0.22μm MF Membrane. It is hard to tell the effects of transmembrane on the flux decline rate using the J/J_0 versus time plot. A comparison of the permeate flux curves at 5psi and at 10psi (Figure 41a), MF 0.22μm shows pressure effects very similar to Omega300K—the permeate flux declines faster at a higher transmembrane pressure. A comparison of the permeate flux curves at 10psi and at 15psi (Figure 41a) shows that the flux decline curve at 15psi does not seem to follow the same trend. However, the pressure effects appear clearer when the slopes in Figure 41c are compared. The slope tends to increase with the transmembrane pressure.

The actual permeate flux is proportional to the transmembrane pressure (Figure 42b) (i.e., still in the pressure independent region) while there is no detrimental effects of transmembrane pressure on the flux recovery (Figure 42a).

The effects of stirring for MF 0.22μm are the same for those of Omega300K, i.e., the unstirred condition shows a filtration rate greater than the stirred. A comparison of the slopes in Figure 41c shows that the slope of unstirred is less than that of stirred, which agrees well with the reversible/irreversible cake resistance data in Table A6.

4.1.6 Effects of PAC on Flux Decline Behavior of Sample #1

As discussed in Section 4.1.3.2, sample #1 had a significant amount of dissolved organic matter, which caused severe fouling of UF membranes in addition to NC fines. The addition of powdered activated carbon (PAC) is known to be effective for organics removal as a pretreatment before membrane processing (Adham 1993). The effects of PAC were investigated by performing 3-stage flux tests with the permeate and raw of sample #1 and Omega100K UF membrane.

Table 6 lists the physical properties of PAC used (WPH, manufactured by Calgon Carbon Corporation, PA). The PAC adsorption isotherm test was conducted for the adsorption of TOC from sample #1 as described in Section 3.1.4, and fit by the Freundlich equation:

$$q_e = K C_e^{\frac{1}{n}} \quad \text{Eq 13}$$

where:

q_e = equilibrium carbon surface adsorbate concentration

C_e = equilibrium adsorbate concentration (i.e., TOC at equilibrium)

K and 1/n = the equilibrium constants related to the adsorbent capacity and the strength of adsorption.

The range of PAC loadings for adsorption isotherm was 0 to 400mg/L, and the experimental results are shown in Figure 43 (a). The equilibrium constants are:

$$K = 12.8\ (mg/g)\ (L/mg)^{1/n}$$
$$1/n = 0.82$$

if comparing the above constant values to other Freundlich adsorption constants for toxic organic compounds listed in Water Quality and Treatment (AWWA 1990).

K is relatively low, which implies the smaller capacity of the adsorbent (PAC) for the adsorbate (TOC) whereas 1/n is relatively high, which implies a weaker adsorption bond. The above equilibrium constants are close to those for carbon tetrachloride (K=11 and 1/n=0.83).

Table 6. Manufacturer's specifications of WPH (after Adham 1993).

Iodine No.	1199
Ash Content, %	6
Moisture, %	3
Specific Gravity, g/cm^3	2.3
Packing Density, g/cm^3	0.4 - 0.7
% Passing 325 Mesh (44mm)	98
Geometric Mean Diameter, mm	10

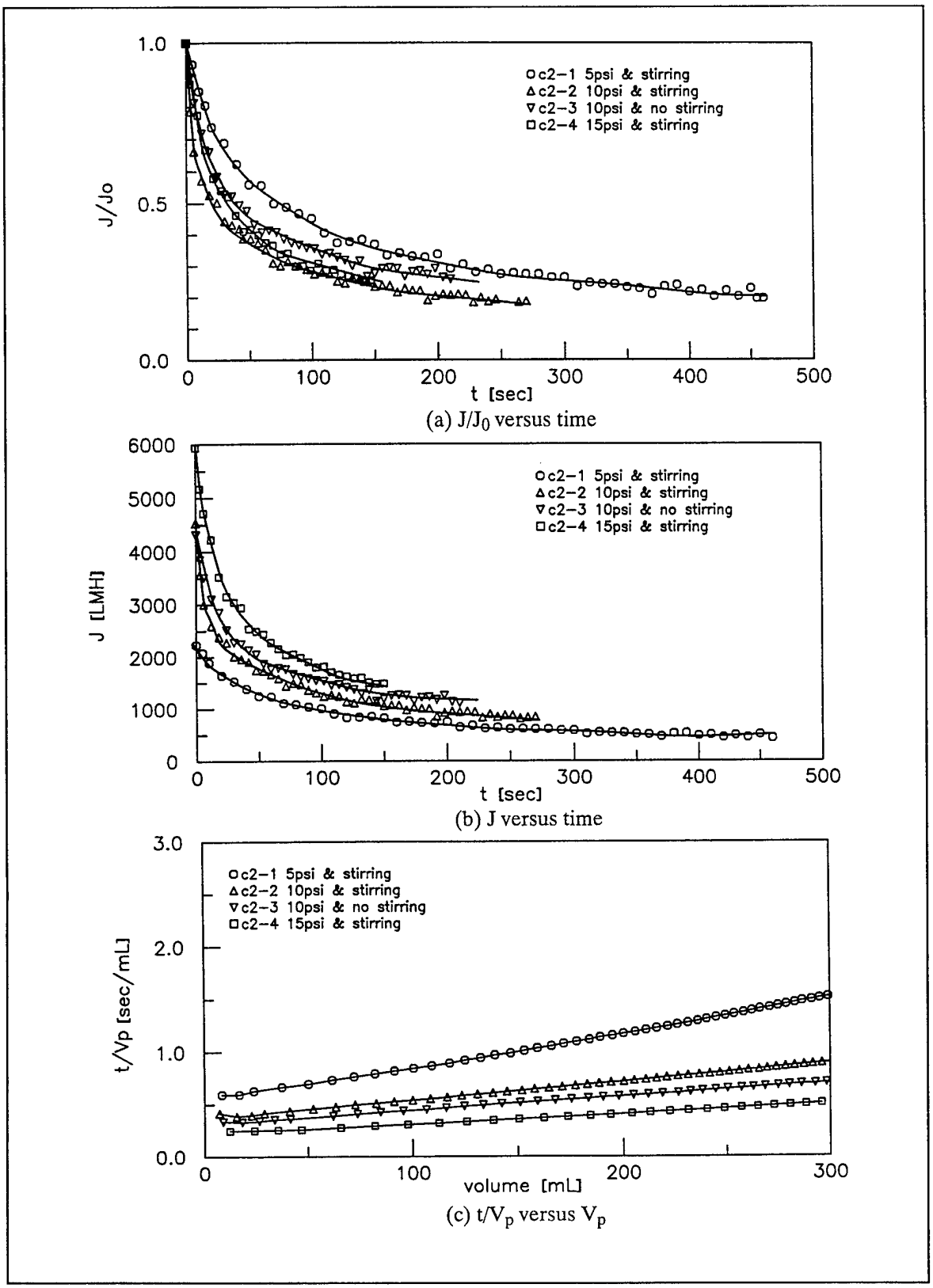

Figure 41. Effects of pressure on flux of sample #3 (MF 0.22μm).

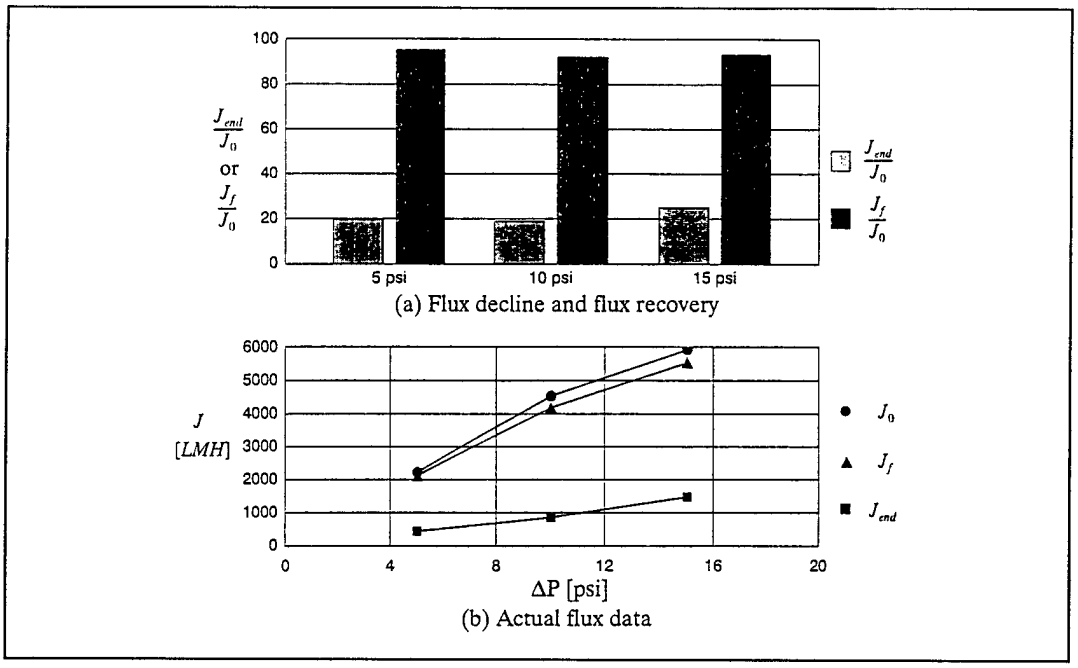

Figure 42. Effects of pressure on flux decline and recovery of sample #3 (MF 0.22μm).

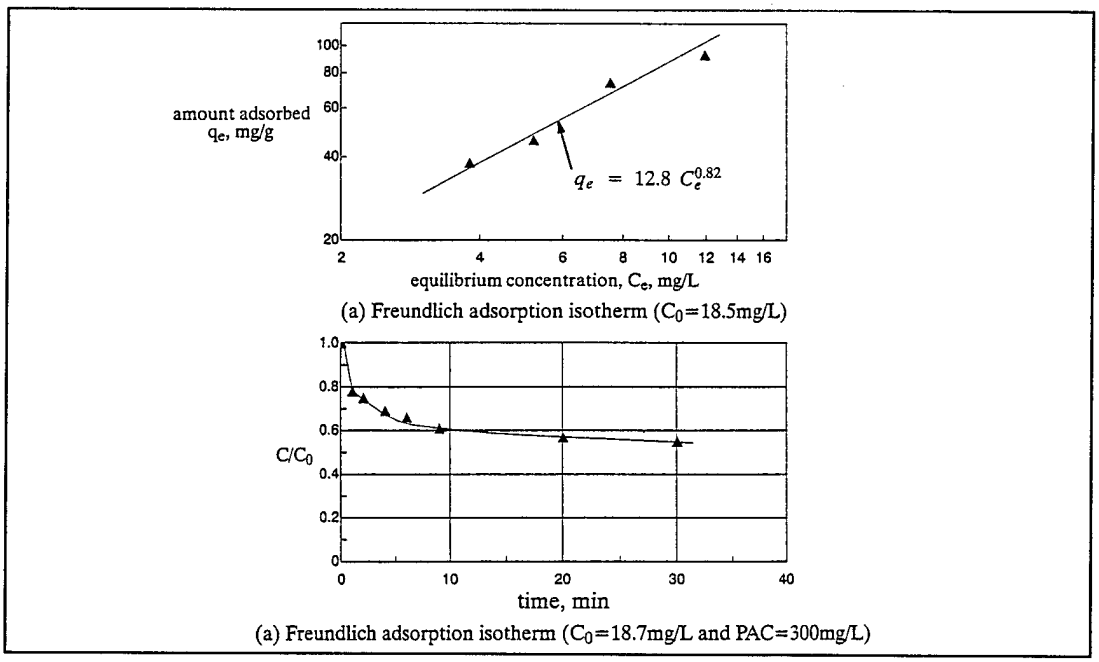

Figure 43. Adsorption isotherm and kinetics of TOC from sample #1 with WPH.

The batch kinetic test for TOC adsorption from sample #1 was also conducted as described in Section 3.1.4. The PAC dosage was 300mg/L, which corresponds to C_0=18.7 and C_e=4.5mg/L according to the Freundlich isotherm equation determined by the adsorption isotherm test results. As shown in Figure 43 (b), the adsorption rate appears to be relatively slow (the initial 40 percent

adsorption occurs pretty fast), and the adsorption occurred during 30 minutes contact time is only about 2/3 of the total adsorption at equilibrium (C_e/C_0 should be 0.24 at PAC dosage=300mg/L). Two possible explanation for this relatively slow kinetics are:

1. NC fine particles in sample #1 also compete and interfere with the organics adsorption.
2. The molecular size of organics in sample #1 may be large. As the molecular size of organics increases, the diffusion rate decreases. For example, a 10,000 molecular weight fulvic acid requires about 17 hr to come to equilibrium, and a 50,000 molecular weight humic acid requires about 2 days (AWWA, *Water Quality and Treatment*, 1990).

To achieve a certain concentration level within the less contact time, a PAC dose should be increased to compensate.

Two kinds of 3-stage flux tests were performed to investigate the efficiency of PAC pretreatment: (1) 3.0g/L of WPH PAC was added to the permeate of sample #1 passing Omega0.3μm, and after 2 hr contact time the 3-stage flux test was performed; (2) 600mg/L of WPH PAC was added to the sample #1 raw, and after 6 hr contact time the 3-stage flux test was performed. Table A7 and Figure 44 give the experimental results.

Figures 44 and 45 show how the flux can be dramatically improved by PAC pretreatment that is supposed to remove the organic matter in sample #1. In the case of a sufficient amount of PAC added (permeate #1 + 3.0g/L PAC), there was only less than 10 percent of flux decline during 300mL permeate production, and the flux was recovered to almost 100 percent by backflush. In the case of 600mg/L of PAC added to raw sample #1, the ending flux was about two times grater than that without PAC (improved from 240LMH to 400LMH), and the flux recovery was also improved by about 20 percent (from 70 to 88 percent). Therefore, it is evident that severe organic foulants exist in sample #1 in addition to NC fines, and that the organic fouling can be reduced by PAC pretreatment, although the captured NC, organic matter and PAC must be disposed of.

A comparison of the reversible/irreversible resistance components in Table A7, shows a significant amount of resistance reduction when PAC added. This becomes even clearer when the slopes in Figure 44c are compared—the slope tends to decrease significantly when PAC is added.

4.1.7 Summary of Phase I: Dead-End Filtration

A total of six different types of NC wastewater samples from each NC manufacturing and purification process were analyzed and classified into three categories based on the analytical experimentation results, including turbidity, TSS, UV absorbance, TOC, alkalinity, pH, and hardness.

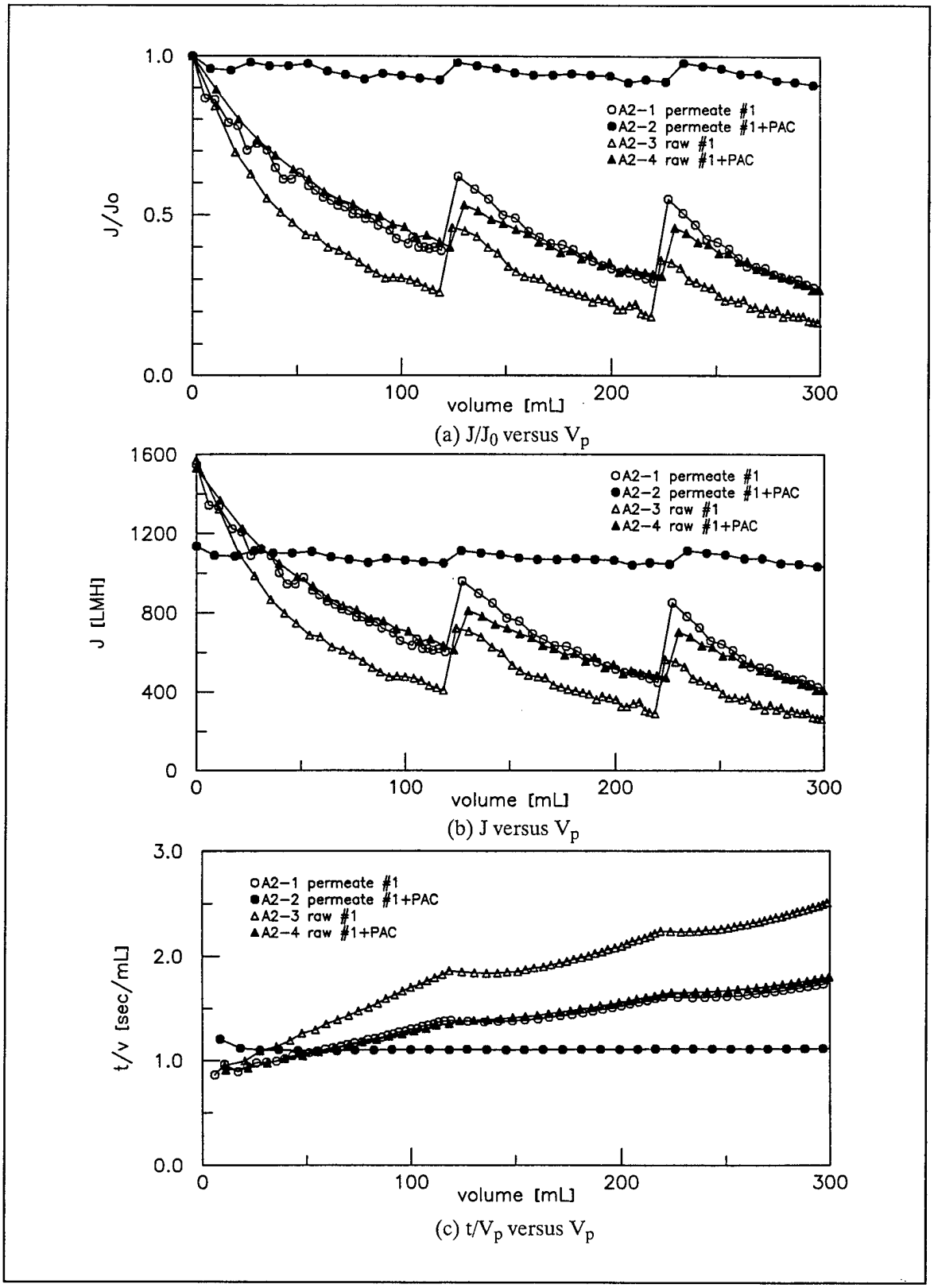

Figure 44. Effects of PAC on flux decline behavior of sample #3 (Omega100K).

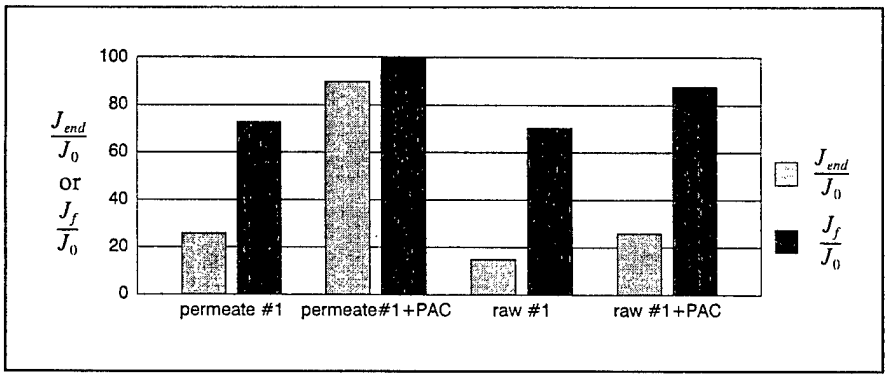

Figure 45. Effects of PAC on flux performance of sample #1 (Omega100K).

The NC wastewater samples in Category 1 (sample #5 and #8) did not appear to need any further experimentation in regard to membrane filtration because of their high quality (no detectable TSS). The flux test results showed that the NC wastewater sample in Category 2 (sample #1) had a significant amount of dissolved organic foulants in addition to colloidal NC foulants, and that UF membranes were more susceptible to organic fouling because of their smaller pore sizes while MF membranes were more susceptible to colloidal fouling due to pore blockage by NC fines. The flux performance of sample #1 could be dramatically improved by PAC pretreatment for organic removal. In the case of the samples in Category 3 (sample #3, #10 and #11), colloidal and supracolloidal sizes of NC fines were found to be the major foulants to cause flux decline and reversible/irreversible fouling during filtration. Microscopy and image analysis showed that the NC cake formed during filtration of sample #3 was denser and more compact than that of sample #1. The wide size distribution of NC fines and their various shapes resulted in formation of a dense and compact NC cake layer.

The following common characteristics were found from analyzing 1-stage flux test results of sample #1 and sample #3:

1. Generally, UF membranes showed slower flux decline rate and the higher flux recovery than MF membranes, which agrees well with the effects of membrane pore size and particle size discussed in Section 4.1.2. However, there is trade-off in using a UF membrane because of its relatively low permeate production rate compared to MF membranes. Omega series UF membranes have an advantage at this point due to their higher pore density and/or porosity.

2. A comparison of the flux test results of Omega series membranes showed that a critical membrane pore size exists that shows the worst flux performance. Among Omega100K, Omega300K, Omega 0.16μm, and Omega 0.3μm, the Omega 0.16μm showed the worst reversible and irreversible fouling. It is very interesting that this pore size is similar to the critical

particle size (about 0.1μm) observed by Fane (1984), at which the steady-state flux is minimum since neither the molecular diffusion process nor the shear-induced hydrodynamic diffusion process is predominant (Lee 1993).

3. The membrane base material is another critical factor affecting the flux performance. The cellulose-based membranes (YM100 and MF 0.22μm) showed the best performance among membranes tested. Polypropylene (YC01 0.2μm) also showed relatively good performance regardless of its naturally hydrophobic characteristics. It is interesting that regardless of hydrophilicity, the PES-based MF membranes (Omega 0.16μm and Omega 0.3μm) showed very poor flux performance (flux recovery=63-75 percent for sample #1, and 79-87 percent for sample #3) whereas the PES UF membranes showed excellent flux performance (flux recovery=100 percent for both samples). This could be explained in relation to the smaller pore size of UF membranes as described in (1). Finally, the acrylo-based (XM300 and FN 0.2μm) and PTFE-based (RC02 0.2μm) membranes showed relatively low flux recovery, which implies strong interactions between these membranes and NC fines/NC wastewater.

In selecting the candidate membranes for UF/MF membrane process of NC wastewater, the following three factors should be accounted for: (1) flux decline rate, (2) degree of reversible and irreversible fouling, and (3) permeate production rate. Three steps of systematic membrane screening criteria were established, including both short-term and long-term effects. The experimental results for sample #3 yield the following conclusions:

1. All membranes showed similar and satisfactory permeate quality in terms of TSS and TOC.

2. As filtration proceeds, the NC cake layer resistance becomes predominant over the intrinsic membrane resistance, and the permeate flux starts to be controlled by the NC cake layer.

3. When filtration continued for a long period, as in the 3- or 6-stage flux tests, the differences of the permeate flux of each membrane narrowed down regardless of its initial clean water flux. Especially, the permeate flux of Omega300K, Omega 0.3μm, and MF 0.22μm approached to the same steady-state value.

4. Omega300K and MF 0.22 μm were found to be the best among the membranes tested; they were selected as the candidate membranes.

With the selected candidate membranes, the effects of transmembrane pressure and stirring on flux of sample #3 were investigated. Increasing the transmembrane pressure resulted in accelerating the flux decline rate. However, the actual permeate flux of both membranes was proportional to the transmembrane pressure (5 to 15 psi), which implied that the permeate flux was still in the pressure-controlled region. Therefore, we can expect a higher permeate production rate by increasing the transmembrane pressure. Both

membranes showed rather unexpected effects of stirring. The unstirred conditions produced a greater permeate flux than the stirred although the difference was small. This result could be explained in relation to the different nature of NC cake formation under the stirred and unstirred conditions. Kim et al. (1993) also observed a similar trend with colloidal silver particles.

4.2 Phase II: Crossflow Filtration

4.2.1 Analytical Experiment Results for NC Wastewater Samples

Raw NC wastewater samples were analyzed for hardness, alkalinity, pH, total suspended solids (TSS), turbidity, and UV absorption. The experimental results are shown in Table 7.

Table 8 shows the quality of the permeates passing through each membrane. The permeates of the beater decant (sample #1-1) were crystal clear, and their quality was good enough for reuse/recycle. The permeates of other samples except the poacher decants had similar quality to the permeate of the beater decant. However, the permeates of the poacher decants (samples #2-1, #2-2, #2-3) showed relatively poor quality, and their color was slightly yellow, which indicated a significant amount of dissolved organic materials. The organic materials in the poacher decants also cause membrane fouling in addition to colloidal NC fines.

4.2.2 Pilot-Scale Flux Test Results

Using the pilot system shown in Figure 11, the flux performance of each sample was investigated with various membranes listed in Table 4. All pilot tests were run in the constant transmembrane pressure mode, and the transmembrane pressure was set to produce an initial clean water flux of 750 $L/m^2/hr$ (LMH). The crossflow velocity was set at 0.4 m/sec. The flow path during each pilot test is shown in Figure 46. The initial clean water flux (J_0) was measured before applying the NC wastewater sample: valves B were open while valves A were closed. At this time the transmembrane pressure was adjusted to keep an initial clean water flux of 750 LMH. After the transmembrane pressure was set up, the flow path was switched to the NC wastewater—valves A were open while valves B were closed.

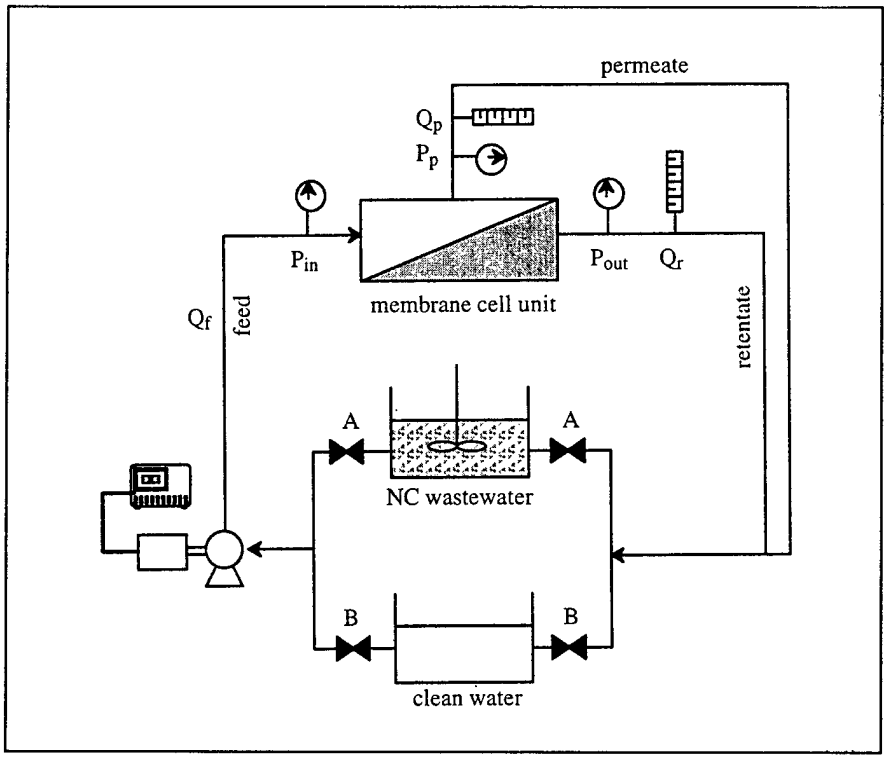

Figure 46. Flow path of the pilot system.

After 30 minutes of filtration, the membrane cell was dissembled and the characteristics of NC cake formed on the membrane surface were qualitatively examined, such as apparent density, thickness, and attachment to membrane surface. The NC cake was removed from the membrane surface by washing and spraying. Then, the membrane cell was reassembled with the membrane skin facing the permeate side, and a backflush (P_{in}=15 psi) was applied for about 1 minute. Finally, the final clean water flux (J_f) test was again performed at the same transmembrane pressure to measure the irreversible fouling component.

Flux Performance of Beater Decant Sample. The beater decant sample had the lowest TSS value. Figure 47 shows that the UF100K membrane was superior to any other membrane tested; after 30 minutes filtration, there was only 40 percent of flux decline and there was almost no irreversible fouling. The UF300K membrane showed better flux performance than the MF0.22, but its flux recovery (60 percent) was worse than the MF0.22 (80 percent). This could be explained by the hydrophobicity of the UF300K membrane, i.e., hydrophobic membranes are more severely fouled by hydrophobic materials like NC fines. Although the MF0.22 is hydrophilic, its flux performance was the worst—more than 50 percent flux decline within several minutes. As found in Section 4.1.2, the particle sizes of NC fines are widely distributed from submicrometer to several hundred micrometers. The pore size of the MF0.22 microfiltration membrane is not small enough to reject all NC fines, so some small particles could block membrane pores or could be entrapped inside of membrane pores during filtration. This results in the worst flux performance.

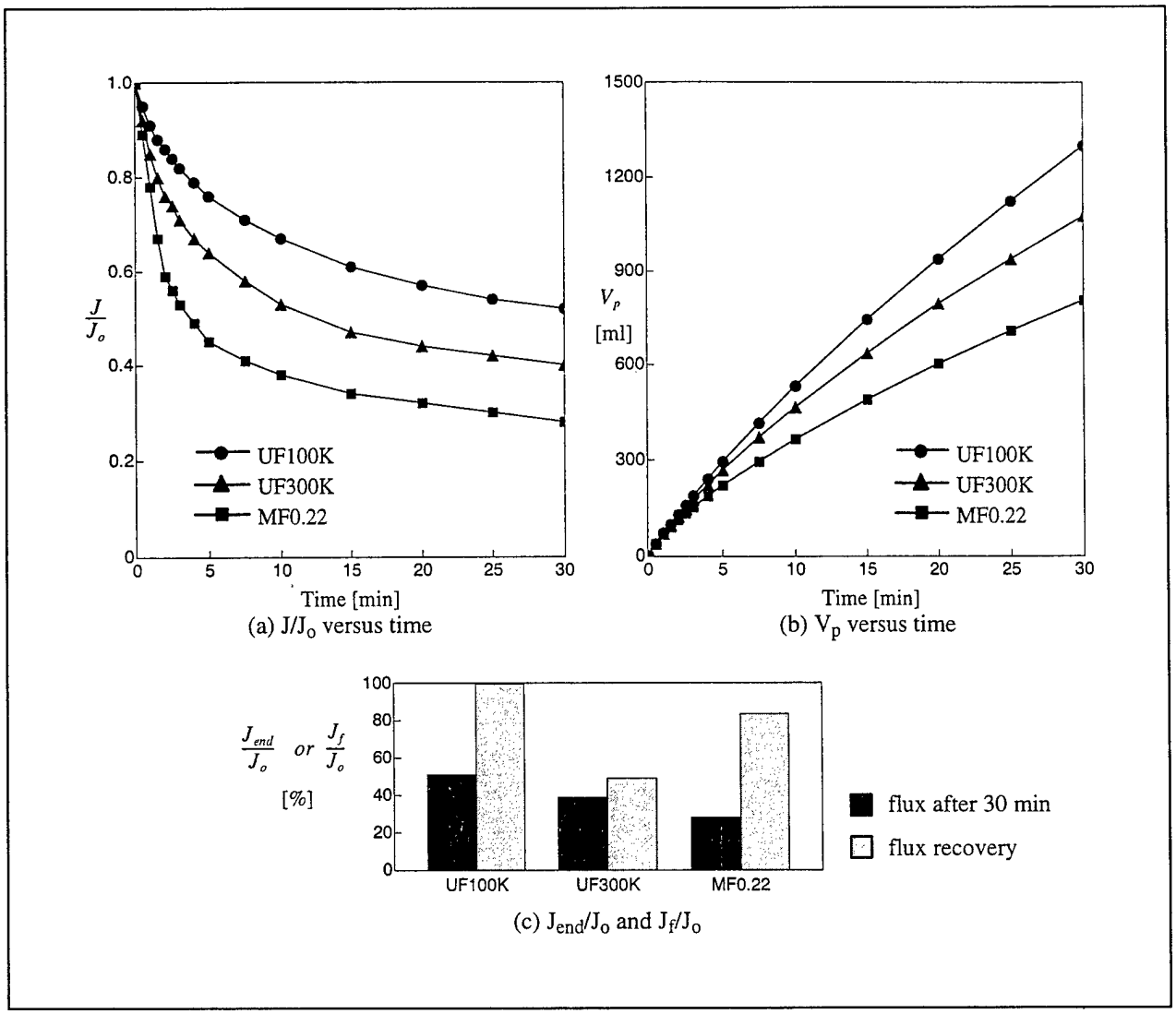

Figure 47. Flux test results of beater decant (J_o=750LMH and U_0=0.4m/sec).

Flux Performance of Poacher Decant Samples. The flux decline of poacher decants was much more severe than the other samples; more than 70 percent flux loss occurred within 5 minutes of filtration. A higher TSS value resulted in a thicker NC cake layer. Figure 48 shows the flux test results of poacher 1-hr decant (sample #2-1). Again, the UF100K membrane shows the best flux performance. The flux decline of the UF300K membrane was similar to that of the UF100K membrane, but the UF100K membrane showed almost 100 percent flux recovery after backflush while the UF300K membrane showed the worst flux recovery (60 percent).

The other two poacher decants (sample #2-2 and #2-3) showed a similar flux performance to sample #2-1. Figure 49 shows the flux test results of the poacher 4 hr decant (sample #2-3). The UF100K membrane showed much greater permeate production than the other membranes.

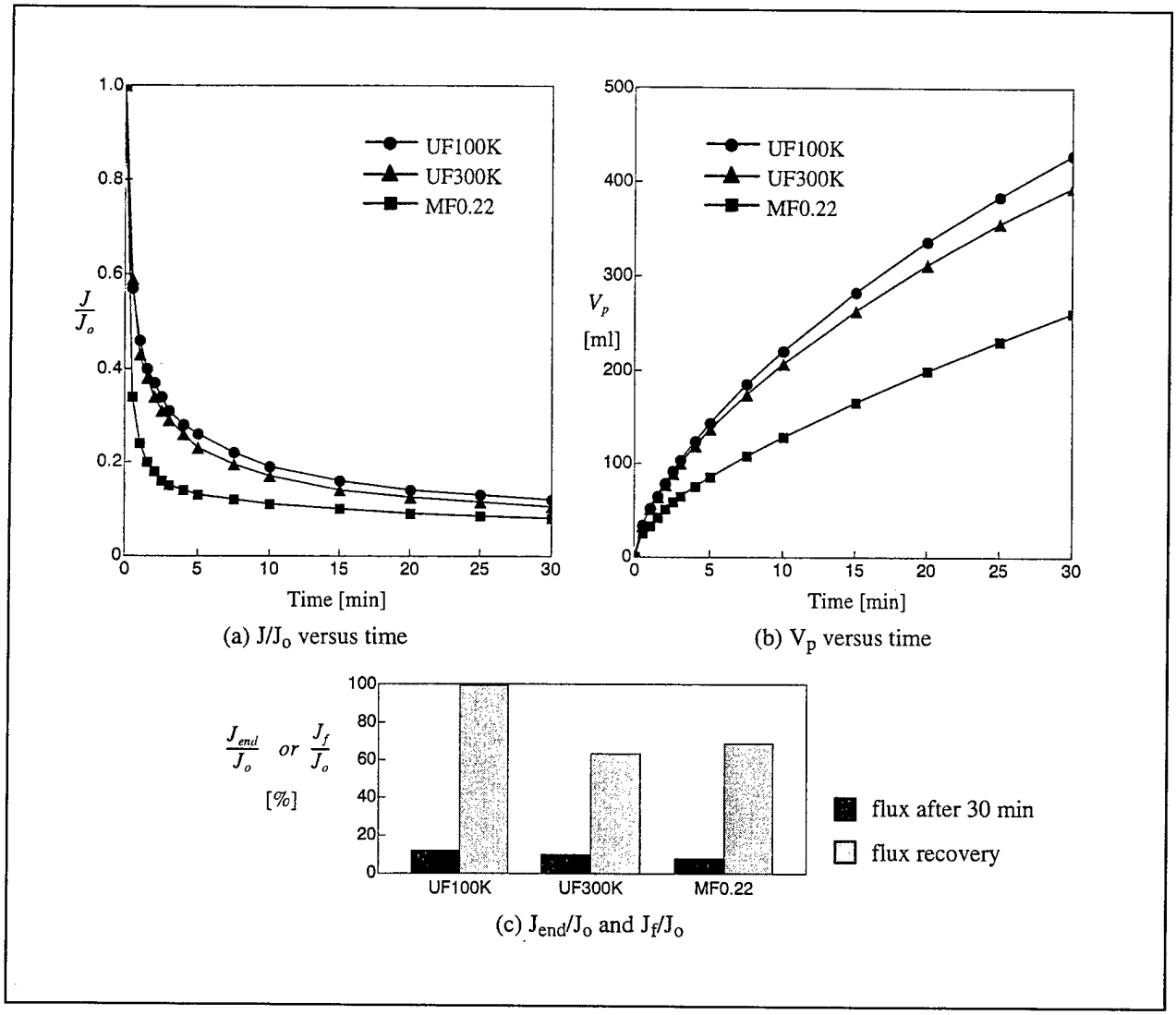

Figure 48. Flux test results of poacher 1-hr decant (J_0=750LMH and U_0=0.4m/sec).

Flux Performance of Blender Decant Sample. Figure 50 shows the flux test results of the blender decant (sample #3). The flux decline curve of the UF100K membrane is quite different from those of the UF300K and MF0.22 membranes. It was interesting that the NC cake layer on the UF100K membrane was thicker than on the UF300K and MF0.22 membranes while the apparent cake density of the UF100K was lower than the others. Furthermore, in the case of the UF100K, the NC cake was like a thin sheet and easily detachable while the NC cakes on the UF300K and MF0.22 were like a very thin gel layer and they were very hard to detach. These results imply that the UF100K has a weaker interaction with NC fines than others because of its base material and hydrophilicity.

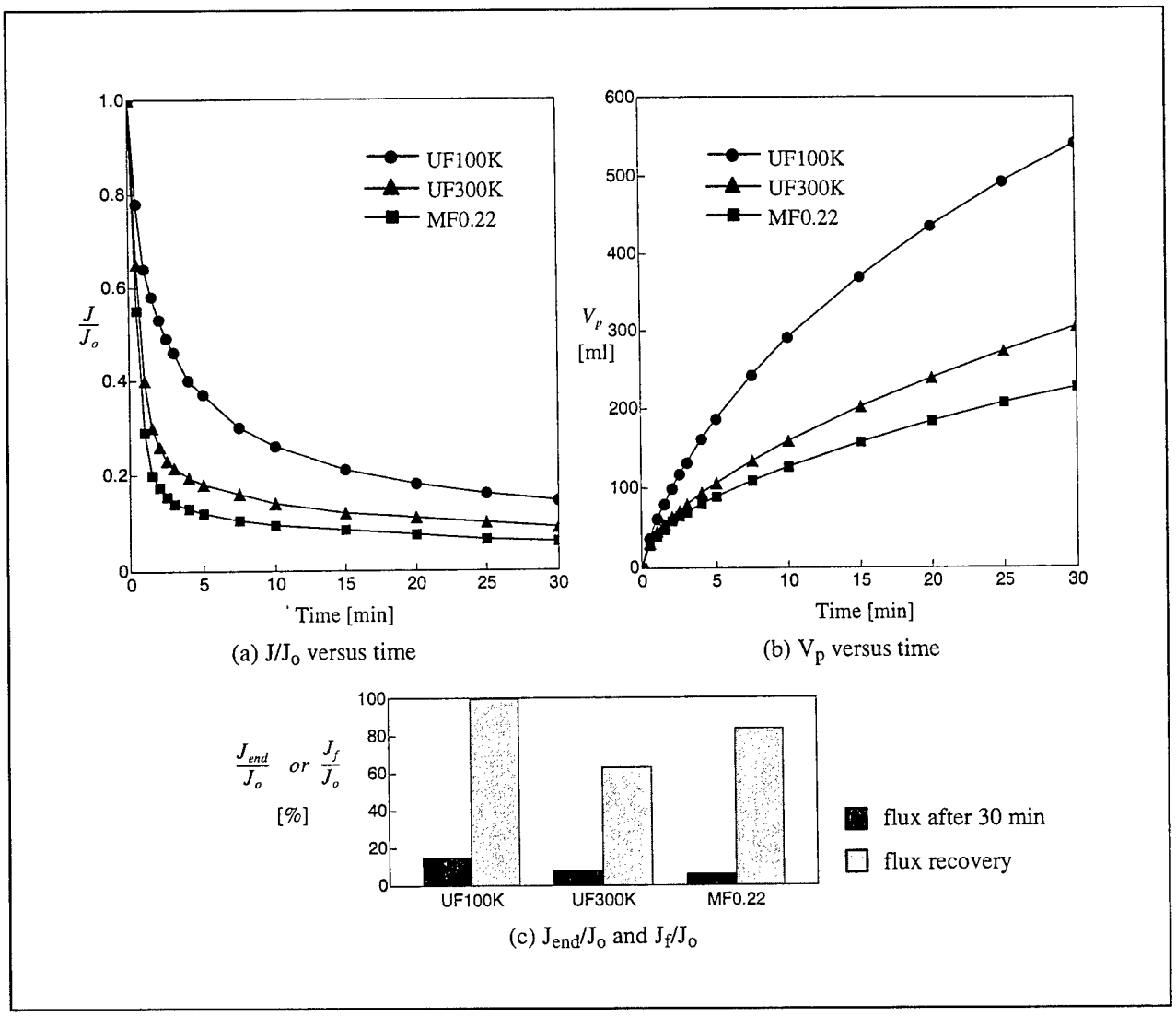

Figure 49. Flux test results of poacher 4-hr decant (J_0=750LMH and U_0=0.4m/sec).

Flux Performance of Wringer Decants. Figure 51 shows that the full basket sample (sample #4-2) had a slightly better flux performance than the empty basket (sample #4-1). The NC cakes of both samples were gel-like and very hard to detach. Again, the flux recovery of the UF100K membrane was almost 100 percent.

Summary. Figures 47 to 51 show that, among the membranes tested, the UF100K was the best for treating any NC wastewater stream; it showed almost no irreversible fouling. Each NC wastewater stream showed a quite different flux decline (see Figure 52). Generally speaking, the rate and degree of flux decline became worse as the TSS value increased—the beater decant, which had the lowest TSS, showed the best flux performance, while the poacher decants, which had the highest TSS, showed the worst flux performance.

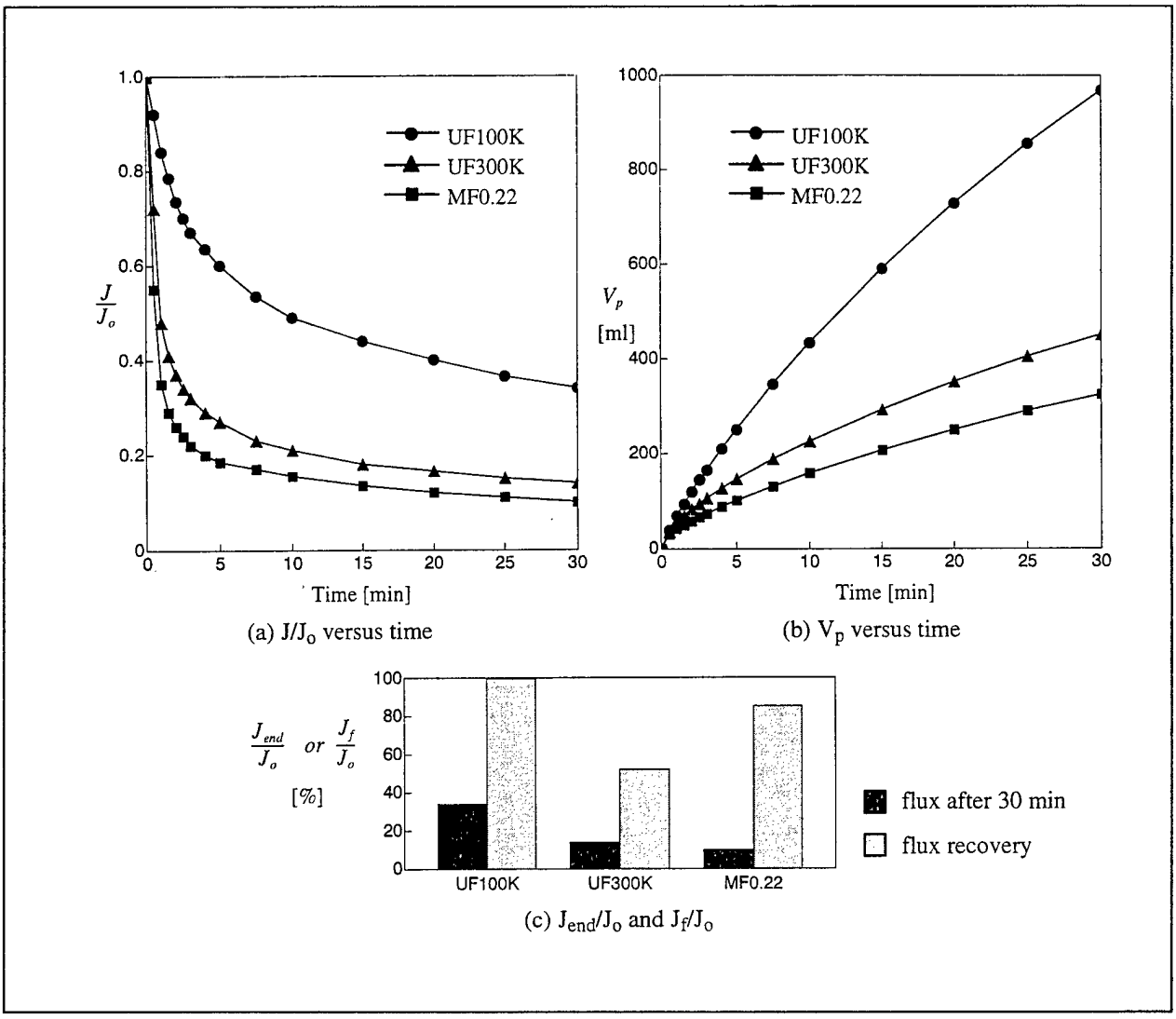

Figure 50. Flux test results of blender decant (J_0=750LMH and U_0=0.4m/sec).

Except for the poacher house decants, all NC wastewaters could be successfully treated using the crossflow membrane filtration with the UF100K membrane. In the case of the poacher house decants, more frequent backflush cycle would be necessary because the NC cake build-up is too fast.

4.2.3 Effects of Transmembrane Pressure and Crossflow Velocity

Effect of Transmembrane Pressure on Flux Performance. The effect of transmembrane pressure was investigated with the UF100K membrane. Figure 53 shows the flux test results at three different transmembrane pressures for the poacher 1-hr decant. The actual permeate flux increased with the transmembrane pressure throughout the filtration period (Figure 53a).

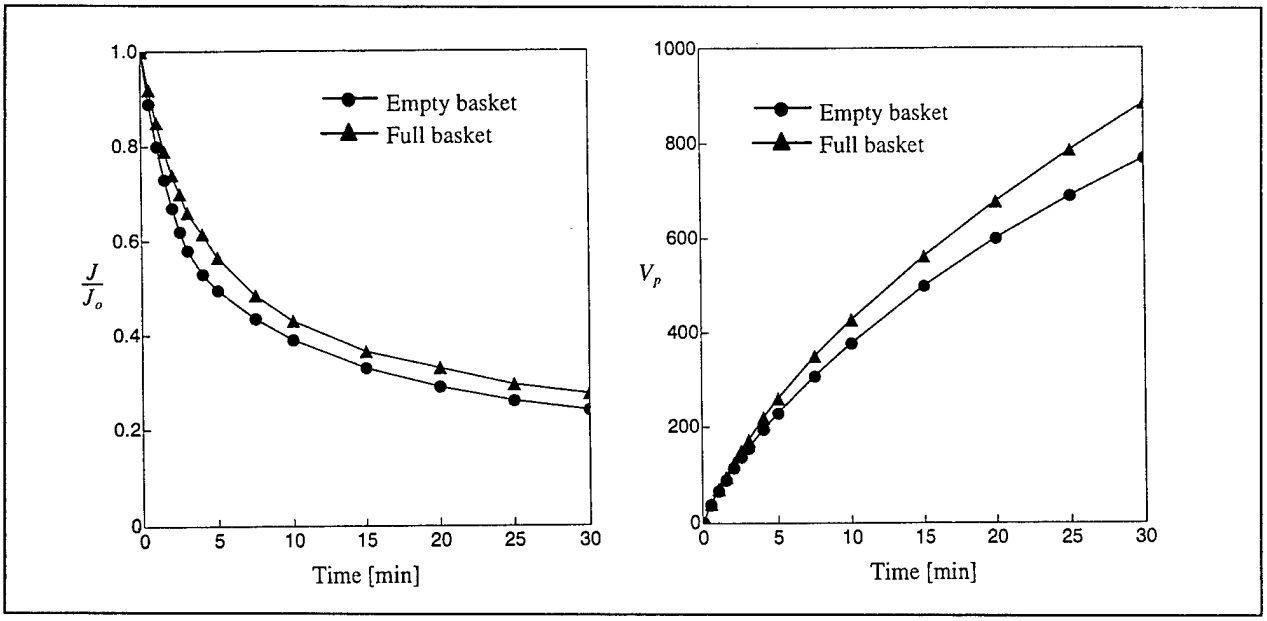

Figure 51. Flux test results of wringer decants with UF100K (J_0=750LMH and U_0=0.4m/sec).

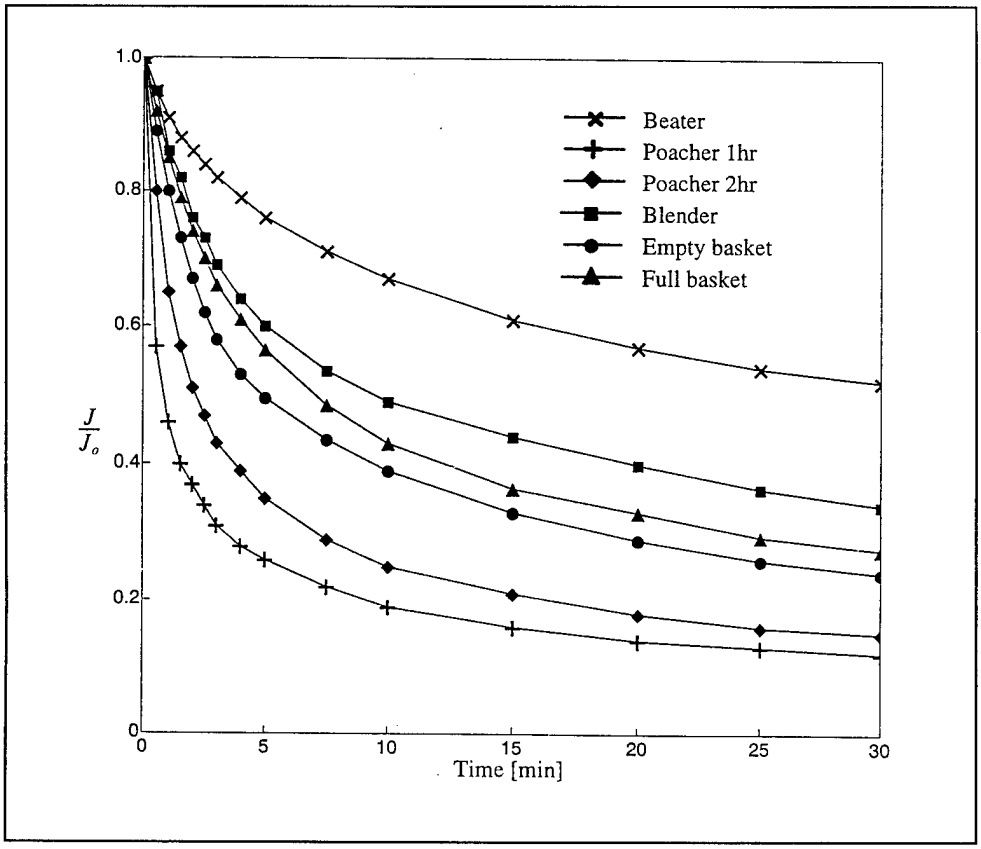

Figure 52. Flux test results of each sample with UF100K (J_0=750LMH and U_0=0.4m/sec).

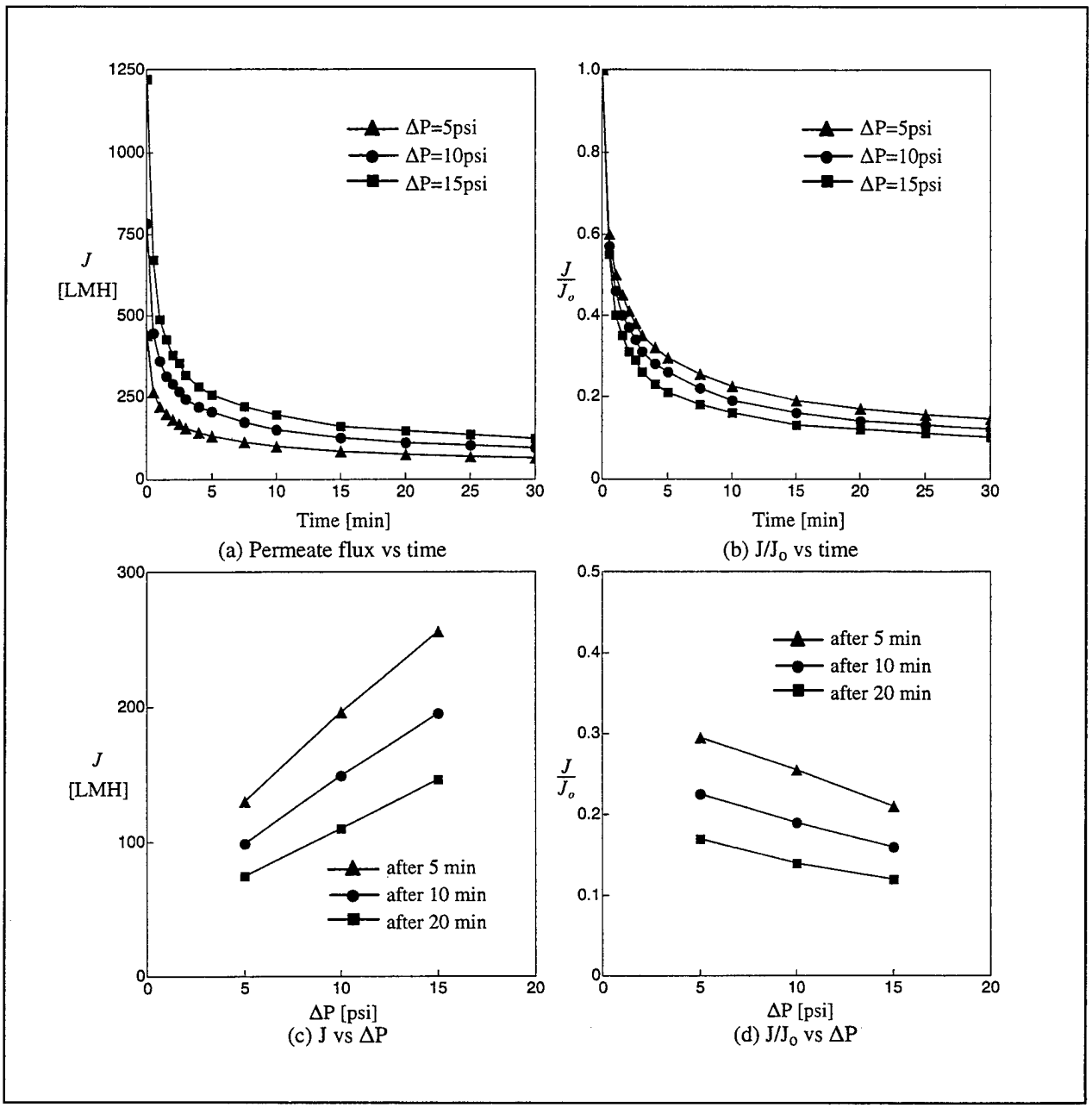

Figure 53. Effect of transmembrane pressure with poacher 1-hr decant and UF100K (U_0=0.4m/sec).

However, the flux decline rate became rapid as the transmembrane pressure increased (Figure 53b) since a higher permeate flux due to a higher transmembrane pressure resulted in more rapid NC cake formation on membrane surface.

Figure 53 (c) and (d) show the permeate flux after 5, 10, and 15-minute filtration periods. The actual permeate flux increases linearly with the transmembrane pressure, which means the membrane process is still in the pressure-controlled

region. Unlike the mass transfer controlled region, higher permeate production rate can be achieved by increasing the transmembrane pressure.

Effect of Crossflow Velocity on Flux Performance. The effect of crossflow velocity was investigated with the UF100K membrane for the blender decant sample. Figure 54 shows the flux test results at three different crossflow velocities. In the study of Phase I, the unstirred conditions during dead-end filtration gave a higher flux performance than the stirred conditions. A similar result was also found with the crossflow membrane filtration tests: increasing the crossflow velocity resulted in deleterious effects on the flux performance. As the crossflow velocity increases, the NC cake layer became denser and more gel-like although it was always reversible.

4.2.4 Summary of Phase II: Crossflow Filtration

The UF100K membrane showed the best flux performance for all NC wastewater samples. Although there is not much difference in membrane pore sizes between the UF100K and the UF300K, the hydrophilic UF100K membrane showed much better flux performance than the hydrophobic UF300K membrane. The UF100K membrane showed no irreversible fouling (i.e., 100 percent flux recovery after backflush) for all NC wastewater samples while the UF300K membrane showed severe irreversible fouling (40 to 60 percent flux recovery). Both the UF100K and MF0.22 membranes are hydrophilic, but the flux performance of the UF100K membrane was much better than that of the MF0.22 membrane. This can be explained by the deleterious effect of membrane pore size. If the membrane pore size is not small enough, particles could block membrane pores or could be entrapped inside of membrane pores during filtration. Consequently, it was recommended to use a hydrophilic ultrafiltration membrane like the UF100K for the NC wastewater treatment.

The flux decline behavior of each NC wastewater stream was quite different. This study was done with the UF100K membrane. The poacher decant samples, which had the highest TSS value, showed the worst flux decline—more than 60 percent flux loss occurred within 5 minutes, and more than 80 percent flux loss after 30 minutes filtration. The beater house decant sample, which had the lowest TSS value, showed the best flux performance, only 40 percent flux decline after 30 minutes filtration. The blender and wringer decant samples, which had mid-range TSS values, showed 60 to 70 percent flux decline after 30 minutes filtration. However, there was no irreversible fouling for all NC wastewater samples with the UF100K membrane. All flux decline during filtration was almost 100 percent recoverable by backflush. So, the crossflow membrane filtration technique could be successful for the NC wastewater treatment.

The transmembrane pressure and crossflow velocity are the most important operating parameters in membrane filtration process. These factors are directly connected to the cost of membrane process. The effect of transmembrane pressure on flux decline behavior was investigated up to 15 psi. Shen et. al (1993) found that the flux performance decreased with transmembrane pressure.

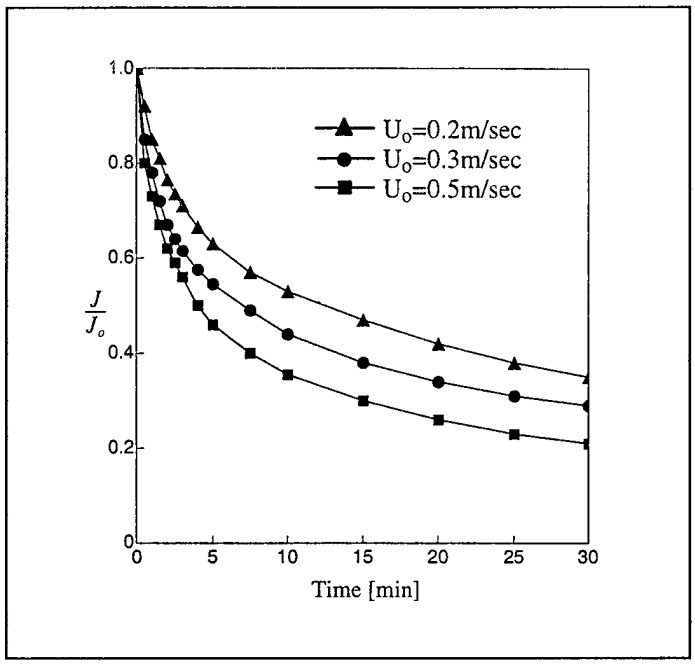

Figure 54. Effect of crossflow velocity with UF100K for blender decant (ΔP=10psi).

However, in this study, it was found that there was no deleterious effect of increasing the transmembrane pressure. The pilot test results showed that the permeate flux increased linearly with the transmembrane pressure, i.e., the membrane process was still in the pressure-controlled region. So, if necessary, the transmembrane pressure could be increased without any deleterious effect on the flux performance. One advantage in the crossflow membrane filtration technique is that a shearing effect arising from crossflow reduces cake build-up on membrane surface. As a result, the flux performance is usually expected to increase with the crossflow velocity since the shearing effect is proportional to crossflow velocity.

However, the pilot test results showed that lower crossflow velocity gave better flux performance. This is consistent with dead-end filtration results. The unstirred conditions gave a higher flux performance than the stirred conditions, as shown in section 4.1.5. These unexpected results were explained in relation to the different nature of cake formation on the membrane surface under stirred and unstirred conditions. Baker et al. (1985) found that the portion of smaller particles are greater in the cake layer than in the feed stream. During the crossflow membrane filtration process, larger NC fines have more tendency to move back into feed stream due to their higher inertia arising from shear force, so the NC cake layer would consist of smaller NC fines. This results in a greater cake resistance. The experimental results showed that the NC cake layer became denser and more gel-like as the crossflow velocity increased.

5 Conclusions

Rinsing and purification processes in the beater, poacher, blender, and wringer houses generate very turbid NC wastewater, of which the TSS ranges from about 30 to over 1000 mg/L. The membrane filtration technique has a great potential in treatment of the NC wastewater. The NC wastewater samples were taken from each house decant. The flux decline behavior of each NC wastewater sample was investigated with a Amicon dead-end membrane filtration cell (Phase I) and with a pilot-scale crossflow membrane filtration system (Phase II).

The flux performance during membrane filtration depends on physicochemical reactivities with the membrane as well as an NC wastewater characteristics. In implementing membrane process, selecting a proper membrane (membrane type, pore size, and base material) would be the first essential step to minimize reversible and/or irreversible fouling and to enhance the flux performance. Based on the experimental results of the Phase I study, it is concluded that:

1. UF membranes have a lower flux decline rate and a higher flux recovery than MF membranes, but UF membranes have a relatively low permeate production rate compared to MF membranes.
2. A critical membrane pore size (about 0.1μm) exists, at which point the worst flux performance occurs.
3. The cellulose-based hydrophilic membranes have the best flux performance.

The above results should be considered when determining a membrane for the NC wastewater treatment. The Amicon UF100K membrane used in Phase II is one of the best membranes that meet the above considerations.

The Amicon dead-end filtration apparatus used in Phase I is not appropriate to simulate a flux decline behavior during a practical membrane filtration process of the NC wastewater. So, a pilot-scale crossflow membrane filtration system was constructed, and the following conclusions are drawn from the Phase II study:

1. The flux decline behavior is quite different from one NC wastewater stream to another. Under the same operating conditions (i.e., DP and U_o), the flux decline becomes severe as the TSS value increases.
2. Up to 15 psi, the permeate flux increases linearly with the transmembrane pressure (pressure controlled region). Increasing the transmembrane pressure has no effect on the flux decline.

3. The flux decline becomes worse as the crossflow velocity increases. This agrees with the results of dead-end filtration (Phase I)—the unstirred conditions produced a greater permeate flux than the stirred conditions.

References

Adham, S.S., *Evaluation of the Performance of Ultrafiltration With Powdered Activated Carbon Pretreatment for Organic Removal*, Ph.D. Thesis (University of Illinois, Urbana-Champaign, 1993).

Albert and Weston, H., *A Manual on Explosives* (Routledge and Sons, Ltd., London, 1917).

Alleman, J.E., B.J. Kim, D.M. Quivey, and L.D. Equihua, "Alkaline Hydrolysis of Munitions-Graded Nitrocellulose," *NC Fines Separation and Treatment Workshop Proceedings* (Purdue University, Lafayette, IN 1993).

Allen, T., *Particle Size Measurement*, 4th ed. (Chapman and Hall, New York, 1990).

American Public Health Association (APHA), *Standard Methods for the Examination of Water and Wastewater*, 14th ed. (Washington, DC, 1975).

American Water Works Association (AWWA), *Water Quality and Treatment*, 4th ed. (Denver, CO, 1990).

Arthur D. Little, Inc., *Engineering/Cost Evaluation of Options for Removal, Disposal of NC Fines*, Final Report to U.S. Army Toxic and Hazardous Material Agency (1987).

Baker, R.J., A.G. Fane, C.J.D. Fell, and B.H. Yoo, "Factors Affecting Flux in Crossflow Filtration," *Desalination* (1985), vol 53, pp 81-93.

Cheryan, M., *Ultrafiltration Handbook* (Technomic Publishing Company, Inc., Lancaster, PA, 1986).

Clark, M.M., Memorandum, Subject: A Resistance Model for Predicting Flux Decline in Pilot Scale Hollow Fiber Ultrafiltration (19 April 1991).

Clark, M.M., and K.S. Heneghan, "Ultrafiltration of Lake Water for Portable Water Production," *Desalination* (1991), vol 80, pp 243-249.

Ellis, H.V., III, J.J. Kowalski, J.R. Hodgson, J.C. Bhandari, J.L. Sanyer, T.W. Reddig, J.L. Mirror, and C.C. Lee, *Mammalian Toxicity of Munitions Compounds: Phase III. Effects of Life-time Exposure; Part III. Nitrocellulose*, Report No. 9 (Midwest Research Institute, Kansas City, MO, 1980).

Ellis, H.V., III, J.J. Kowalski, J.R. Hodgson, J.C. Bhandari, J.L. Sanyer, T.W. Reddig, J.L. Mirror, and C.C. Lee, *Mammalian Toxicity of Munitions Compounds: Phase I. Acute Oral Toxicity, Primary Skin and Eye Irritation, Dermal Sensitization, Disposition and Metabolism, and Ames Tests of Additional Compounds*, Report No. 6/ADA060333 (Midwest Research Institute, Kansas City, MO, 1978).

Ellis, H.V., III, J.J. Kowalski, J.R. Hodgson, J.C. Bhandari, J.L. Sanyer, T.W. Reddig, J.L. Mirror, and C.C. Lee, *Mammalian Toxicity of Munitions Compounds: Phase II. Effects of Multiple Doses; Part IV. Nitrocellulose*, Report No. 5/ADA062016 (Midwest Research Institute, Kansas City, MO, 1976).

Ewing, T.W., and F.T. Kristoff, "Assessment of the Explosion Hazard During Continuous Purification of Nitrocellulose in the Coincell," *Journal of Harzardous Material* (1986), vol 13, No. 2.

Fane, A.G., "Ultrafiltration of Suspensions," *Journal of Membrane Science* (1984) vol 20, No. 3, pp 249-259.

Heffinger, J.G., and W.J. Worrell, *Microfiltration of Nitrocellulose Fines*, Final report to U.S. Army Construction Engineering Research Laboratory (1992).

Khanna, K., Memorandum, Subject: Nitrocellulose Health Advisory (Office of Drinking Water, U.S. Environmental Protection Agency, 1988).

Kim, Kyu-Jin, V. Chen, and A.G. Fane, "Ultrafiltration of Colloidal Silver Particles: Flux, Rejection, and Fouling," *Journal of Colloid and Interface Science* (1993), vol 155, pp 347-359.

Lâiné, J.M., J.P. Hagstrom, M.M. Clark, and J. Mallevialle, "Effects of Ultrafiltration Membrane Composition," *Journal AWWA* (1989), vol 81, No. 11, pp 61- 67.

Lee, Y., *Modeling of Flux Decline Behavior During the Crossflow Ultrafiltration Membrane Process*, MS Thesis (University of Illinois, Urbana-Champaign, 1993).

Lee, C.C., et al., *Mammalian Toxicity of Munitions Compounds: Phase I. Acute Oral Toxicity, Primary Skin and Eye Irritation, Dermal Sensitization, and Disposition and Metabolism*, Report No. 1/ADB011150L (Midwest Research Institute, Kansas City, MO, 1975).

Merin, U., S. Ordin, and G.B. Tanny, "Microfiltration of Sweet Cheese Whey," *Dairy Science Technology* (1983) vol 18, p 153.

Patel, P.N., *Membrane Filtration of Microbial Cells: Processing of Saccharomyces Cerevisiae in Hollow Fiber and Pleated Filter Cross-Flow Modules*, MS Thesis (University of Illinois, Urbana-Champaign, 1985).

Rogres, P.L., K.J. Lee, and D.E. Tribe, "High Productivity Ethanol Fermentations as a Potential Liquid Fuel or Fuel Supplement With Zymomonas Mobilis Used in Tropical Countries for Making Alcoholic Beverages, Palm and Cactus Wines," *Process Biochemistry* (1980), vol 15, pp 7-11.

Ryon, M.G., *Water Quality Criteria for Nitrocellulose*, Document No. AD-ORNR-6179 (U.S. Army Medical Research and Development Command, Fort Detrick, Frederick, MD, 1986).

Stryer, Lubert, *Biochemistry* (W.H. Freeman & Company, New York, 1988).

Quinchon, J., and J. Tranchant, *Nitrocellulose: The Materials and Their Applications in Propellants, Explosives and Other Industries* (Ellis Horwood Ltd., Chichester, England, 1989).

Urbanski, T., *Chemistry and Technology of Explosives* (Pergamaon Press, Oxford, U.K., 1965).

Shen, X., J.K. Park, and B.J. Kim, "Separation of Nitrocellulose Manufacturing Wastewater by Bench-Scale Flat Sheet Cross-Flow Microfiltration Units," *NC Fines Separation and Treatment Workshop Proceedings at Purdue University* (Purdue University, Lafayette, IN, 1993).

Sullivan, J.H., H.D. Putnam, M.A. Keirn, B.C. Pruitt, and J.C. Nichols, *A Summary and Evaluation of Aquatic Environmental Data in Relation to Establishing Water Quality Criteria for Munitions Unique Compounds*, Final report to U.S. Army Medical Research and Development Command, Fort Detrick, Frederick, MD (1978).

Van Den Berg, G.B., and C.A. Smolders, "Flux Decline in Ultrafiltration Processes," *Desalination* (1990), vol 77, pp 101-133.

Appendix A: Flux Test Results

Table A.1 1-stage flux test results for sample #1

: total permeate vol.=120mL

: operated at 10 psi with stirring

ID	Membrane	Flux in [LMH]			% Flux		resistance(x e^11) [1/m]				Permeate quality		
		Jo	Jend	Jf	Jend/Jo	Jf/Jo	Rt	Rm	Rc	Ri	NTU	UV	TOC
A1	Nova100K	1296	570	1296	44	100	4.34	1.91	2.43	0.00	0.8	0.50	-
A2	Omega100K	1207	567	1207	47	100	4.37	2.05	2.31	0.00	0.5	0.52	42.6
A3	Omega300K	1988	954	1908	48	96	2.60	1.25	1.30	0.05	0.3	0.51	-
A4	Omega 0.16	5344	1015	3367	19	63	2.44	0.46	1.70	0.27	0.7	0.52	-
A5	Omega 0.3	6374	2295	4781	36	75	1.08	0.39	0.56	0.13	0.6	0.52	41.9
B1	YM100	455	282	455	62	100	8.78	5.44	3.34	0.00	0.4	0.60	-
B2	XM300	929	223	752	24	81	11.11	2.67	7.82	0.63	0.3	0.51	42.6
C1	FN 0.2	5338	907	4164	17	78	2.73	0.46	2.13	0.13	0.2	0.51	-
C2	MF 0.22	4983	2193	4634	44	93	1.13	0.50	0.60	0.04	0.3	0.52	41.9
D1	RC02 0.2	4974	1791	4427	36	89	1.38	0.50	0.82	0.06	0.4	0.48	-
D2	YC01 0.2	2424	1091	2303	45	95	2.27	1.02	1.20	0.05	0.3	0.47	-

Jo = initial clean water flux

Jend = local flux when the permeate volume reachs 120 mL.

Jf = water flux after backwash

sample #1 raw	910.0	2.79	383.4
DI water	0.2	0.00	0.273
Tap water	1.0	0.03	0.793

Table A.2 1-stage flux test results for permeate #1

: total permeate vol.=300mL(1st stage=120ml, 2nd stage=100ml, 3rd stage=80ml)

: operated at 10 psi with stirring

ID	Membrane	Flux in [LMH]			% Flux		resistance(x e^11) [1/m]			
		Jo	Jend	Jf	Jend/Jo	Jf/Jo	Rt	Rm	Rc	Ri
A2	Omega100K	1549	403	1129	26	73	6.15	1.60	3.96	0.59
A3	Omega300K	1860	651	1395	35	75	3.81	1.33	2.03	0.44
A4	Omeag0.16	5639	4793	5312	85	94	0.52	0.44	0.05	0.03
B1	YM100	445	289	445	65	100	8.56	5.57	3.00	0.00
C2	MF 0.22	4155	4072	4097	98	99	0.61	0.60	0.00	0.01

Jo = initial clean water flux

Jend = local flux when the total permeate volume reaches 300mL

Jf = water flux after backwash

Table A.3 1-stage flux test results for sample #3

: total permeate vol.=120mL

: operated at 10 psi with stirring

ID	Membrane	Flux in [LMH]			% Flux		resistance(x e^11) [1/m]				Permeate quality		
		Jo	Jend	Jf	Jend/Jo	Jf/Jo	Rt	Rm	Rc	Ri	NTU	UV	TOC
A1	Nova100K	1406	970	1406	69	100	2.55	1.76	0.79	0.00	0.8	0.052	-
A2	Omega100K	1394	990	1394	71	100	2.50	1.78	0.73	0.00	0.4	0.050	1.837
A3	Omega300K	2367	1420	2320	60	98	1.74	1.05	0.68	0.02	0.2	0.048	-
A4	Omega 0.16	6235	2120	4926	34	79	1.17	0.40	0.67	0.11	0.8	0.049	-
A5	Omega 0.3	5326	2663	4634	50	87	0.93	0.47	0.40	0.07	0.4	0.045	1.796
B1	YM100	433	325	433	75	100	7.63	5.72	1.91	0.00	0.3	0.044	-
B2	XM300	935	299	608	32	65	8.28	2.65	4.20	1.43	0.2	0.040	1.802
C1	FN 0.2	5534	719	3320	13	60	3.44	0.45	2.70	0.30	0.2	0.043	-
C2	MF 0.22	4799	1872	4703	39	98	1.32	0.52	0.80	0.01	0.2	0.045	1.951
D1	RC02 0.2	5516	1931	4633	35	84	1.28	0.45	0.75	0.09	0.3	0.057	-
D2	YC01 0.2	2537	1269	2385	50	94	1.95	0.98	0.91	0.06	0.2	0.052	-

Jo = initial clean water flux

Jend = local flux when the permeate volume reachs 120 mL.

Jf = water flux after backwash

sample #1 raw	540.0	2.630	12.3
DI water	0.2	0.000	0.273
Tap water	1.0	0.03	0.793

Table A.4 3-stage flux test results for sample #3

: total permeate vol.=300mL

: operated at 10 psi with stirring

ID	Membrane	Flux in [LMH]			% Flux		Time in sec		resistance(x e^11)			[1/m]
		Jo	Jend	Jf	Jend/Jo	Jf/Jo	T(0.5Jo	Tend	Rt	Rm	Rc	Ri
A1	Nova100K	1566	564	1478	36	94.4	190	440	4.39	1.58	2.72	0.09
A2	Omega100K	1511	604	1423	40	94.2	240	420	4.10	1.64	2.36	0.10
A3	Omega300K	2446	807	2253	33	92.1	120	300	3.07	1.01	1.97	0.09
A4	Omega 0.16	6065	849	4118	14	67.9	10	260	2.92	0.41	2.32	0.19
A5	Omega 0.3	6340	1268	5135	20	81.0	25	165	1.95	0.39	1.47	0.09
B1	YM100	501	301	499	60	99.6	N/A	930	8.24	4.94	3.28	0.02
B2	XM300	(Eliminated because of its low Jo and low recovery)										
C1	FN 0.2	(Eliminated because of its low Jend and low recovery)										
C2	MF 0.22	4537	862	4188	19	92.3	25	270	2.87	0.55	2.28	0.05
D1	RC02 0.2	5248	1102	3967	21	75.6	20	210	2.25	0.47	1.62	0.15
D2	YC01 0.2	2393	742	2175	31	90.9	140	315	3.34	1.04	2.20	0.10

Jo = initial clean water flux

Jend = local flux when the total permeate volume reaches 300mL.

Jf = water flux after backwash

T(0.5Jo) = time required for the local flux to reach a half of the initial flux

Tend = time required for the permeate volume to reach 300mL

Table A.5 6-stage flux test results for sample #3

: total permeate vol.=600mL(1st stage=120ml, 2nd=100ml, 3rd=100ml
4th=100ml, 5th=90ml, and 6th=90ml)

: operated at 10 psi with stirring

ID	Membrane	Flux in [LMH]			% Flux		Time in sec		resistance(x e^11)			[1/m]
		Jo	Jend	Jf	Jend/Jo	Jf/Jo	T(0.5Jo	Tend	Rt	Rm	Rc	Ri
A1	Nova100K	(Eliminated because its flux decline behavior is worse than Omega 100k)										
A2	Omega100K	1428	386	1341	27	93.9	280	1200	6.43	1.73	4.58	0.11
A3	Omega300K	2139	471	1976	22	92.4	160	900	5.26	1.16	4.01	0.10
A4	Omega 0.16	(Eliminated because of its bad recovery and no superious Jend)										
A5	Omega 0.3	5221	470	4177	9	80.0	25	770	5.27	0.47	4.68	0.12
B1	YM100	(Eliminated because its low Jo and longer Tend)										
B2	XM300	(Already eliminated based on 1st criteria)										
C1	FN 0.2	(Already eliminated based on 1st criteria)										
C2	MF 0.22	4695	470	4249	10	90.5	35	750	5.28	0.53	4.69	0.06
D1	RC02 0.2	(Eliminated because of its low recovery)										
D2	YC01 0.2	2402	312	2176	13	90.6	80	1250	7.93	1.03	6.79	0.11

Jo = initial clean water flux

Jend = local flux when the total permeate volume reaches 600mL.

Jf = water flux after backwash

T(0.5Jo) = time required for the local flux to reach a half of the initial flux

Tend = time required for the permeate volume to reach 600mL

Table A.6 Effects of pressure and stirring on flux of sample #3 (Omega 300K and MF 0.22um)
: total permeate vol.=300mL(1st stage=120ml, 2nd stage=100ml, 3rd stage=80ml)

ID	variables	Flux in [LMH]			% Flux		Time in sec		resistance(x e^11)			[1/m]
		Jo	Jend	Jf	Jend/Jo	Jf/Jo	T(0.5Jo	Tend	Rt	Rm	Rc	Ri
A3	5 psi w/ stir	910	337	910	37	100.0	340	720	3.68	1.36	2.32	0.00
	10 psi w/ stir	2139	813	1970	38	92.1	160	300	3.05	1.16	1.79	0.10
	10 psi w/o stir	1955	880	1806	45	92.4	230	300	2.82	1.27	1.44	0.10
	15 psi w/ stir	3664	1282	3023	35	82.5	85	190	2.90	1.01	1.67	0.22
C2	5 psi w/ stir	2232	446	2129	20	95.4	70	460	2.77	0.55	2.19	0.03
	10 psi w/ stir	4537	862	4188	19	92.3	25	270	2.87	0.55	2.28	0.05
	10 psi w/o stir	4317	1122	4131	26	95.7	40	210	2.21	0.57	1.61	0.03
	15 psi w/ stir	5937	1484	5545	25	93.4	35	150	2.50	0.63	1.83	0.04

Jo = initial clean water flux
Jend = local flux when the total permeate volume reaches 300mL or 600mL
Jf = water flux after backwash
T(0.5Jo) = time required for the local flux to reach a half of the initial flux
Tend = time required for the permeate volume to reach 300mL or 600mL

Table A.7 Effects of PAC addition to sample #1 (Omega100K)
: total permeate vol.=300mL(1st stage=120ml, 2nd stage=100ml, 3rd stage=80ml)
: pressure= 10psi with stirring

ID	variables	Flux in [LMH]			% Flux		Time in sec		resistance(x e^11)			[1/m]
		Jo	Jend	Jf	Jend/Jo	Jf/Jo	T(0.5Jo	Tend	Rt	Rm	Rc	Ri
A2	permeate	1549	403	1129	26	72.9	70	520	6.15	1.60	3.96	0.59
	permeate+PAC	1136	1022	1130	90	99.5	> 330	330	2.42	2.18	0.23	0.01
	raw	1571	236	1104	15	70.3	50	750	10.51	1.58	8.27	0.67
	raw+PAC**	1530	398	1345	26	87.9	100	540	6.23	1.62	4.39	0.22

Jo = initial clean water flux
Jend = local flux when the total permeate volume reaches 300mL
Jf = water flux after backwash
T(0.5Jo) = time required for the local flux to reach a half of the initial flux
Tend = time required for the permeate volume to reach 300mL
* PAC dose = 3.0g/L: contact time = 2hrs
** PAC dose = 600mg/L: contact time = 6hrs

Appendix B: List Of Membrane Manufacturers

Company	Products	Address	Phone	FAX
Filtron Corp.	Nova10K Omega100K Omega300K Omega0.16μm Omega0.3μm	50 Bearfoot Road Nothborough, MA 01532	508/393-1800 800/FILTRON	508/393-1874
Amicon, Inc.	YM100 YM300	72 Cherry Hill Drive Beverly, MA 01915	508/777-3622 800/343-0696	508/777-6204
Costar	Filinert 0.2μm Membra-Fil 0.22μm	One Alewife Center Cambridge, MA 02140	617/868-6200 800/492-1110	617/868-2076
Osmonics, Inc.	RC02 0.2μm YC01 0.2μm	5951 Clearwater Drive Minnetonka, MN 55343	612/933-2277 800/351-9008	612/933-0141
Millipore Corp.	UF 100K UF 300K	80 Ashby Road Bedford, MA 01730	617/275-9200 800/632-2708	617/275-5550

USACERL DISTRIBUTION

Chief of Engineers
ATTN: CEHEC-IM-LH (2)
ATTN: CEHEC-IM-LP (2)
ATTN: CECG
ATTN: CECC-P
ATTN: CECC-R
ATTN: CECW
ATTN: CECW-O
ATTN: CECW-P
ATTN: CECW-PR
ATTN: CEMP
ATTN: CEMP-E
ATTN: CEMP-C
ATTN: CEMP-M
ATTN: CEMP-R
ATTN: CERD-C
ATTN: CERD-ZA
ATTN: CERD-L
ATTN: CERD-M
ATTN: CERM
ATTN: DAEN-ZC
ATTN: DAIM-FDP

CECPW 22310-3862
ATTN: CECPW-E
ATTN: CECPW-FT
ATTN: CECPW-ZC
ATTN: DET III 79906

US Army Engr District
ATTN: Library (40)

US Army Engr Division
ATTN: Library (12)

US Army Europe
ATTN: AEAEN-EH 09014
ATTN: AEAEN-ODCS 09014

INSCOM
ATTN: IALOG-I 22060
ATTN: IAV-DPW 22186

USA TACOM 48397-5000
ATTN: AMSTA-XE

Defense Distribution Region East
ATTN: ASCE-WI 17070-5001

US Army Materiel Command (AMC)
Alexandria, VA 22333-0001
ATTN: AMCEN-F
Installations: (19)
Army Munitions Plants (8)

FORSCOM
Forts Gillem & McPherson 30330
ATTN: FCEN

TRADOC
Fort Monroe 23651
ATTN: ATBO-G

Fort Belvoir 22060
ATTN: CETEC-IM-T
ATTN: CETEC-ES 22315-3803
ATTN: Water Resources Support Ctr
ATTN: Australian Liaison Office

USA Natick RD&E Center 01760
ATTN: STRNC-DT
ATTN: ORDNA-F

US Army Materials Tech Lab
ATTN: SLCMT-DPW 02172

USARPAC 96858
ATTN: DPW
ATTN: APEN-A

CEWES 39180
ATTN: Library

CECRL 03755
ATTN: Library

USA AMCOM
ATTN: Facilities Engr 21719
ATTN: AMSMC-EH 61299
ATTN: Facilities Engr (3) 85613

USA Engr Activity, Capital Area
ATTN: Library 22211

US Army ARDEC 07806
ATTN: SMCAR-ISE

Engr Societies Library
ATTN: Acquisitions 10017

Defense Nuclear Agency
ATTN: NADS 20305

Defense Logistics Agency
ATTN: MMDIS 22060-6221

Walter Reed Army Medical Center 20307

National Guard Bureau
ATTN: NGB-ARI

US Military Academy
ATTN: MAEN-A
ATTN: Facilities Engineer
ATTN: Geography and Envr Engrg

Naval Facilities Engr Command
ATTN: Facilities Engr. Command (8)
ATTN: Naval Facilities Engr Service Center93043

8th US Army Korea
Env Program Office 96301
ATTN: FKEN-E

USA Japan (USARJ)
ATTN: APAJ-EN-ES

416 Engineer Command 60623
ATTN: Gibson USAR Ctr

Tyndall AFB 32403
ATTN: Engrg & Srvc Lab

American Public Works Assoc. 64104-1806

US Army Envr Hygiene Agency
ATTN: HSHB-ME 21010

US Gov't Printing Office 20401
ATTN: Rec Sec/Deposit Sec (2)

Nat'l Institute of Standards & Tech
ATTN: Library 20899

Defense Tech Info Center 22060-6218
ATTN: DTIC-O (2)

155
7/97

This publication was reproduced on recycled paper.